

AD-753 914

DIELECTRIC LENS MODEL

Philip L. Bachman

E-Systems, Incorporated

Prepared for:

Rome Air Development Center

November 1972

DISTRIBUTED BY:

**NTIS**

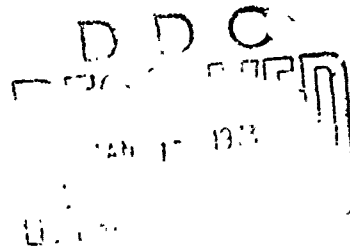
National Technical Information Service  
U. S. DEPARTMENT OF COMMERCE  
5285 Port Royal Road, Springfield Va. 22151

AD753914

RADC-TR-72-299  
Final Technical Report  
November 1972



DIELECTRIC LENS MODEL  
Melpar Division, E-Systems, Inc.



Approved for public release;  
distribution unlimited.

NATIONAL TECHNICAL  
INFORMATION SERVICE

Rome Air Development Center  
Air Force Systems Command  
Griffiss Air Force Base, New York

131

UNCLASSIFIED

Security Classification

DOCUMENT CONTROL DATA - R & D		
<i>(Security classification of title, body of abstract and indexing annotation must be entered when the overall report is classified)</i>		
1. ORIGINATING ACTIVITY (Corporate author) Melpar Division, E-Systems, Inc., 7700 Arlington Boulevard, Falls Church, Virginia 22046		2a. REPORT SECURITY CLASSIFICATION UNCLASSIFIED
		2b. GROUP N/A
3. REPORT TITLE DIELECTRIC LENS MODEL		
4. DESCRIPTIVE NOTES (Type of report and inclusive dates) Final Report		
5. AUTHOR(S) (First name, middle initial, last name) Philip L. Bachman		
6. REPORT DATE November 1972	7a. TOTAL NO OF PAGES <del>124</del> 131	7b. NO OF REFS 12
8a. CONTRACT OR GRANT NO F30602-71-C-0129  Job Order No. 45191604	8b. ORIGINATOR'S REPORT NUMBER(S) 1057.00100	
9d. OTHER REPORT NO(S) (Any other numbers that may be assigned this report) RADC-TR-72-299		
10. DISTRIBUTION STATEMENT Approved for public release; distribution unlimited.		
11. SUPPLEMENTARY NOTES None	12. SPONSORING MILITARY ACTIVITY Rome Air Development Center (DCRR) Griffiss Air Force Base, New York 13441	
13. ABSTRACT A study was conducted to determine the design data and measure the performance of phase-corrected horn antennas employing the dielectric lenses. The objective is to provide data for a dielectric lens antenna system to be evaluated in a satellite communications link. The frequency range of interest is from 15 to 60 GHz with maximum interest from 20 to 30 GHz. Computer programs were used to design lenses having two refracting surfaces and uniform amplitude distributions across the apertures for maximum gain. Four 18-inch diameter lens-horn antennas were fabricated using cross-linked styrene for the lens material. Their performance was measured both individually and in array combinations, and the performance of larger arrays was predicted. Element aperture efficiencies over 70% were obtained, and the gain and antenna patterns followed predicted values over wide frequency bandwidths. These results are attributed to the ability to fabricate lenses to close tolerances required for the frequencies of interest. The use of lens surface-matching layers reduced reflections and increased gain and efficiency in accord with predicted results although the improvement is relatively small. Arrays of four lens-corrected horns were constructed and tested in three configurations. Results agreed closely with calculated values. The large electrical size of the apertures in wavelengths results in grating lobes when arrayed. These side lobes are close to the main beam and can be tolerated for applications involving satellite links. The array factor for the electrically large elements limits the capability for beam steering to very small angles. An optical simulation of the array patterns was accomplished by the use of a laser beam and		

DD FORM 1 NOV 61 1473

UNCLASSIFIED

Security Classification

UNCLASSIFIED

Security Classification

14 KEY WORDS	LINK A		LINK B		LINK C	
	ROLE	WT	ROLE	WT	ROLE	WT
Antennas Lenses Horns Military Satellite Communications Link Millimeter Waves Matching Layers Arrays Laser Optical Simulation						
13. Abstract (continued)						
photographic images of various array configurations. The array diffraction pattern is recorded photographically and side-lobe structure in the plane of the array becomes evident.						
ib						

SAC--Griffiss AFB NY

UNCLASSIFIED

Security Classification

**DIELECTRIC LENS MODEL**

**Philip L. Bachman**

**Melpar Division, E-Systems, Inc.**

**Approved for public release;  
distribution unlimited.**

**Do not return this copy.  
Retain or destroy.**

*ic*

FOREWORD

This Final Report describes a study accomplished by Melpar Division, E-Systems, Inc., 7700 Arlington Boulevard, Falls Church, Virginia, under contract F30602-71-C-0129, Job Order Number 45191604, for Rome Air Development Center, Griffiss Air Force Base, New York. Contractor's report number is 1057.00100. Mr. Rodney C. Pratt (DCRR) was the RADC Project Engineer.

This report has been reviewed by the Information Office (OI) and is releasable to the National Technical Information Service (NTIS).

This technical report has been reviewed and is approved.

*Rodney C. Pratt*  
Approved: RODNEY C. PRATT  
Project Engineer

*Joseph L. Ryerson*  
Approved: JOSEPH L. RYERSON, Technical Director  
Communications & Navigation Division

FOR THE COMMANDER:

*Fred I. Diamond*  
FRED I. DIAMOND  
Chief, Plans Office

## ABSTRACT

A study was conducted to determine the design data and to accurately measure the performance of phase-corrected horn antennas which employ dielectric lenses to achieve high antenna efficiency. The ultimate goal of this investigation is to provide necessary data for a dielectric lens antenna system which would be evaluated in a military satellite communication link. The frequency range of interest is from 15 to 60 GHz with maximum interest from 20 to 30 GHz.

Computer programs were used to design lenses having two refracting surfaces and uniform amplitude distributions across the apertures to achieve maximum efficiency. Four 18-inch diameter lens-corrected horn antenna elements were designed and fabricated using cross-linked styrene for the lens material. The performance of these elements was measured both individually and in array combinations, and the performance of larger arrays was predicted. Surface-matching layers for the lenses were also designed and evaluated for reduction of reflections and increased efficiency.

Very good element aperture efficiencies were obtained, and the gain and antenna patterns closely followed predicted values over wide frequency bandwidths. These results are attributed, in part, to the ability to fabricate lenses to highly accurate tolerances required for the frequencies of interest. The use of surface-matching layers increased gain and efficiency in accord with predicted results.

Arrays of four lens-corrected horns were constructed and tested in three configurations. Results agreed closely with calculated values for arrays of the electrically large apertures. The wide spacing between element centers in an array results in large grating lobes. These side lobes are close to the main beam and can be tolerated for applications involving satellite links. The array factor for the electrically large elements limits the capability for beam steering to very small angles.

An optical simulation of the array patterns was accomplished by the use of a laser beam and photographic images of various array configurations. The array diffraction pattern is recorded photographically and the side-lobe structure in the plane of the array becomes evident. This is a very useful technique for studying array combinations and evaluating the characteristic diffraction patterns.

## Evaluation

The purpose of the study was to determine the characteristics of a dielectric lens system for application in a ground based communications terminal. The frequencies of interest were those above 15 GHz, with particular attention at 20 and 30 GHz.

The results of the study did not provide all of the expected benefits, but did reveal that a very efficient antenna can be provided, and when placed in an array, has the capability of a small degree of electronic tracking.

Although the antenna works extremely well at the design frequencies, (above 80% efficiency in some cases) its cost and weight may not compete favorably with parabolic reflectors of the same effective aperture. However, the fact that the surface tolerance is only one third as critical as with a reflecting antenna allows the useable frequency to be three times higher with comparable machining procedures. The greatest benefit, from this study, appears to be at frequencies far above any in present use and from the standpoint of surface tolerance, at least, the constructed antenna would perform well up to approximately 400 GHz.

*Rodney C. Pratt*  
RODNEY C. PRATT  
Project Engineer

## TABLE OF CONTENTS

<u>Section</u>		<u>Page</u>
I	INTRODUCTION	1
	1. Objective	1
	2. Scope	1
	3. Approach	1
II	LENS DESIGN	4
	1. Two-Surface Lens with Constant Amplitude	4
	2. Two-Surface Plano-Convex Lens	9
	3. Lens Fabrication and Tolerances	11
III	SURFACE-MATCHING LAYERS FOR LENSES	13
	1. Discussion of the Problem	13
	2. Theoretical Design	15
	3. Design Calculations and Fabrication	17
IV	HORN ANTENNA DESIGN	21
	1. General Design Discussion	21
	2. Predicted Antenna Element Performance	22
	3. Horn Feeds and Mechanical Design	24
V	ANTENNA ARRAY ANALYSIS	29
	1. One-Dimensional Array Distributions	29
	2. Two-Dimensional Array Configurations	32
	3. Beam Steering	38

## TABLE OF CONTENTS (Continued)

<u>Section</u>		<u>Page</u>
VI	EXPERIMENTAL RESULTS	43
	1. Element Performance	43
	2. Matching Layers	54
	3. Array Performance	57
	4. Beam-Steering Characteristics	73
VII	LASER OPTICAL SIMULATOR	77
	1. Technique	77
	2. Results	79
VIII	CONCLUSIONS	87
IX	RECOMMENDATIONS	89
APPENDIX I	Computer Program for Constant-Amplitude Lens Design	91
APPENDIX II	Computation of Aperture Amplitude Distribution for Plano-Convex Lens	99
APPENDIX III	Aperture Efficiency Versus Amplitude Distributions	105
APPENDIX IV	Computer Program for Linear Antenna Array	115
REFERENCES		123

## LIST OF ILLUSTRATIONS

<u>Figure</u>		<u>Page</u>
1	Lens-Corrected Horn Antenna	2
2	Two-Surface Lens Geometry	4
3	Departure from a Plano First Lens Surface versus Parameters of a 20-inch Diameter Lens	7
4	Contour Plot of Constant-Amplitude and Plano-Convex Lenses	8
5	Comparison of Amplitude Distributions versus Aperture Radius	10
6	Calculated Matching Layer Thickness	18
7	Calculated Matching Layer Dielectric Constant	18
8	Matching Layer Thickness for Two Frequencies	19
9	Plano-Convex Lens with Matching Layer Applied	20
10	Lens-Horn Configuration and Mounting Structure	25
11	VSWR of Rectangular to Circular Waveguide Transitions	28
12	Calculated Side-Lobe Levels versus Four-Element Array Parameters	31
13	Geometry of Symmetrical One-Dimensional Array	33
14	Configuration of 4 x 4 Square Array	35
15	Calculated Antenna Patterns of 14-Element Diamond Array Compared to 16-Element Square Array	36
16	Fourteen-Element Diamond Array Configuration	37

LIST OF ILLUSTRATIONS (Continued)

<u>Figure</u>		<u>Page</u>
17	Four-Element Diamond Array Configuration	39
18	Calculated Antenna Patterns of Four-Element Diamond Array	40
19	Measured and Theoretical Antenna Gain	46
20	E-Plane Element Pattern, 20 GHz	48
21	H-Plane Element Pattern, 20 GHz	49
22	Measured Points and Theoretical Antenna Beamwidths	50
23	E- and H-Plane Element Side-Lobe Levels	52
24	E-Plane Antenna Pattern Comparison for Uniform Amplitude, 20 GHz	53
25	2 x 2 Lens-Horn Array	58
26	4 x 1 Lens-Horn Array and Waveguide Feeds	59
27	Diamond-Shaped Array of Lens-Corrected Horns	60
28	Feed Arrangements Showing Relative Polarizations, Planes of Bends, and Ports	61
29	E-Plane Pattern of 2 x 2 Array	63
30	H-Plane Pattern of 2 x 2 Array	64
31	E-Plane Pattern of 4 x 1 Array	65
32	H-Plane Pattern of 4 x 1 Array	66
33	E-Plane Pattern of Diamond Array, Azimuth Rotation	68

LIST OF ILLUSTRATIONS (Continued)

<u>Figure</u>		<u>Page</u>
34	H-Plane of Diamond Array Azimuth Rotation	69
35	E-Plane Pattern of Diamond Array Elevation Rotation	70
36	H-Plane Pattern of Diamond Array Elevation Rotation	71
37	Comparison of Performance of Element and Arrays	72
38	One-Half Degree Beamsteering with 4 x 1 Array	75
39	Coherent Optical Image-Processing Apparatus	78
40	Variations in Array Configurations	80
41	Diffraction Pattern of 4 x 4 Array, Short Exposure	81
42	Diffraction Pattern of 4 x 4 Array, Long Exposure	81
43	Diffraction Pattern of 12-Element Cross	82
44	Diffraction Pattern of 14-Element Diamond	82
45	Diffraction Pattern of 2 x 2 Array	84
46	Diffraction Pattern of 4 x 1 Array	84
47	Diffraction Pattern of 4-Element Diamond	85
48	Diffraction Pattern of 7-Element Hexagon	85
49	Typical Aperture Distribution Functions	106
50	Aperture Efficiency Relative to Uniform Illumination	107
51	Measured Aperture Distributions of Lens-Horn, 18 GHz	108
52	Measured Aperture Distributions of Lens-Horn, 20 GHz	109

LIST OF ILLUSTRATIONS (Continued)

<u>Figure</u>		<u>Page</u>
53	Measured Aperture Distributions of Lens-I. n., 26.5 GHz	110
54	Measured Aperture Distributions of Lens-Fiorn, 30 GHz	111
55	Array Parameters Used in Computer Program	116

## SECTION I

### INTRODUCTION

#### 1. OBJECTIVE

The purpose of this study is to determine the design parameters and to accurately measure the performance of dielectric lens antennas. It is based upon the background concepts that are described in RADC-TR-70-109, titled "Dielectric Lens Study," reference 1. The antenna element is a horn with a phase-correcting dielectric lens which achieves a high antenna efficiency. The objective is to obtain the data necessary to construct a dielectric lens antenna system which will be evaluated in terms of military satellite communication link.

#### 2. SCOPE

Four lens-corrected horn antenna elements were designed, fabricated, and tested individually and in array combinations. Figure 1 is a photograph of one of the elements showing the dielectric lens, the spun aluminum horn, the mounting flanges, and a waveguide feed transition section. The overall goal is to provide performance information which will allow the design of an array of dielectric lens-corrected horn elements equivalent to a 6-foot effective aperture diameter. Recommendations as to the design of a future satellite communication antenna are to be derived, and consideration is given to a few degrees of beamsteering of the final antenna array. The results of the study will also provide the answers as to whether surface-matching of the lens elements is a desirable feature. The frequency range of interest is from 15 to 60 GHz with maximum interest from 20 to 30 GHz.

#### 3. APPROACH

The design of the lenses was treated first, and section II begins with the design of constant-amplitude lenses as developed in reference 1. The computer program for this design was corrected and modified and the results are noted. Another computer program was developed based upon conventional lens design methods, and a plano-convex lens compared very favorably with the constant-amplitude lens design. The plano-convex design was adopted because the lens is less expensive to fabricate and its predicted performance is equivalent to the double convex, constant-amplitude design. The lenses were machined to close

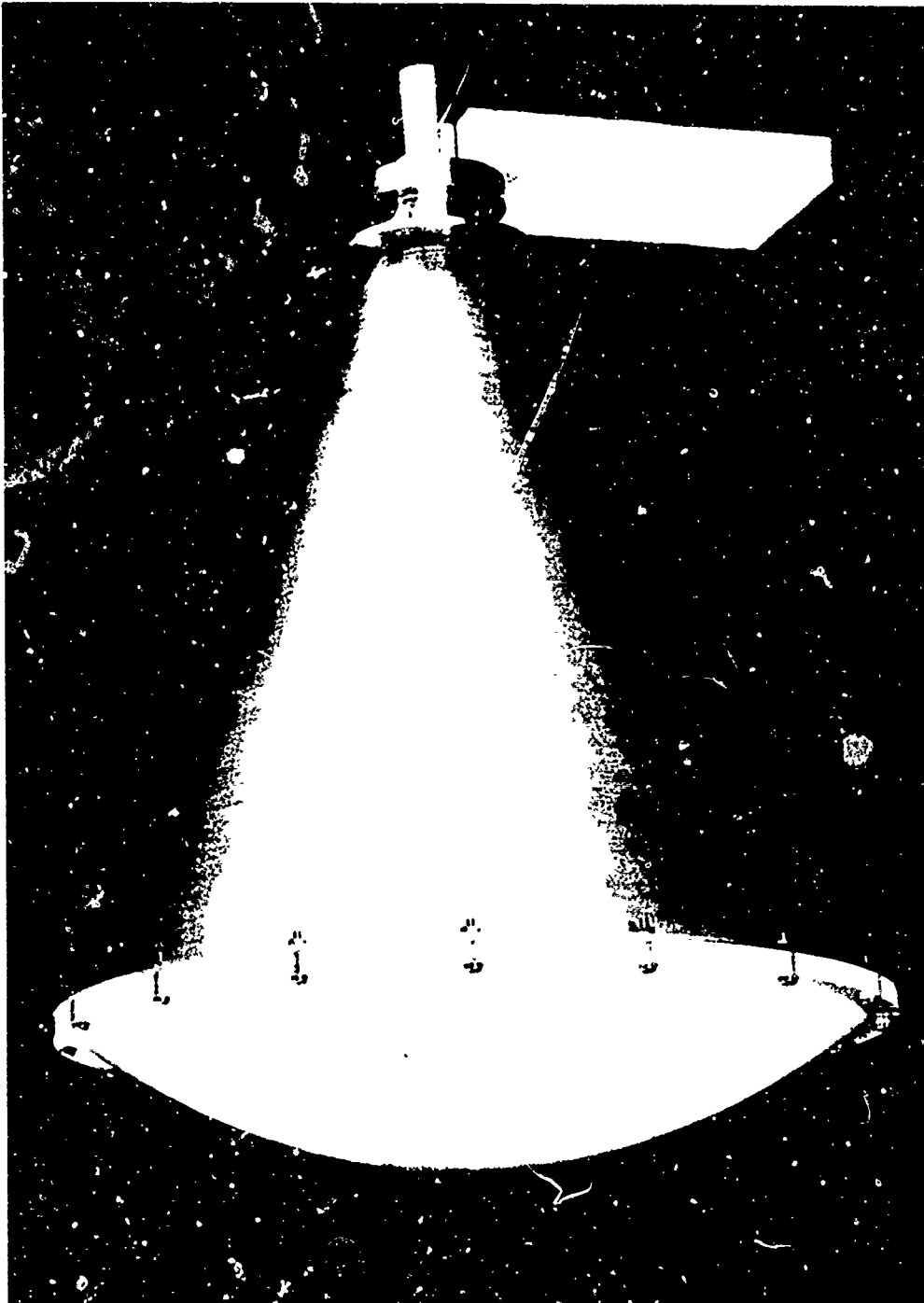


Figure 1. Lens-Corrected Horn Antenna

tolerances out of blanks of cross-linked styrene material which has excellent electrical and mechanical properties.

Surface-matching layers were designed for the purpose of reducing reflections from the lens at the air-to-dielectric interface and are discussed in section III. These layers are nominally one quarter wavelength in thickness and did reduce the reflected transmission losses. The maximum measured improvement is 0.4 dB for the high gain elements when using a layer on each lens surface. The addition of matching layers had little effect on the patterns and side lobes.

Details of the horn antenna design are covered in section IV. Included are the design of the conical horn and the rectangular to circular waveguide transitions. The design allows the rectangular waveguide inputs to be changed so that different frequency bands can be covered. Transitions for the 18- to 26.5-GHz and the 26.5- to 40-GHz waveguide sizes were made and tested. The predicted element performance is treated under this section and in the referenced appendices. The maximum element aperture efficiency was calculated to be 83%.

Detailed analyses of arrays of the large aperture elements were made to determine the expected performance and to evaluate different array configurations. This effort is described in section V. Computer programs were set up to study the effect of element spacings, size, and position with respect to array patterns and side-lobe levels. Physically placing the apertures close together is necessary to minimize side-lobe levels and to maintain high efficiency. The phasing of array elements to achieve beam steering and the limiting factors are also covered.

The experimental results for the individual element and the arrays are given in section VI. Typical element gain at 20 GHz was 39.2 dB or an aperture efficiency of 73%. When matching layers are added to both lens surfaces the aperture efficiency was increased to as high as 81.7% and compares closely to the maximum predicted value of 83%. Array performance followed predicted results for 2 x 2, 4 x 1, and diamond arrangements of the four lens-corrected horn elements. Results show the gain is high but so are side-lobe levels; as a result of the tests, variations in array configurations are suggested to help minimize side-lobe levels.

An added experiment was performed using a laser beam and photographic images of array configurations. This technique for optical simulation is described in section VII. It gives a very graphic presentation of the side-lobe structure as viewed in the plane of an array and is a useful technique for studying array combinations.

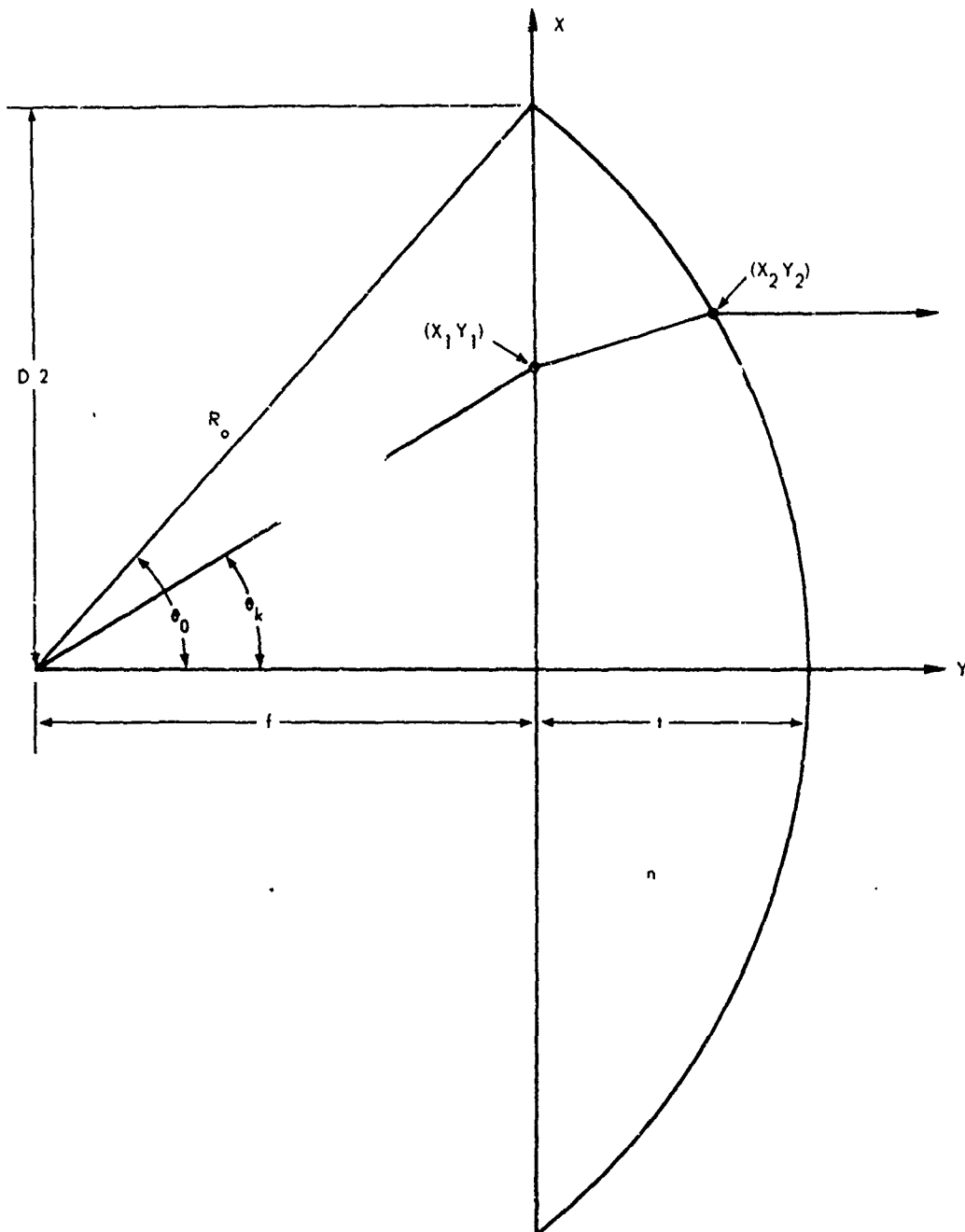


Figure 2. Two-Surface Lens Geometry

## SECTION II

### LENS DESIGN

#### 1. TWO-SURFACE LENS WITH CONSTANT AMPLITUDE

The two-surface lens is one with a constant index of refraction and two refracting surfaces. The previous work performed by J. F. Kauffman (1, 2) solved the problem of designing a two-surface lens with not only a constant phase distribution over the lens aperture but with a uniform amplitude distribution as well. The method of solution computes the nonspherical contours of a dielectric lens for the case of an impinging spherical wave with constant power per unit solid angle. The advantage of a lens providing uniform phase and amplitude distributions when related to a microwave antenna is that the maximum antenna gain and efficiency can be achieved for a given aperture.

The lens design effort was begun with a review of the original computer program. This program was modified by W. V. Goodell and J. Kuhns and rewritten into a more versatile format capable of solutions for different selections of input parameters. These parameters are: index of refraction, lens diameter, total subtended angle from the focus, and thickness of the lens at its center. The output is a common set of tabulated coordinates in X and Y for the two surfaces of refraction. These data provide the information for the fabrication of templates needed to machine the lenses. A copy of the program, written in FORTRAN II for the IBM-360/25 computer, is included in appendix I.

The results obtained in reference 1 indicated that there is a family of solutions to the design of the constant-amplitude lens and that a plano-convex solution to the two-surface lens is possible at a particular index of refraction. This solution is of interest because of the lower cost of fabricating a plano-convex lens as compared to a doubly curved lens. The family of lens solutions varies from double-convex to plano-convex to concave-convex lenses with increasing dielectric constant lens material.

The geometry of the two-surface lens is as shown in figure 2. Series of lens parameters were put into the computer for indices of refraction ( $n$ ) from 1.585 to 1.789 and for total angles subtended by the edges of the lens ( $2\theta_0$ ) from the focal point varying in  $3^\circ$  steps from  $30^\circ$  to  $60^\circ$ . The lens diameter was selected to be 20 inches at the point where the lens thickness

becomes zero. Although the lens-corrected horn apertures under this contract are expected to be 18 inches, the 20-inch diameter was chosen for typical calculations to allow for sufficient mounting flange thickness at the edge of the lens. The results of the computations are summarized in figure 3. It is seen that the first lens surface is convex through an index of refraction of 1.719 but becomes concave, as evidenced by the negative numbers, at an  $n$  of 1.789. By interpolation, the plano-convex solution occurs for a lens material having an index of refraction of 1.757.

A lens material adjusted to the correct index of refraction for a plano-convex solution to the constant amplitude lens would have to be very accurately controlled. Homogeneity of the material would also be a factor because of significant changes in computed lens thickness for small changes in dielectric properties. A very desirable material for use in making lenses is cross-linked styrene. This material has been used successfully in the fabrication of operational lenses and has the following properties:

Dielectric constant	=	2.530
Index of refraction	=	1.590
Loss tangent	=	0.00066 (at 10 GHz)
Specific gravity	=	1.05
Coefficient of linear thermal expansion	=	$7 \times 10^{-5} / ^\circ\text{C}$

It is available under the trade name of Rexolite 1422. The dielectric constant and loss tangent of this material are very stable throughout the frequency range of interest.

The design parameters for a constant-amplitude, two-surface lens were computed for the cross-linked styrene material. The subtended angle from the focus ( $2\theta_0$ ) was chosen as  $45^\circ$ ; the reasons for choosing this angle will become more apparent in later discussions on reflections from the lens surfaces. A plot of the curvature of this lens, given in figure 4, is from the data output derived in appendix I. It can be seen that the lens is double convex, having a maximum thickness of 3.371 inches while the departure from a plane first surface is 0.361 inches.

INDEX OF REFRACTION	TOTAL ANGLE SUBTENDED BY LENS FROM FOCUS	MAXIMUM LENS THICKNESS (INCHES)	DEPARTURE FROM PLANE FIRST SURFACE (INCHES)
1.590	30°	2.231	.245
	45°	3.371	.361
	60°	4.542	.468
1.600	30°	2.194	.227
	45°	3.315	.333
	60°	4.466	.432
1.719	30°	1.831	.045
	45°	2.767	.064
	60°	3.727	.074
1.789	30°	1.669	-.036
	33°	1.838	-.040
	36°	2.007	-.046

Figure 3. Departure from a Plano First Lens Surface versus Parameters of a 20-inch Diameter Lens

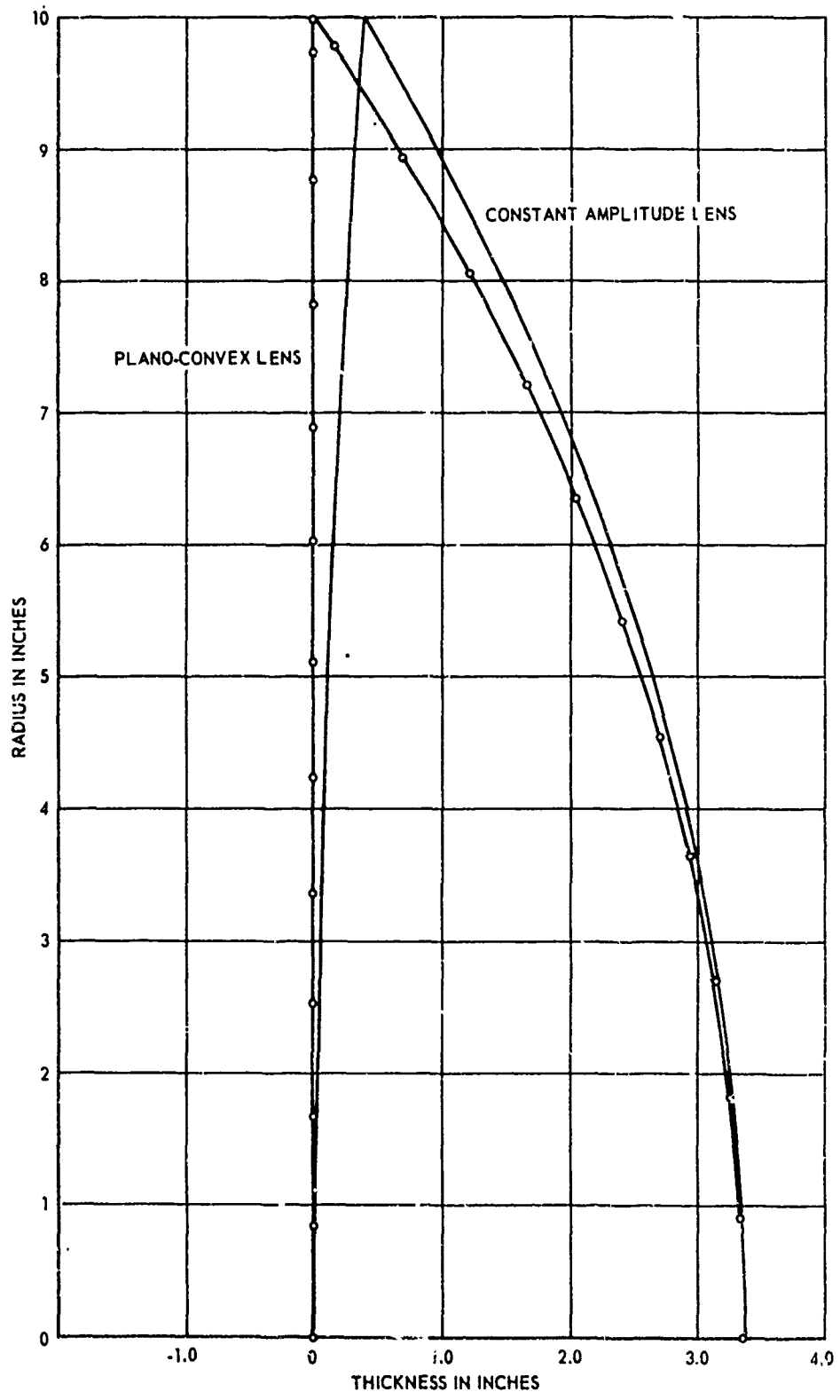


Figure 4. Contour Plot of Constant-Amplitude and Plano-Convex Lenses

The question naturally arises as to what effect a plano-convex lens has on the aperture distribution and the resultant antenna performance. Because of the advantages in lower fabrication costs, this subject is explored in the next paragraphs.

## 2. TWO-SURFACE PLANO-CONVEX LENS

A new computer program was written for a plano-convex lens using the same input parameters as for the previous lens design. This program is based upon the design solutions given in chapter 11 of reference 3, and chapter 14 of reference 4. The analysis of the problem, the computer program, and a set of lens coordinates are given in appendix II. The plot of the lens curvature is given in figure 4, and can be compared to that for the constant-amplitude design. The maximum thickness is identical, 3.371 inches, which means that the weight and the materials cost of the two designs are the same.

Both lens design solutions are basically accomplished by a ray-tracing method which means that, in the case of the constant amplitude design, equal angular increments beginning at the focus will emerge from the lens equally spaced. Hence, the constant amplitude condition is proven. By analyzing the change in spacing for the emergent rays of the plano-convex solution, the amplitude distribution can be determined as explained in appendix II. Figure 5 shows the plots of the amplitude distribution across the aperture of each type of lens. As can be seen, the variation in amplitude introduced by the plano-convex lens design is only 0.74 dB. It is noted that the calculated amplitude increases toward the outer edges of the lens and is caused by closer spacing of the emergent rays. This increase in amplitude can be expected to compensate slightly for the amplitude taper expected in an actual antenna and feed.

The effect of the theoretical increase in amplitudes on the antenna gain and side-lobe levels is considered to be negligible. Approximate calculations indicate that the effect on antenna gain caused by an amplitude distribution tapering by 0.74 dB is less than 0.01 dB. On the basis of the design analysis and of previous successful uses of similar lenses, it was decided to fabricate lenses using the plano-convex design for the experimental studies. The plano-convex design also has advantages when used with quarter-wave matching layers as will become evident in later discussions.

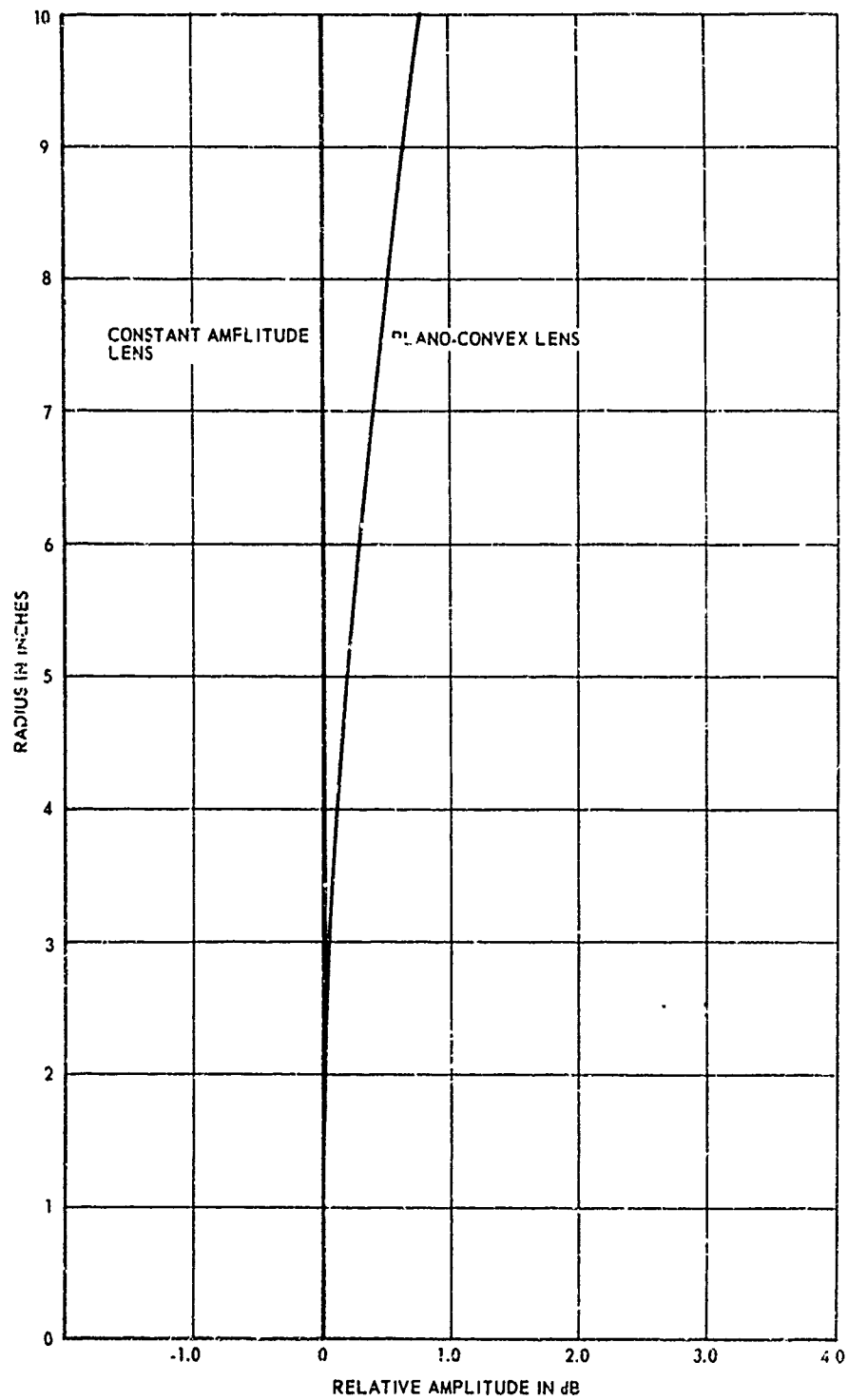


Figure 5. Comparison of Amplitude Distributions versus Aperture Radius

### 3. LENS FABRICATION AND TOLERANCES

Four plano-convex lenses were machined for experimental evaluation of single elements and different array combinations. The refracting diameters of these lenses are 18.00 inches with a 0.75-inch-wide by 0.50-inch-thick mounting flange, giving an overall diameter of 19.50 inches. The flange width was determined to be the practical minimum for attaching to the horn flange and for permitting alignment adjustments. To obtain the lens contours and to allow the half-inch flange thickness, it was necessary to calculate the lens for a 48° total subtended angle with a lens radius (at zero thickness) of 9.689 inches. The resulting lens thickness is 3.493 inches at the center of the lens. The actual weight of the lens is 20.25 pounds.

The fabrication tolerances on the X and Y coordinates of the lenses were held to  $\pm 0.005$  inches. This is only  $\pm 0.013$  wavelengths at 30 GHz and is much less than the usual one-sixteenth wavelength criteria ( $\pm 0.025$  inches) which is frequently allowed. One of the advantages of the lens antenna is the ability to hold close tolerances and thereby minimize losses due to phase error effects.

The lens also offers advantages in surface tolerances over those of a paraboloidal (dish) antenna by nature of its principle of operation. This problem has been treated in reference 1. Interesting comparative results can be obtained by considering the case for relatively small angles of incidence and a surface tolerance of  $\Delta T$ . Taking the example of a lens with an index of refraction  $n = 1.590$ , the path length difference through the lens is:

$$\Delta L_l = (n - 1) \Delta T = 0.59 \Delta T$$

For a reflector, the path length difference is:

$$\Delta L_r = 2 \Delta T$$

This is true because the surface error occurs for both the incident and the reflected ray. For an equal surface tolerance,  $\Delta T$ , in both the reflector and the lens, the following relation holds:

$$\Delta L_r = \frac{2 \Delta L_l}{.59} = 3.4 \Delta L_l$$

Thus, for a given surface tolerance, the corresponding path length or phase error for a reflector is 3.4 times that for the lens. In other words, the allowable fabrication surface tolerance for a lens is 3.4 times greater than that for a reflector for an equivalent phase error.

## SECTION III

### SURFACE-MATCHING LAYERS FOR LENSES

#### 1. DISCUSSION OF THE PROBLEM

The use of matching layers to reduce reflection losses from dielectric-to-air interfaces has been used in various forms for many years. Coated optical lenses, quarter-wave impedance-matching transformers, and matching layers for microwave lenses all use the same principle. There were several possible approaches which could have been used to evaluate the effects of the matching layers on lens performance. One approach is to use artificial dielectric techniques and make lenses with and without these layers as part of the lens. For instance, machined grooves in the lens surfaces could provide the artificial dielectrics of the desired dielectric constant and thickness. At frequencies of 20 or 30 GHz such grooves become very small, expensive, and fragile, and could not be removed from the lenses for other measurements. It was decided to make separate layers of an intermediate material which could be applied and removed from the lenses as desired for accurate performance comparisons.

A study of the literature on surface matching of lenses revealed a small number of references with limited experimental results published. References 4 (pages 14-12 to 14-21), 5, 6, 7, 8, and 9 give the basic analytical information needed.

References 5 and 6 are essentially the same article, and references 5, 6, 7, and 8 are summarized in reference 4, pages 14-12 to 14-21. Reference 9 contains the results of some additional work by Cummins and by Collin plus that presented in references 5, 6, 7, and 8. Much of the effort described in these references relates to the use of artificial dielectric layers made by removing part of the base material or by use of embedded metallic obstacles. Theoretical analysis is complete, although the experimental results are not sufficient to evaluate the present design application.

Typical values of reflection coefficients versus angles of incidence at the air-to-lens interfaces are given in reference 4, pages 14-12 to 14-21. Examples of the effect of quarter-wave matching of surfaces are also given. The plots of reflection coefficient show that polarization perpendicular to the lens surface reflects more energy than polarization parallel to the lens surface. This difference is more pronounced as the angle approaches the Brewster angle, which is

approximately  $55^\circ$ . Thus, there is more uniform amplitude distribution for E and H planes and less forward scattered energy with lower values of the angle of incidence.

Addition of quarter-wave matching layers greatly reduces the reflections at the air-to-lens interfaces for both polarizations. Here, again, the improvement is greatest at values of incidence angles less than approximately  $20^\circ$ . Thickness of the quarter-wave layer is also more nearly constant for the smaller angles.

The magnitude of the reflected energy from the lens-to-air interfaces is dependent upon the dielectric constant of the lens material. The cross-linked styrene material has a K of 2.35. With conventional wave propagation formulas it can be determined that the mismatch at each surface equals a reflection coefficient of 0.228 or a 0.23-dB reflection at normal incidence. The condition for maximum reflection between the first and second surfaces can result in a maximum loss of 0.91 dB. However, this value will vary because of the differences in lens thickness, and numerous sinusoidal fluctuations can occur across the aperture. In both references 1 and 4 (pages 14-12 to 14-21) an average total reflection loss of 0.5 dB is derived.

The use of quarter-wavelength-thick layers means that the frequency bandwidth for elimination of reflections is limited. It is a slowly varying function which optimizes at one-quarter wavelength and is a minimum at one-half wavelength thickness (or multiples thereof). However, at a thickness of one-half wavelength the matching layer has no beneficial action and reflections are the same as if no layer were present. Thus, the matching layer reduces reflections or offers no detrimental effects over a frequency bandwidth of greater than one octave. This fact assumes that the dissipation losses are negligible, and that is a reasonable assumption for materials whose loss tangent is low. In reference 1, the total calculated lens loss for a material whose loss tangent is 0.001 is approximately 0.2% and is, therefore, negligible.

Under the present study there are advantages to be derived in the use of the plano-convex lens having two refracting surfaces over the single-surface lenses used in the referenced articles. The first advantage is the fact that the double-refracting lens has the plane surface toward the feed rather than the curved surface as in the case of single-refracting surface lenses. This means that the angle of incidence is reduced by approximately one-half, and, consequently, the reflected energy is greatly reduced.

A significant factor discussed in reference 8 was the reflections between the horn walls and the lens, especially at the edges of the lens where the angles of incidence are greatest. This condition is alleviated by the present design and did not show up in the experimental results. Secondly, there is no lens surface of constant phase to reflect energy back into the system in one direction or have an appreciable effect on input VSWR. Finally, the total included angle of 45° was chosen for horn design, and results in a maximum angle of incidence of 22.5°. Thus, the matching layer parameters fall on the flattest portion of the design curve and a uniform, homogeneous material can be used.

## 2. THEORETICAL DESIGN

The design of the thickness and dielectric constant of the matching layer may be determined by using the explanation found in reference 9. It is well known, from the theory of propagation and reflection of waves, that quarter-wave-thick matching layers can be used to cancel reflections from dielectric interfaces if the matching layer has a dielectric constant of:

$$K_2 = \sqrt{K_1 K_3} \text{ and } t = \frac{\lambda_0}{4 \sqrt{K_2}}$$

where  $K_1$  = Dielectric constant of 1st material, for air = 1.0

$K_2$  = Dielectric constant of the matching layer

$K_3$  = Dielectric constant of the 3rd material, for lens = 2.53

$t$  = Thickness of the matching layer

$\lambda_0$  = Wavelength in free space.

The above criteria holds only for normal incidence of the wave onto the dielectric material. For a lens with  $K_3 = 2.53$  in air, the matching layer should have a value of  $K_2 = 1.590$  and  $t = 0.117$  inches at 20 GHz, or  $t = 0.078$  inches at 30 GHz.

For angles of incidence greater than  $0^\circ$ , the wave impedances for a plane wave in air incident upon the lens is:

$$Z_1 = \frac{Z_0}{\sqrt{1 - \sin^2 \theta_1}}$$

where  $Z_0$  is the intrinsic impedance of free space and  $\theta_1$  is the angle of incidence relative to the interface normal. The wave impedances for this plane wave in the matching layer and the lens are, respectively:

$$Z_2 = \frac{Z_0}{\sqrt{K_2 - \sin^2 \theta_1}} \quad \text{and} \quad Z_3 = \frac{Z_0}{\sqrt{K_3 - \sin^2 \theta_1}}$$

A quarter-wave transformer that will match the lens to free space without reflections is obtained if  $K_2$  is so chosen that  $Z_2 = \sqrt{Z_1 Z_3}$  and the thickness,  $t$ , of the layer equals  $\lambda_g/4$ . The wavelength in the matching layer is.

$$\lambda_g = \frac{\lambda_0}{\sqrt{K_2 - \sin^2 \theta_1}}$$

From the above requirements, the dielectric constant  $K_2$  is given by:

$$K_2 = \sin^2 \theta_1 + \cos^2 \theta_1 \sqrt{K_3 - \sin^2 \theta_1}$$

and the thickness of the layer is given by:

$$t = \frac{\lambda_g}{4} = \frac{\lambda_0}{4 \sqrt{K_2 - \sin^2 \theta_1}}$$

It is apparent that both the thickness and the dielectric constant of the matching layer are a function of the angle of incidence upon the lens surfaces. Calculations to determine the amount and the significance of the variations in  $K_2$  and  $t$  are required for the practical application and are given in the following paragraphs.

### 3. DESIGN CALCULATIONS AND FABRICATION

The thickness,  $t$ , and the dielectric constant,  $K_2$ , of the matching layer for the present lens design have been calculated. The lens has a dielectric constant of  $K_3 = 2.53$  and a maximum angle of incidence of  $22.5^\circ$  on the feed side of the horn. The angle of incidence of plane wave incident upon the curved surface of the lens reaches a maximum of  $30^\circ$  at the outer edges of the lens. The calculated thickness in free-space wavelengths and the dielectric constant are shown in figures 6 and 7 as a function of the angle of incidence.

The actual thickness of the matching layers for 20 and 30 GHz are plotted in figure 8. It can be seen from the graphs that, by designing the lens for low angles of incidence, the matching layers are very nearly constant in thickness and in dielectric constant.

Calculations were made for the actual thickness of a matching layer having a dielectric constant of 1.60 instead of the varying theoretical values shown in figure 7. This was done to determine any deviations that might occur through the use of homogeneous material in constructing the matching layers. The results showed that the thicknesses for the 20-GHz and 30-GHz layers were nearly identical to the calculated values given in figure 8 out to an angle of incidence of  $30^\circ$ . The maximum deviation was only -0.002 inches at  $30^\circ$  although the difference becomes greater as the angle of incidence increases.

It was concluded that a homogeneous material could be used and that a constant thickness layer, for all practical purposes, would satisfy the design criteria over the angles of incidence encountered. The material which was chosen to make the matching layers is a polystyrene foam whose density is adjusted to give a dielectric constant of  $1.60 \pm 0.02$ . This material is available from Emerson and Cumming, Inc., as ECCO FOAM PS in standard sheet sizes of 1 x 18 x 30 inches. Two sheets were machined to a thickness of 0.120 inches as designed for operation at 20 GHz. One sheet was cut into pieces and applied with adhesive to the curved surface of a lens, as illustrated in figure 9. The second sheet was flat and was attached or removed from the flat sides of the lenses to obtain comparative data.

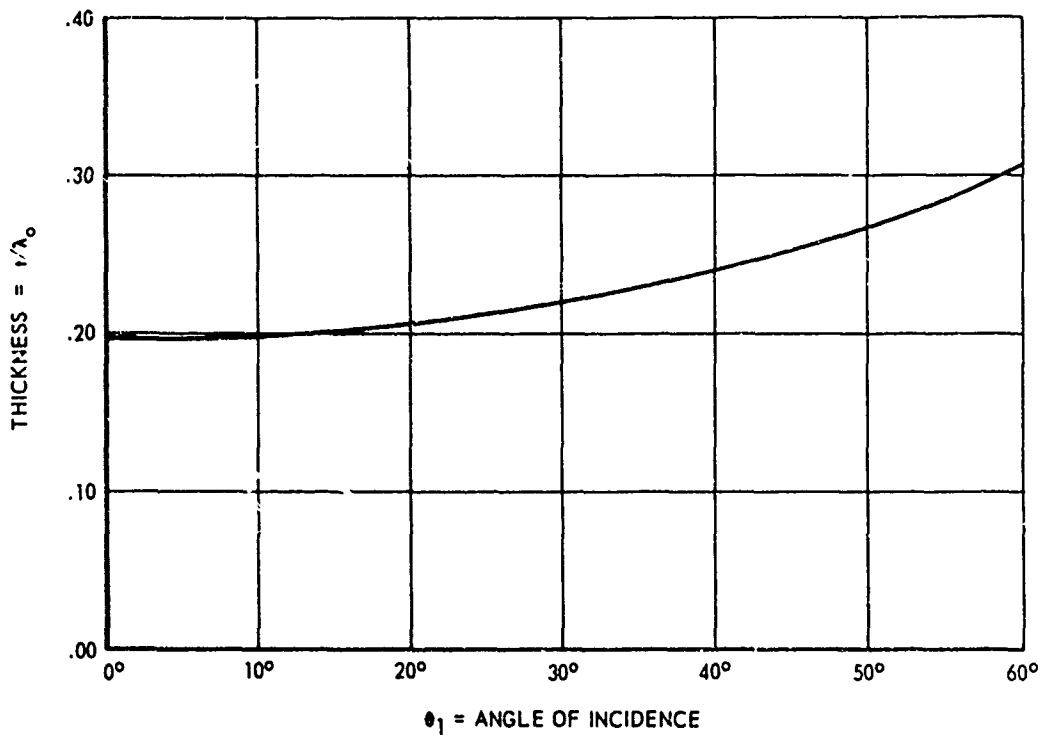


Figure 6. Calculated Matching Layer Thickness

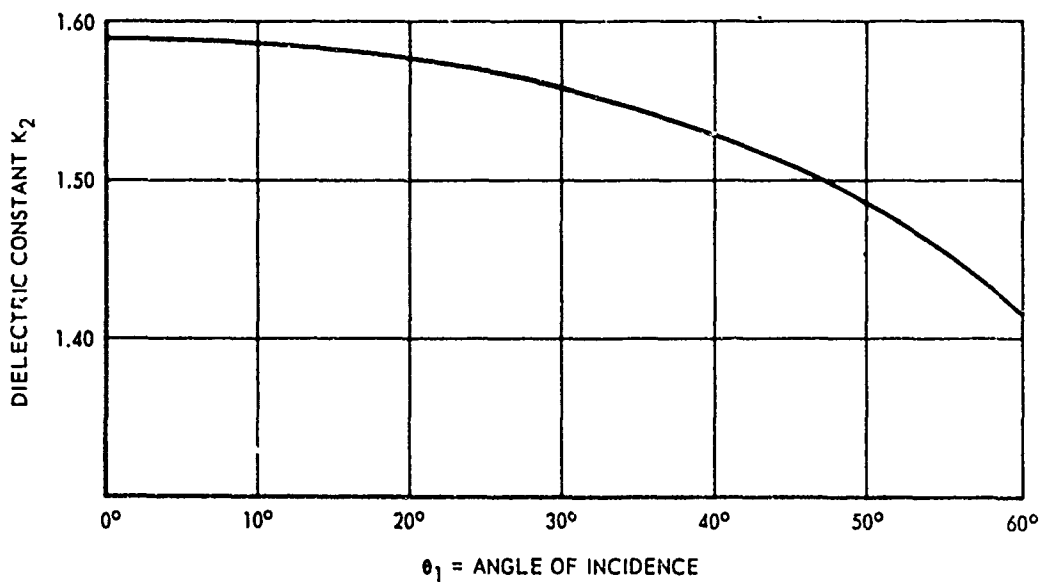


Figure 7. Calculated Matching Layer Dielectric Constant

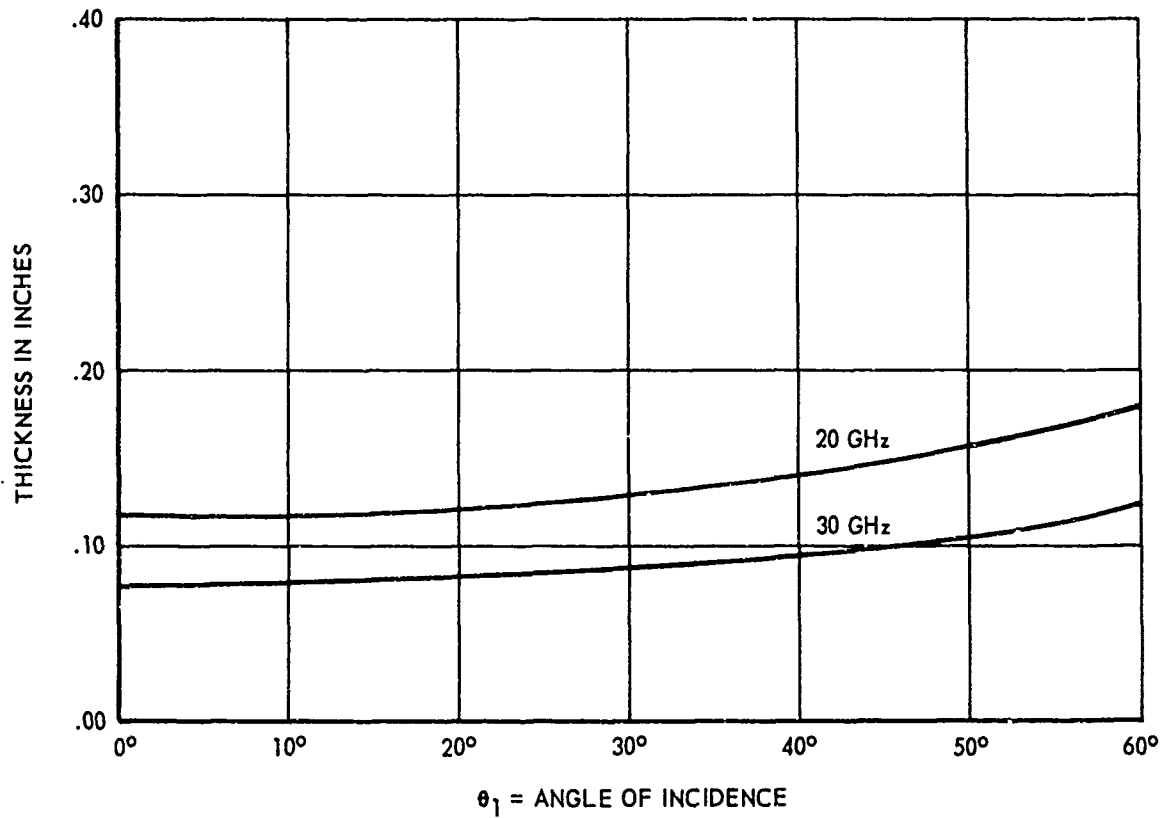


Figure 8. Matching Layer Thickness for Two Frequencies

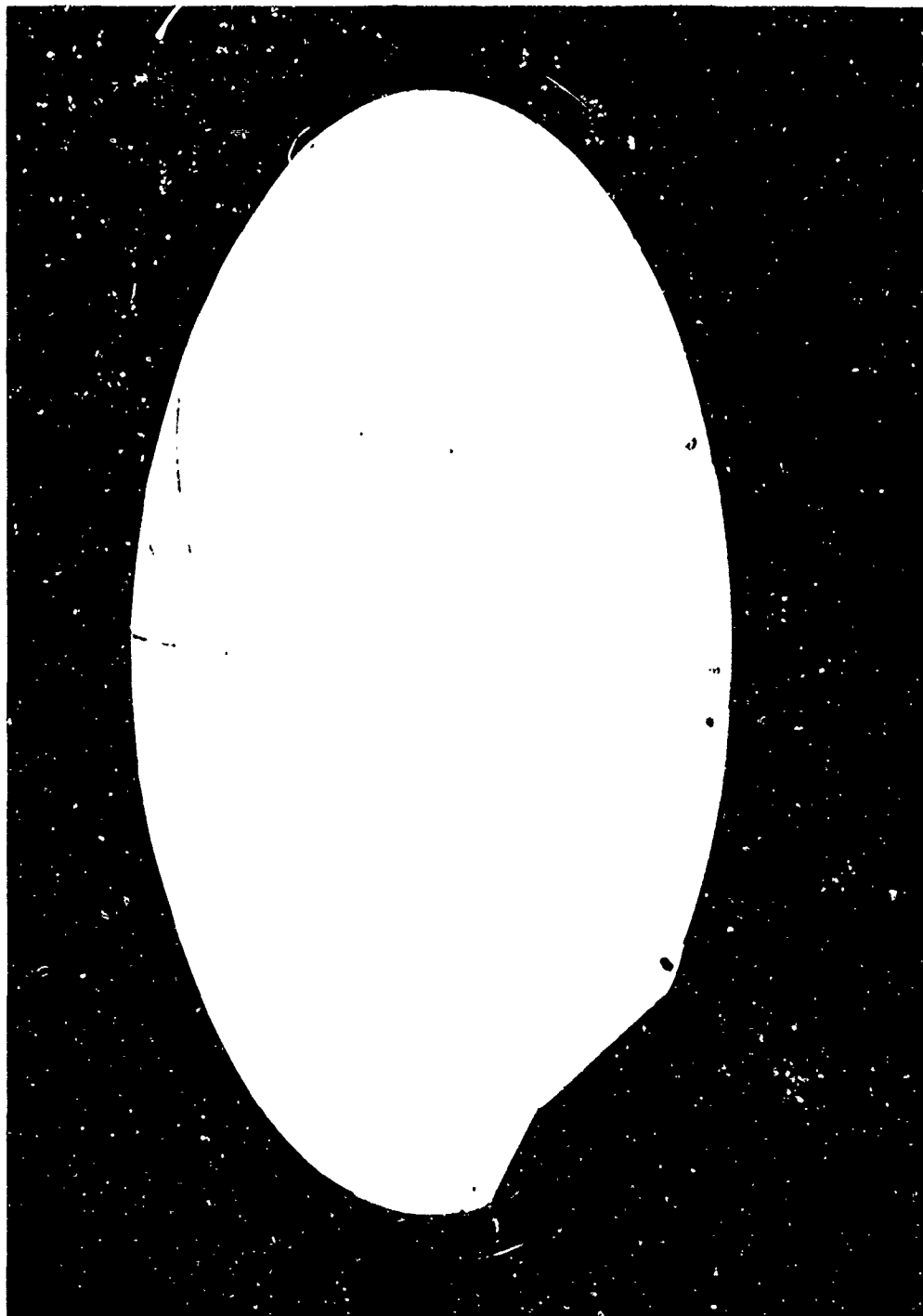


Figure 9. Plano-Convex Lens with Matching Layer Applied

## SECTION IV

### HORN ANTENNA DESIGN

#### 1. GENERAL DESIGN DISCUSSION

The lens-corrected horn antenna as illustrated in figure 1 offers several potential advantages, especially in the 12- to 60-GHz frequency range. As discussed in section III, the lens has a 3.4-to-1 advantage over a parabolic dish with respect to surface tolerances for equivalent performance, and this is significant at the higher frequencies and shorter wavelengths. The lens-horns do not suffer from the spillover losses of conventional parabolic dishes, nor do they have the aperture blockage problem by the feeds.

A horn with an electrically large aperture is an efficient antenna but would have to be very long. The lens enables the horn to be shortened by correcting the phase of the wavefront. The aperture distribution for the lens-corrected horn is such that its aperture efficiency is much higher than reflector or array type antennas, and the phase corrections by the lens allows this high efficiency to be maintained. The lenses are designed on the basis of geometrical optics and are basically frequency-independent devices. The lens-horns have very low wide-angle side-lobe and back-lobe levels by virtue of the enclosed structure. Being a closed structure, the lens-horn has its own built-in radome against environmental conditions.

The design of the horn is dependent upon the lens design and vice versa. Difficulty occurs when one attempts to make a horn that is too short, because the phase curvature across its aperture is greater and the amplitude distribution is altered. The lens corrects for the phase front curvature; but as the horn becomes shorter the lens becomes thicker, the angles of incidence at the edges of the lens are greater, and there are more reflections off the lens which affect the antenna side lobes and gain. A total included horn angle of  $45^\circ$  was chosen as being a good compromise between angles of incidence at the lens surfaces and the length of the horn.

The gain of the antenna and its aperture efficiency are dependent upon the phase and amplitude distributions across the aperture. The phase is corrected by the lens, but the amplitude is primarily affected by the conducting walls of the horn. The amplitude is essentially uniform in the E plane of the horn, but tapers to zero in the H plane because of the boundary conditions for a parallel

electric field. The predicted antenna performance based upon both calculated values and measured data is covered in detail in paragraph 2 of this section. The design of the replaceable feeds for the horn and the mechanical design features are discussed in paragraph 3 of this section.

## 2. PREDICTED ANTENNA ELEMENT PERFORMANCE

The antenna patterns of rectangular and circular apertures are available in pages 2-25 to 2-30 of reference 4 and pages 182 to 195 of reference 3. The calculated values relate antenna beamwidths, side-lobe levels, and relative gain to various amplitude distributions across the apertures. Rectangular apertures may be treated as separable functions where the antenna pattern in each principal plane is that of the line source distribution for that plane. Circular apertures are calculated by integrating the field in the aperture plane over polar coordinates, but are usually treated as having circularly symmetric amplitudes. As the amplitude distribution across the apertures becomes more and more tapered from the uniform case, the beamwidth broadens, the side lobes become lower, and the gain reduces. The side-lobe levels of a uniformly illuminated circular aperture are -17.6 dB from the beam peak, while those of a rectangular aperture are -13.2 dB. This is apparent if the projection of the circular aperture illumination is made onto a line, producing an equivalent line source which is no longer uniform but has some degree of tapering. The antenna patterns for all large apertures are normalized by the factor  $\lambda/D$  (wavelength over diameter), so that no change in side lobes occurs for larger or smaller apertures in terms of wavelengths. The angular spread of the pattern is all that changes, assuming uniform phase characteristics and equivalent tolerances.

A significant factor in determining the theoretical gain or efficiency of the lens-horn antenna is the fact that its E- and H-plane amplitude distributions are different from each other. These electric field distributions are also characteristic of the E and H planes of rectangular waveguide horn antennas. Field probing measurements were made to verify and demonstrate the characteristic E- and H-plane amplitudes across the circular aperture of the lens-horn. A detailed discussion and a determination of the theoretical aperture efficiency as compared to a uniformly illuminated circular aperture is given in appendix III.

It is concluded that the aperture efficiency of the lens-corrected horn based upon its characteristic distribution is 93%. This represents a loss of 0.8 dB from a 100% efficient or uniformly illuminated aperture. The difference between the maximum computed efficiency and the measured antenna gain becomes

a problem of accounting for the differences between the maximum theoretical gain and the measured value, and correcting for them, if possible. The other loss factors to which a reduction in efficiency can be attributed are as follows:

- a. Phase errors, which are minimized by the accuracy of the lens construction.
- b. Cross polarization, which has been measured as -38 dB and is considered negligible.
- c. Reflection losses, for which the quarter-wave matching layers provide answers.
- d. Absorption losses, for which calculations given in reference 1 account for approximately 0.1%.
- e. VSWR losses, which can be accounted for or reduced by tuning devices. If the VSWR is 1.36 or less, the maximum mismatch loss is 2.3% or 0.1 dB.
- f. Ohmic losses, which are dependent upon the conductivity of the horn material and are minimal. Feed network losses for an array will be greater and can be measured.

The side-lobe levels predicted for the lens-horn antenna are those of a uniformly illuminated circular aperture in the E plane or a level of 17.6 dB below peak intensity. In the H plane the side-lobe level for the tapered illumination is 24.6 dB below peak intensity. Predicted half-power (3-dB) beamwidths in the E plane should equal:

$$BW = 58.4 \frac{\lambda}{D} \text{ degrees}$$

where  $\lambda$  is the wavelength at the test frequency and D is the aperture diameter and is equal to 18 inches. H-plane beamwidth should equal:

$$BW = 72.8 \frac{\lambda}{D} \text{ degrees}$$

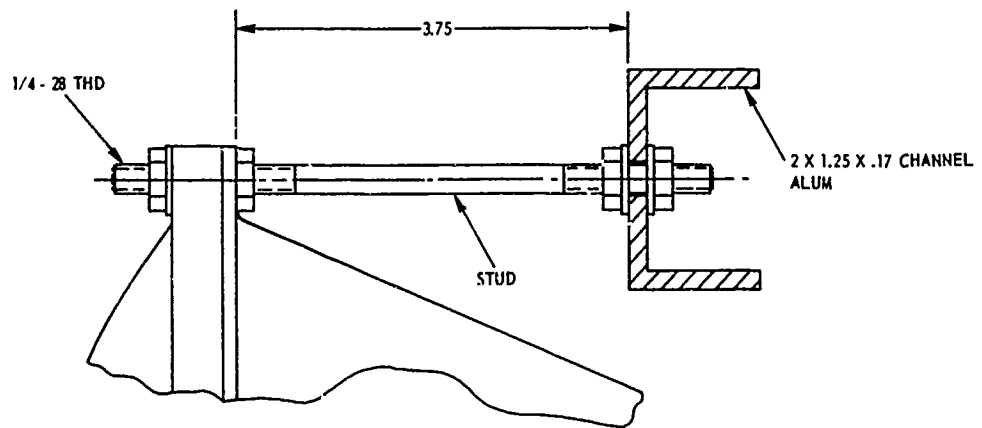
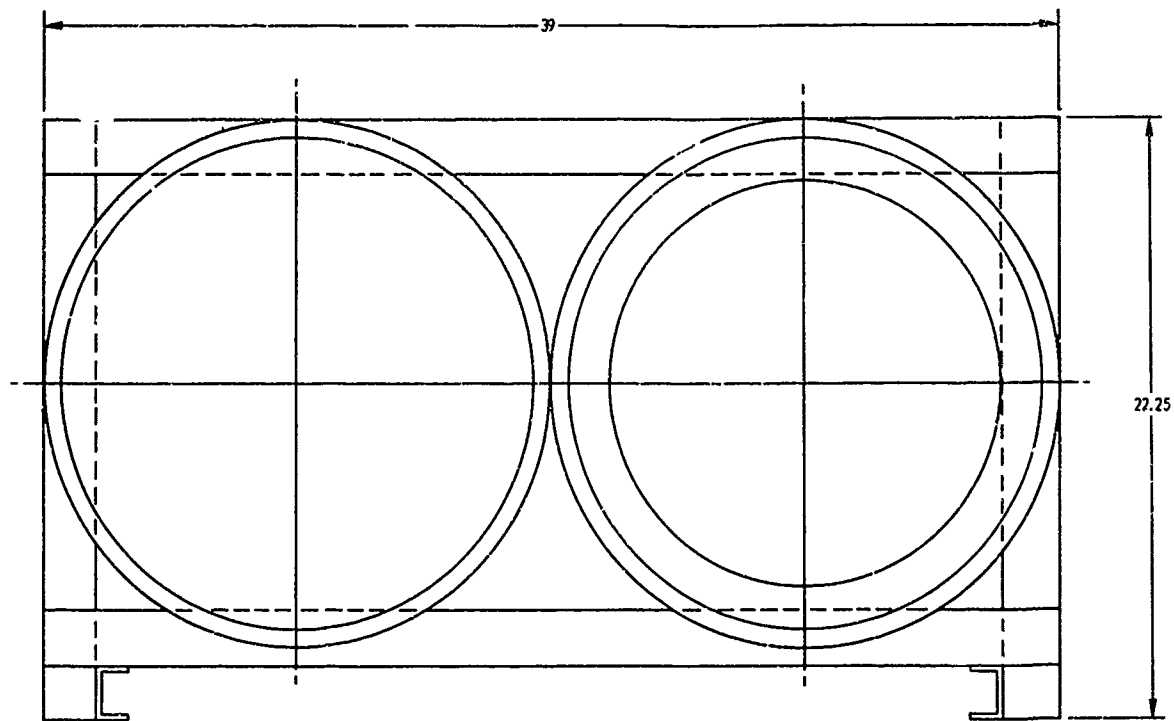
### 3. HORN FEEDS AND MECHANICAL DESIGN

The horn and feed design is illustrated in figure 10. The lens is attached by bolting to the flange of the 45° frustum or spun aluminum horn. A frustum flange is attached to the small end of the 45° frustum and serves as a support mount and as a flange to which feeds are attached. The feed consists of the adapters which can be for the 18- to 26.5-GHz band or the 26.5- to 40-GHz band and the transitions for these respective bands. An adapter is a short section of circular waveguide and the first flared portion of the 45° cone out to an inside diameter of 0.15 inches. The transition transforms from circular waveguide to the rectangular waveguide input.

Several methods for fabricating the 45° frustums or horns were considered, including: (1) spinning, (2) rolling and welding, and (3) fiberglass layup with plated surfaces. The fiberglass layup appears to offer the best control and uniformity of fabrication as well as being light in weight. The fiberglass would be electroplated with copper and a tarnish resistive coating of gold put over the copper. Calculations of skin depth have indicated that a coating of copper one mil thick is sufficient. However, only a few vendors had the capability of plating the fiberglass horns of the size required, and costs for four horns were several thousand dollars which was considered to be excessive. The technique of rolling and welding was also eliminated because of the probability of distortion and lack of symmetry of critical surfaces at the ends of the cones.

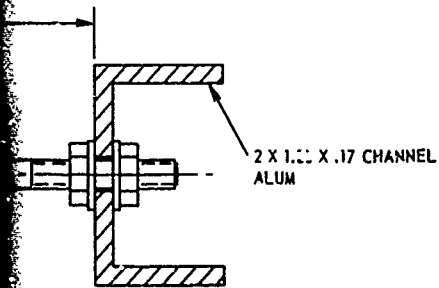
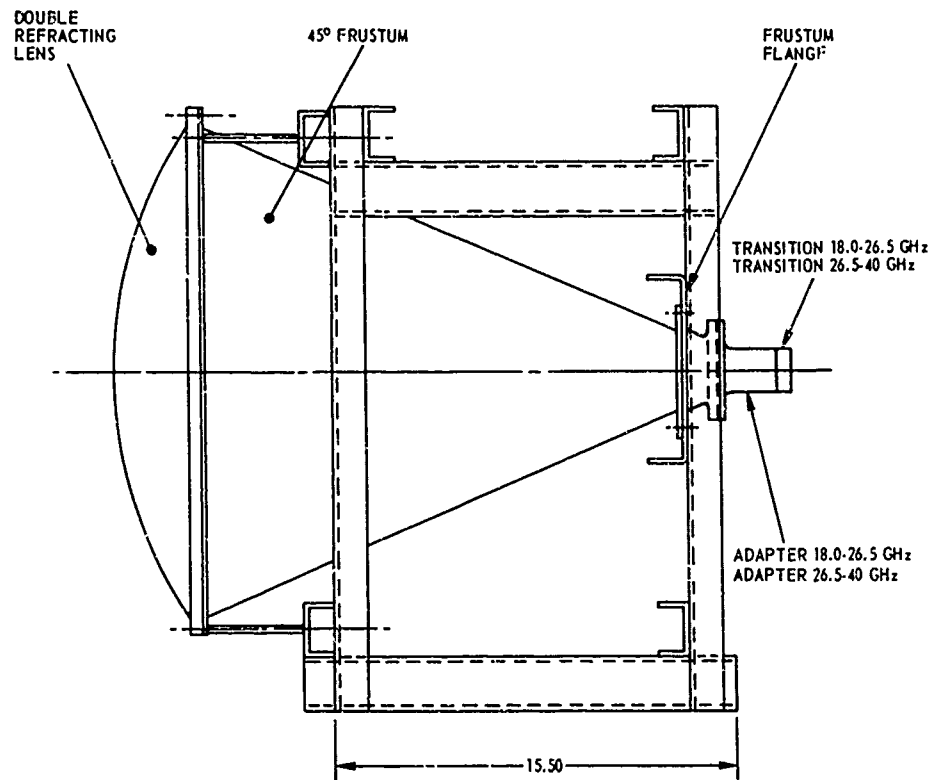
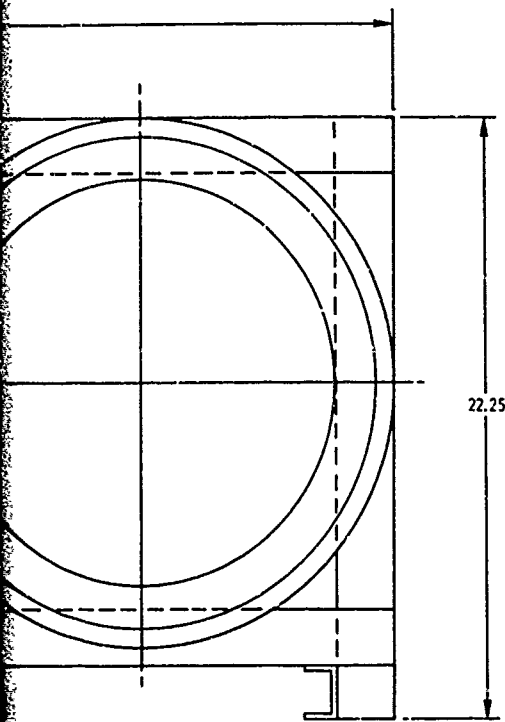
Spinning was then investigated and chosen as the method of fabricating the horns. Prices for four units were less than one thousand dollars, and more manufacturers were available. The spinning process does not lend itself to incorporating a flange on the small end of the horn. Therefore, machined frustum flanges were added, and they serve both as an accurate horn mounting and as a precision surface for attaching the feeds.

The adapters fit onto the frustum flanges and are the first part of the 45° horn, fed by a short section of circular waveguide. The circular waveguide diameters chosen were the same as the width of the rectangular waveguide input feed or equal to: 0.420 inches for the 18- to 26.5-GHz band and 0.280 inches for the 26.5- to 40-GHz band. These sizes are small enough to avoid the propensity for higher-order waveguide modes and sufficiently large to avoid excessive attenuation near guide cutoff frequency.



LENS SUPPORT, 3 PLACES PER LENS

Figure 10



PER LENS

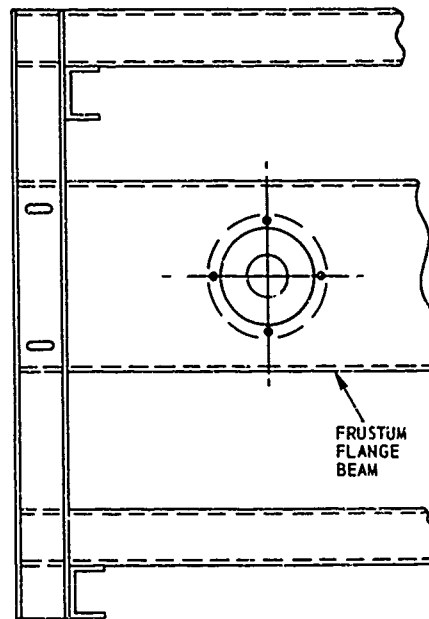


Figure 10. Lens-Horn Configuration and Mounting Structure

The transitions each consist of three quarter-wavelength steps having elliptical cross sections to form a gradual change from circular to rectangular waveguide input. The VSWR of the transitions and adapters are shown in figure 11. Although lower VSWR could be achieved by use of more expensive tapered transitions, the performance was adequate and the configuration was convenient for the experimental measurements. The change from horizontal to vertical polarization was accomplished by unbolting the adapters from the frustum flanges and rotating each adapter with its transition by 90° and refastening.

The weight of each lens-corrected horn element was a total of 27.75 pounds as follows:

Dielectric lens	=	20.25 pounds
Horn and feed	=	7.00
Mounting hardware	=	<u>0.50</u>
Total		27.75 pounds

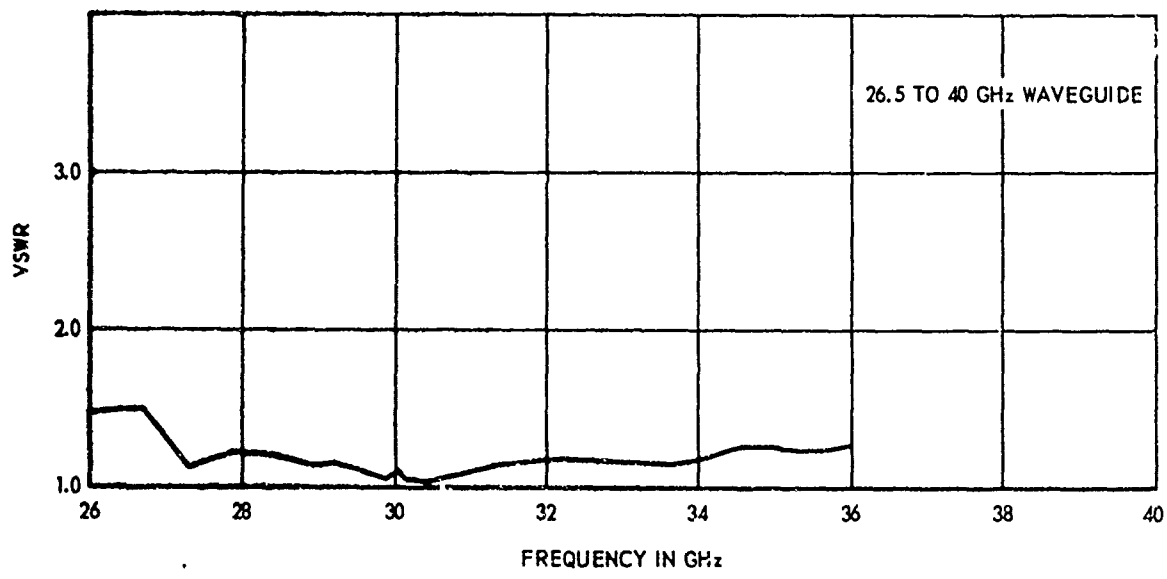
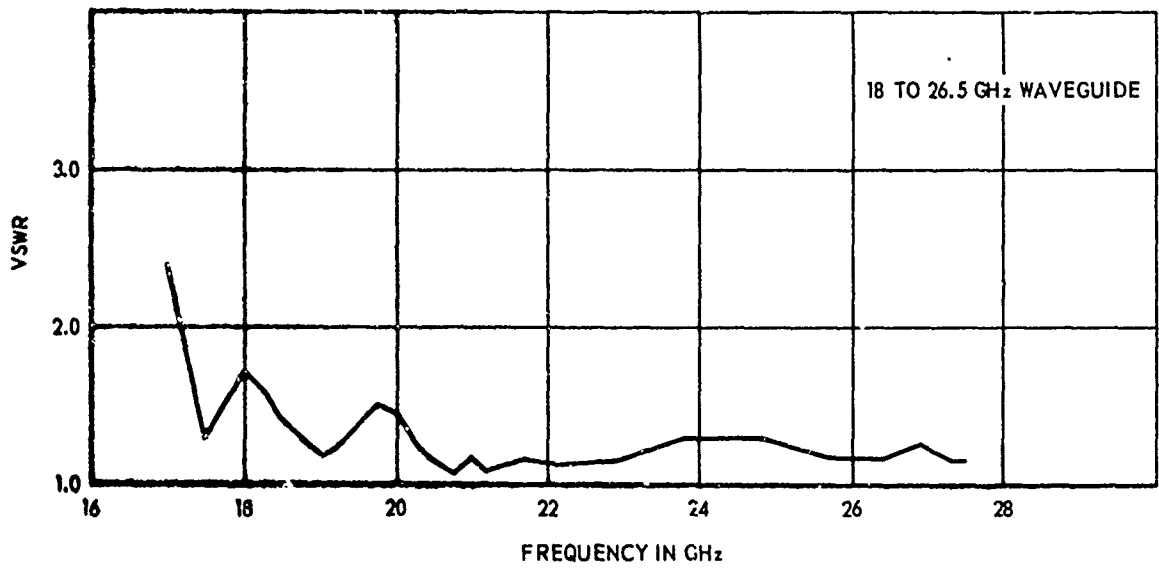


Figure 11. VSWR of Rectangular to Circular Waveguide Transitions

## SECTION V

### ANTENNA ARRAY ANALYSIS

#### 1. ONE-DIMENSIONAL ARRAY DISTRIBUTIONS

Calculations were made with the computer of the secondary radiated patterns of arrays of lens-corrected horn antennas to provide a theoretical basis for the experimental measurements and to predict the optimum design parameters. Variables include the number of elements, the distances between the elements, the size of each aperture, and the amplitude factor of each element.

The pattern of a uniformly illuminated circular aperture was used as the element pattern and was derived as in reference 3. The resulting element pattern function is:

$$g(u) = 2\pi a^2 \frac{J_1(u)}{u}$$

where  $u = \frac{2\pi a}{\lambda} \sin \theta$

$a =$  element aperture radius

$J_1 =$  Bessel function of order one.

The antenna pattern of the element was determined using the 18-inch diameter lens aperture. The actual E-plane measured pattern was found to correspond very closely to the computed pattern, thereby verifying that the expected amplitude distribution and phase correction had been obtained.

A computer program was written for arrays of elements at the outset of the program to verify that the best choice of the number, size, and spacing of elements was made. The capability of using nonuniform amplitude for the array elements was also added to the program. The array patterns,  $F(\theta)$ , were computed for in-phase elements by using the principle of pattern multiplication:

$$F(\theta) = g(\theta) f(\theta)$$

where  $g(\theta) =$  the element pattern factor

$f(\theta) =$  the array pattern factor.

The array pattern factor calculation was based upon the analysis given in reference 11, chapter 4. The equations used and the resulting computer program are given in appendix IV.

This study of array pattern characteristics is somewhat unique because the emphasis is on electrically large apertures. The reason for this is that the lens-corrected horns are used to their greatest advantage when the element apertures are electrically large. The range of values for 18-inch diameter apertures for frequencies between 15 GHz and 60 GHz is from 23 to 92 wavelengths. Element beamwidths will vary from approximately  $3.2^\circ$  to  $0.8^\circ$  and grating lobe spacings will be of similar magnitudes over this range of frequencies. Numerous combinations of the numbers of elements, spacings, amplitude distributions, frequencies, and element diameters were tried using the computer program. Variations in the results of the pattern computations for four uniformly illuminated apertures versus spacing and relative amplitudes are summarized in figure 12. Certain basic characteristics of the arrays can be concluded from the studies that were made:

a. The element spacing in the array determines the angular separation of the grating lobes. The highest side lobes are the first grating lobes and these are the predominant side lobes for all the array configurations.

b. The closer the elements can be located the lower will be the side lobes as a result of the multiplication of the array pattern factor and the element pattern factor.

c. A tight clustering of elements so that the apertures appear to overlap in the plane of the patterns will reduce side lobes. Such arrangements have the effect of decreasing the element spacing and tapering the amplitude distribution across the array.

d. Tapering the illumination of the elements of the array by putting more signal into the center elements has the effect of reducing some of the side lobes. This is sometimes significant, but it offers little improvement for the highest grating lobes and also reduces the efficiency of the array aperture.

e. Computations were run for two to eight elements having diameters totaling a 6-foot-wide array. The high side lobes still occurred because the patterns can be normalized with respect to wavelength over diameter.

SPACING BETWEEN LENS CENTERS	RELATIVE VOLTAGES		HIGHEST SIDELOBES		NOTES
	CENTER PAIR	OUTER PAIR	1st HIGH	2nd HIGH	
20 inches	1.0	1.0	-10.1 dB	-12.5 dB	4" between apertures
19	1.0	1.0	-11.4	-12.6	2" between apertures
18	1.0	1.0	-12.9	-13.1	Apertures touching
9.5	1.0	1.0	-16.7	-19.2	Apertures overlapping
19	2.0	1.0	-11.1	-19.8	2' between apertures tapered amplitude
16	2.0	1.0	-16.7	-26.2	Apertures overlapping tapered amplitude
14	2.0	1.0	-21.9	-23.4	Apertures overlapping tapered amplitude
20	3.0	1.0	- 9.7	-18.5	Binomial taper
20	2.06	1.0	- 9.8	-18.5	Tchebyscheff taper
20	1.43	1.0	-10.0	-17.5	3.1 dB taper

Number of Elements = 4

Aperture Diameter = 18 inches

Frequency = 20 GHz

Figure 12. Calculated Side-Lobe Levels versus  
Four-Element Array Parameters

f. Further investigation of arrangements of elements into a two-dimensional array is indicated with the idea of effectively overlapping the apertures to reduce side lobes. For example, a simple 4 x 4 arrangement of elements may be less desirable than staggered arrangements which permit closer spacing between elements. Also, relocation or elimination of corner elements may prove more effective.

## 2. TWO-DIMENSIONAL ARRAY CONFIGURATIONS

The linear arraying of antenna elements has been studied and the results indicate relatively high grating lobes or side lobes when arraying the electrically large elements. The grating lobe positions and the side-lobe levels are determined by the spacing between elements. In order to make design recommendations for larger arrays for future communication antennas, an investigation of two-dimensional arrays was conducted. Included were different techniques whereby closer spacing can be obtained with a reduction in the side-lobe level.

A method of computing the array patterns of different two-dimensional configurations has been worked out. The patterns of the array are obtained in the conventional manner of calculation: the array-factor patterns and multiplying it by the array-element pattern. To calculate the array factor of a two-dimensional array for a given plane, the phase centers of the array elements are projected into a line in that plane to form a one-dimensional array equivalent for that plane. Where element phase centers coincide on that line, their voltage amplitudes are simply added. The array-factor pattern is then calculated for the one-dimensional equivalent.

In the case of a symmetrical one-dimensional array, the array-factor pattern is, using the geometry of figure 13:

$$E_A = K_0 + \sum_{n=1}^N K_n e^{j\tau_n} + \sum_{n=1}^N K_n e^{-j\tau_n}$$

$$E_A = K_0 + 2 \sum_{n=1}^N K_n \cos \tau_n$$

where  $K_n$  is the voltage amplitude of the  $n^{\text{th}}$  element and

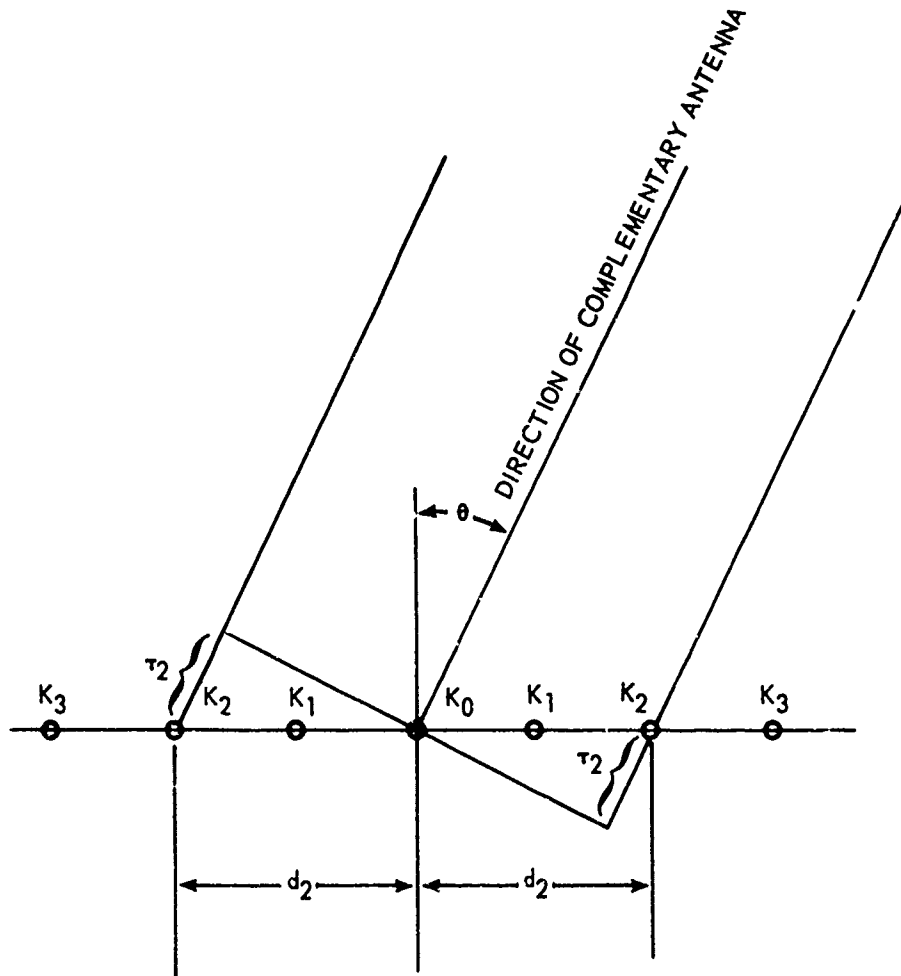


Figure 13. Geometry of Symmetrical One-Dimensional Array

$$\tau_n = \frac{2\pi d_n}{\lambda} \sin \theta$$

If the elements in the "one-dimensional array equivalent" in figure 13 are equally spaced, the pattern equation becomes:

$$E_A = K_0 + 2 \sum_{n=1}^N K_n \cos (n\tau_1)$$

It can be seen from this equation that this array-factor pattern has equal-amplitude maximums at  $\tau_1 = 0, 2\pi, 4\pi$ , etc. When the array-factor pattern is multiplied by the element pattern, the amplitude of the side lobes at the values of  $\theta$  for which  $\tau = 2\pi, 4\pi, 6\pi$ , etc., is down from the peak of the main lobe only as far as the element pattern is down at this angle. These lobes are called grating lobes.

The above method can be accomplished for a two-dimensional array without overlapping element-effective apertures by arranging the element positions so that when projected into a line in the pattern plane the effective apertures of the equivalent array elements are overlapped. This should result in no loss of gain because the collecting aperture area is unchanged.

The 4 x 4 array, composed of 18-inch diameter lens-corrected horns, produced a radiation pattern having an 11.4 dB side lobe when spaced on 19-inch centers. One-half inch was allowed on each horn rim for mounting, which, we believe, is a minimum allowable for mechanical reasons. This 4 x 4 array consists of 16 elements and is illustrated in figure 14, and the calculated principal plane pattern is tabulated in figure 15.

A scheme was devised that produces an array in which the elements are as close together as possible without overlapping. The above procedure was applied to this scheme in order to analyze it as a one-dimensional array.

Figure 16 illustrates this "diamond" array. Calculated patterns were determined at the different "horizontal" cuts which are designated by the letters A, B, C, and D. The numbers beside the circles represent the apparent voltage amplitudes. Figure 15 presents the half-power beamwidth, 10-dB beamwidth, the first null position, and then the first six side-lobe levels with their respective locations from boresight. As can be seen, the highest side-lobe level presented is 16 dB down from the peak amplitude, and other side lobes are also lower than the square array.

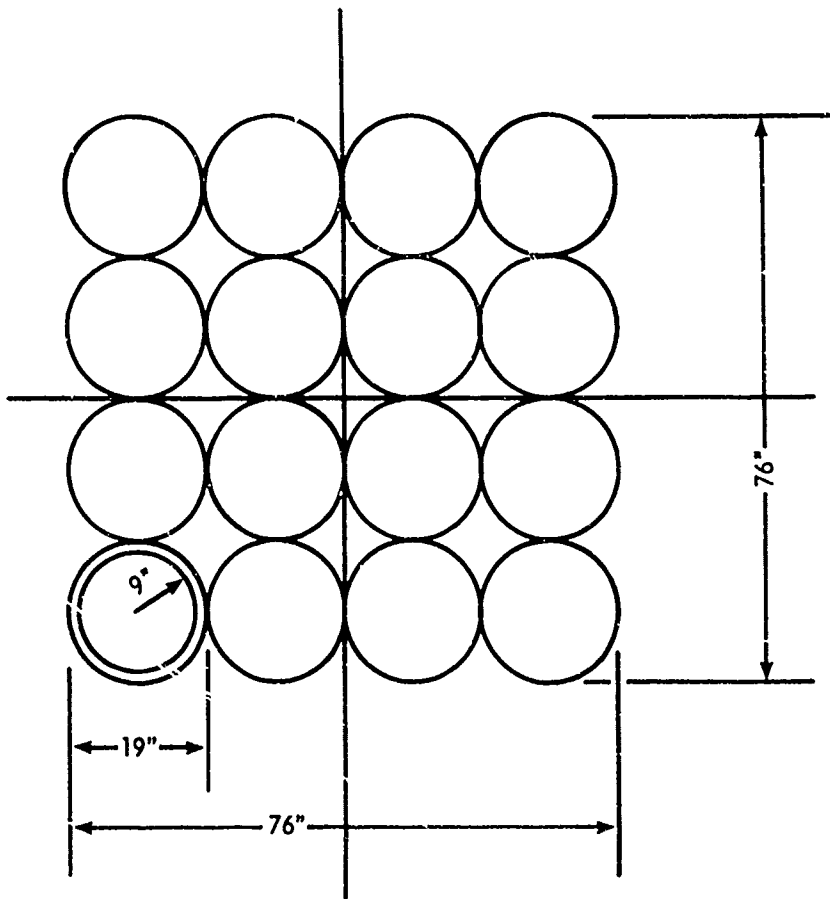


Figure 14. Configuration of 4 x 4 Square Array

CUT NO.	3 dB BW DEGREES	10 dB BW DEGREES	NULL POSITION DEGREES	1ST SIDE LOBE		2ND SIDE LOBE		3RD SIDE LOBE		4TH SIDE LOBE		5TH SIDE LOBE		6TH SIDE LOBE	
				LEVEL dB	POSITION DEGREES										
A	0.53	0.89	0.64	19.3	0.85	28.1	1.65	36.6	2.70	19.7	3.45	41.6	5.3	28.2	7.10
B	0.45	0.74	0.52	16.1	0.70	27.6	1.20	49.1	1.65	32.0	2.85	19.9	3.15	48.6	4.40
C	0.48	0.83	0.55	16.9	0.75	26.4	1.25	16.1	1.8	34.7	2.45	33.3	2.85	33.4	3.30
D	0.43	0.71	0.51	23.3	0.65	20.2	1.00	28.8	2.40	16.9	1.85	38.1	2.40	41.5	2.70

PRINCIPAL PLANE CUT FOR 16 ELEMENT SQUARE ARRAY															
0.40	0.68	0.45	12.6	0.65	15.4	1.10	11.4	1.65	19.9	3.50	24.8	5.30	28.3	7.10	

Figure 15. Calculated Antenna Patterns of 14-Element Diamond Array Compared to 16-Element Square Array

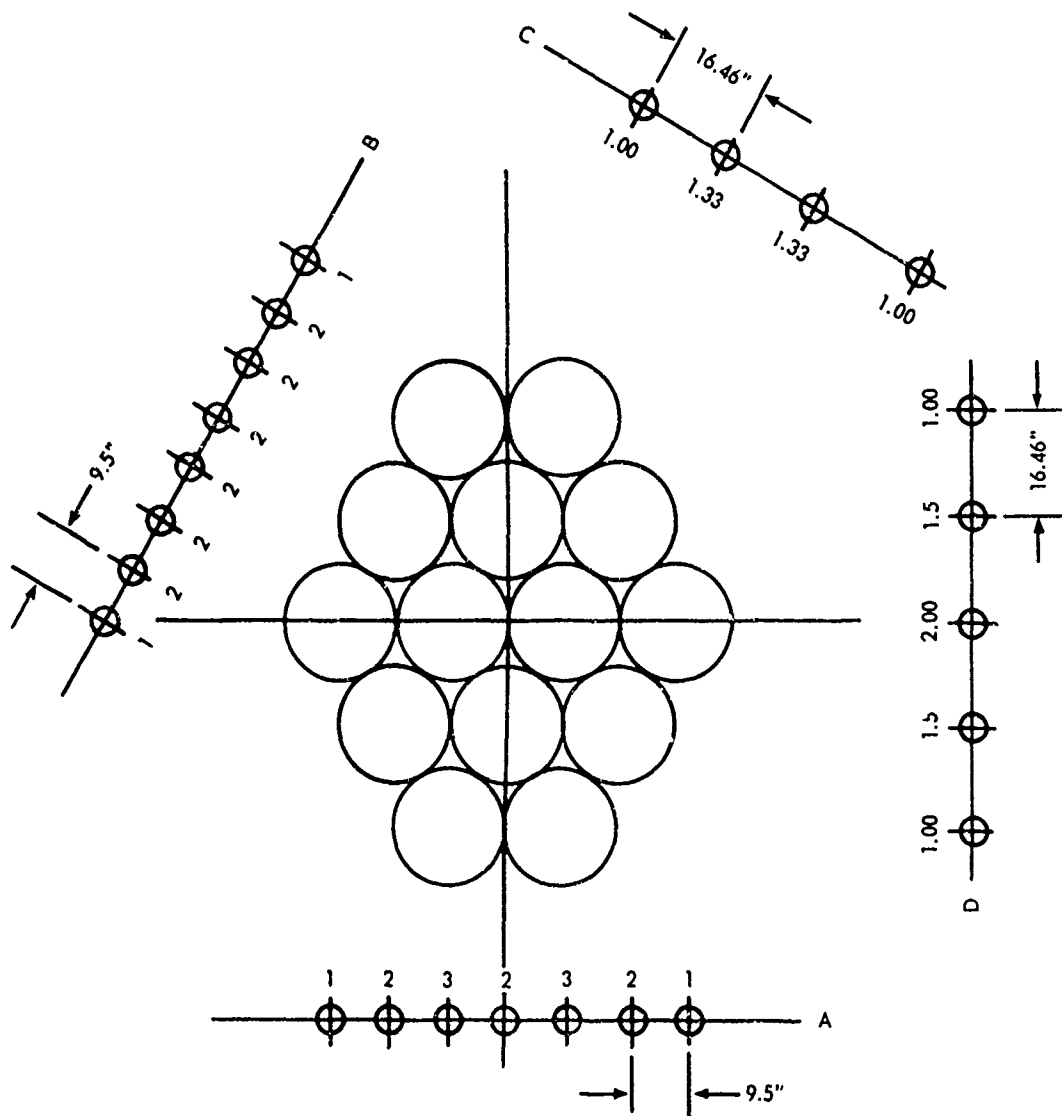


Figure 16. Fourteen-Element Diamond Array Configuration

Under the experimental measurement portion of this contract, four lens-horn elements were built and tested. As a result of the calculations on the 14-element diamond array configuration, a 4-element diamond array, as shown in figure 17, was constructed for testing purposes. Calculated patterns in planes A, B, C, and D were obtained using the computer program and using the voltage excitation and element spacings illustrated in the figure for the appropriate planes of interest. This data is presented in figure 18. Each of the elements were fed in-phase and at equal amplitudes. The numbers by the little circles represent the apparent amplitudes used in calculating the radiation pattern in the appropriate plane.

### 3. BEAM STEERING

The beam of an array antenna can be steered in space, without moving large mechanical masses, by properly varying the phase of the signals applied to (or received from) each element. In the present situation, four equally spaced array elements are considered; they have a geometry similar to that given in figure 13. The spacing between adjacent elements is  $d$ , and the signals at each element are assumed to be of equal amplitude. If the same phase is applied to all elements the relative phase difference,  $\phi$ , is zero and the position of the main beam will be broadside to the array, or  $\theta$  equals  $0^\circ$ . The direction of the main beam is at an angle of  $\theta_0$  when the path length,  $\tau_n$ , or the phase,  $\phi$ , between elements is:

$$\phi = \frac{2\pi d}{\lambda} \sin \theta_0$$

For the case of equally spaced elements the relative phase of the first element is zero, the second element is  $\phi$ , the third element is  $2\phi$ , and the fourth element is  $3\phi$ .

When the array is scanned by use of element phasing to an angle of  $\theta_0$  and the spacing between elements,  $d/\lambda$ , is large, then the grating lobes will occur at angles  $\theta_1$  given by:

$$\sin \theta_1 = \sin \theta_0 \pm \frac{n\lambda}{d}$$

where  $n$  is an integer. The scan angle is limited by the element beamwidths and by the spacing between elements. The element beamwidth limits the relative signal strength as the beam is scanned away from peak, and the spacing between elements determines the grating lobe location and the maximum

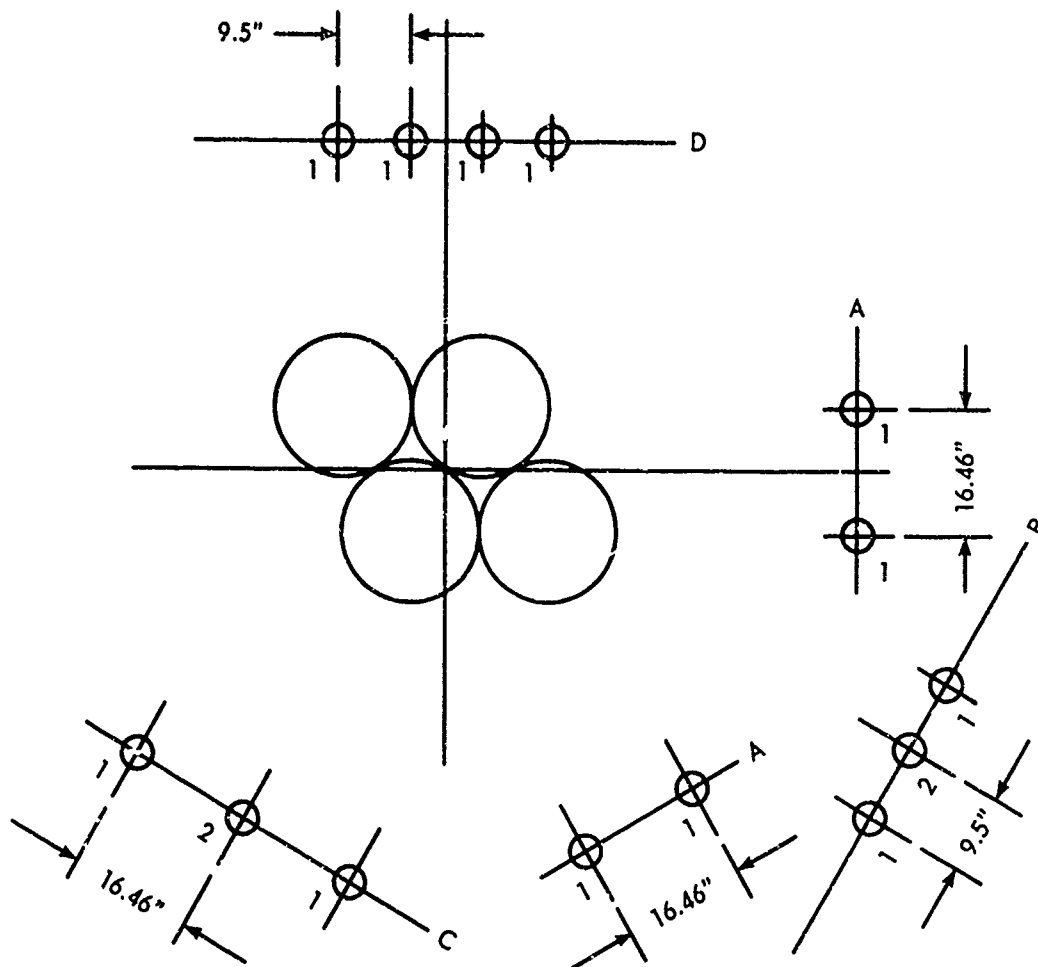


Figure 17. Four-Element Diamond Array Configuration

CUT NO.	3 dB BW DEGREES	10 dB BW DEGREES	NULL POSITION DEGREES	1ST SIDE LOBE		2ND SIDE LOBE		3RD SIDE LOBE		4TH SIDE LOBE		5TH SIDE LOBE		6TH SIDE LOBE	
				LEVEL dB	POSITION DEGREES										
A	0.934	1.53	1.03	11.7	1.50	24.5	2.55	23.9	3.60	29.2	4.65	31.7	5.6	31.6	6.6
B	1.10	1.92	1.80	44.6	2.10	18.6	3.25	35.1	4.55	48.4	5.85	28.0	7.0	47.6	8.3
C	0.72	1.22	1.03	13.8	1.65	27.9	2.55	26.0	3.70	31.6	4.55	34.7	5.7	33.2	6.5
D	0.75	1.28	0.85	16.7	1.20	33.3	2.00	39.1	2.50	19.2	3.40	35.4	4.9	41.5	5.65

Figure 18. Calculated Antenna Patterns of Four-Element Diamond Array

angles of scan.

To illustrate the effects of the scan angle limitation, consider the case for 20 GHz when  $\lambda = 0.590$  inches,  $d = 19.5$  inches and:

$$\sin \theta_1 = \sin \theta_0 \pm \frac{n (.590)}{19.5}$$

From this it is seen that when  $\theta_0 = 0^\circ$  the grating lobes occur at  $\theta_1 = \pm n (1.73^\circ)$  where  $n = 1, 2, 3, 4, 5$ . The multiplication of the element pattern times the array factor means that the array beam peaks will occur at the positions of the grating lobes. As the beam is scanned, the positions of the grating lobes shift by the desired scan angle. The peak gain of the array occurs at  $\theta = 0^\circ$  and the amplitude of the main beam decreases in proportion to the element beamwidths as the array scans away from broadside. In the present example, as the array beam scans away from  $0^\circ$  it reaches a point half way between the grating lobes where two equal beams exist at  $\pm 0.86^\circ$  and these beams will be theoretically 2.5 dB below the peak level obtained at broadside. As the array is scanned further, the "main beam" will continue to decrease in amplitude while the next side lobe will get higher until it peaks again at  $0^\circ$  (or a scan angle of  $1.78^\circ$ ).

Therefore, one can establish scan limits for the array based upon the criteria of maximum main beam gain to the point where there are two equal beams located half way between the grating lobes. A tabulation of the characteristic beamwidths and scan limits that can be expected for 18-inch diameter, uniformly illuminated apertures spaced at 19.5 inches between centers is:

Frequency	Element Beamwidth	Four-Element Array Beamwidth	Array Scan Limits for Max Gain
15 GHz	2.56°	0.60°	1.16°
20	1.91°	0.45°	0.86°
30	1.28°	0.30°	0.58°
40	0.96°	0.22°	0.43°
60	0.64°	0.15°	0.29°

An analysis of the scanned patterns of arrays of these high gain elements should be done in the light of the application involved to be able to completely evaluate the array beam-steering characteristics. Variations in array configurations versus beam-steering characteristics is another area of investigation that would warrant further study.

## SECTION VI

### EXPERIMENTAL RESULTS

#### 1. ELEMENT PERFORMANCE

Lens-corrected horn antenna elements were fabricated for use in the experimental program to accurately determine performance characteristics. Accurate measurements of the gain and aperture efficiency of the antenna element is also important in evaluating the performance of the arrays. Array gain was measured by comparison to a single lens-horn element.

The first gain measurements were made by comparison to a gain-standard horn. The VSWR of the lens-horn antenna was not taken into account in the measurements, but the values of VSWR are low and are considered to be typical for a practical antenna. An E- and H-plane tuner was used in front of the detecting bolometer to ensure good match at each frequency. The results of these first gain measurements were as follows:

<u>Frequency</u> <u>(GHz)</u>	<u>Gain</u> <u>(db over isotropic)</u>
18	37.5
19	38.0
20	38.5
21	39.0
22	39.2
24	40.5
26	40.7
28	41.7
30	42.5

These data were close to the 83% maximum theoretical efficiency level. However, the use of gain-standard horns was not a sufficiently accurate method for three reasons:

- a. The gain calibration is based upon calculated data on the horn aperture size.
- b. The gain of the gain-standard horn is an average of 15 dB below that of the lens-horn antennas and insufficient signal strength was available for accurate readings above 30 GHz.
- c. Significant variations in received power levels were noted for various positions of the gain-standard horn with respect to the location of the antennas under test.

The reasons for the variations in c. are attributed to range reflections which have a greater effect on the broad-beamed gain-standard horn (12°) than the narrow-beamed antennas (2°).

A second method of gain measurement was felt to be more accurate and is called the "absolute gain of identical antennas." Two identical lens-corrected horn antennas were used, one for transmitting and one for receiving. The method is described in reference 11, pages 456 to 457, and would be the same technique used to experimentally determine the gain of gain-standard horn antennas. The technique begins with the fundamental Friis transmission formula:

$$\frac{W_r}{W_t} = \frac{A_{er} A_{et}}{\lambda^2 R^2}$$

where

- $W_r$  = received power
- $W_t$  = transmitted power
- $A_{er}$  = effective aperture of receiving antenna
- $A_{et}$  = effective aperture of transmitting antenna
- $\lambda$  = wavelength at test frequency
- $R$  = range distance between antennas

since:

$$A_{er} = G_0 \frac{\lambda^2}{4\pi R^2}$$

where

$G_0$  = gain of antenna over an isotropic source and because it is assumed when using two identical antennas that  $A_{er} = A_{et}$  the formula becomes:

$$\frac{W_r}{W_t} = \frac{G_0^2 \lambda^2}{(4\pi R)^2}$$

or

$$G_0 = \frac{4\pi R}{\lambda} \sqrt{\frac{W_r}{W_t}}$$

The power ratio  $\frac{W_r}{W_t}$  is, in practice, a measured difference in dB; R was

accurately determined to be 570 feet and the wavelength ( $\lambda$ ) is calculated for each frequency of measurement.

The results of these final gain measurements are plotted in figure 19 and listed as follows:

<u>Frequency</u> <u>(GHz)</u>	<u>Gain in dB</u> <u>over Isotropic</u>	<u>Aperture Efficiency</u> <u>(%)</u>
18	37.4	74.5
19	37.8	72.6
20	38.2	73.0
21	38.6	73.1
22	39.1	72.8
24	39.8	72.8
26	40.4	71.1
28	41.1	71.6
30	41.6	69.9

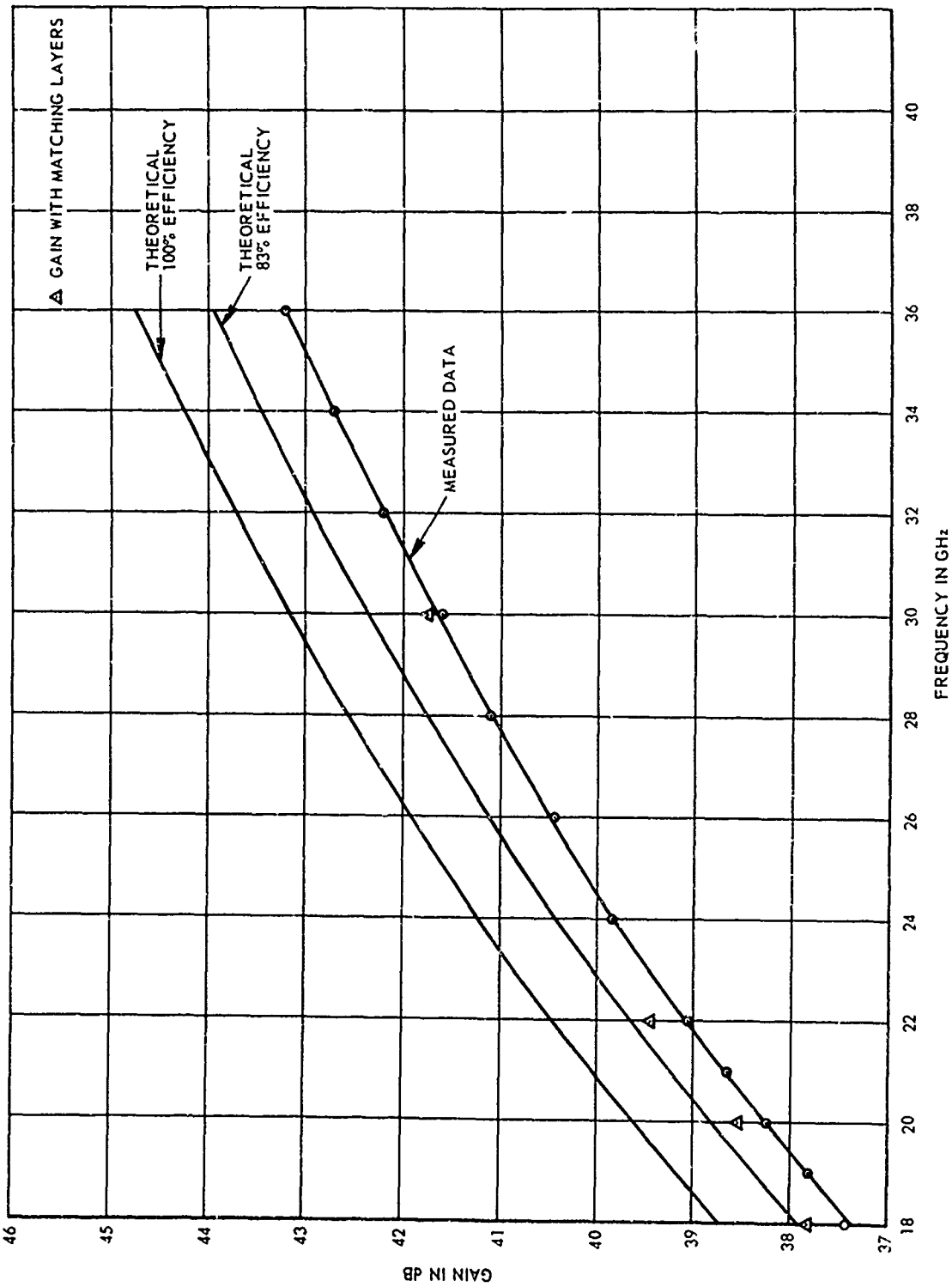


Figure 19. Measured and Theoretical Antenna Gain

<u>Frequency</u> (GHz)	<u>Gain in dB</u> <u>over Isotropic</u>	<u>Aperture Efficiency</u> (%)
32	42.2	70.5
34	42.7	70.4
35.8	43.2	71.1

These values are slightly less than the data measured with the gain-standard horn. Nevertheless, it is felt that these later data are the more accurate. The gradual reduction in efficiency is attributed to increased attenuation losses with increasing frequency. For comparison purposes, the 100% efficiency curve for a uniformly illuminated aperture is shown in the figure; also shown is the 83% efficiency curve which is the calculated maximum gain obtainable from this antenna. The antenna exhibited excellent uniformity of performance and there were no unexpected deviations as the frequency was varied.

The gain of the horn, with the lens removed has a value of only 14.8 dB at 20 GHz. The large reduction in gain for the same aperture dimension is attributed to the fact that the horn is relatively short, has a large included cone angle (45°), and has a  $3\lambda$  phase front curvature at its aperture. The gain falls rapidly with phase front curvature so that the low gain of the horn without the lens to correct the phase is understandable. Another way to look at the situation is to think of the 45° conical horn without the lens as being a very small effective aperture with the rest of the cone having no effect on the wavefront propagation. The measured patterns of the horn without the lens showed irregularities due to phase curvature and approximate E- and H-plane beamwidths of 36° x 22°.

Radiation patterns were measured for the lens-horn element over a two-to-one frequency band. The measured patterns at 20 GHz for the E and H planes are given in figures 20 and 21. These are typical of the patterns obtained throughout the range of frequencies. The measured points for E- and H-plane beamwidths versus the expected calculated values are shown in figure 22. As noted in the section on design predictions, the amplitude illuminations for the E and H planes closely follow the theoretical examples given on page 195 of reference 3. The E-plane illumination is uniform and the theoretical half-power beamwidth equals  $1.02 \frac{\lambda}{D}$  radians or  $58.4 \frac{\lambda}{D}$  degrees. The curves in figure 22 are calculated for the diameter, D, equal to 18 inches and the wavelength,  $\lambda$ , for the corresponding frequencies. Similarly, the tapered illumination in the H plane produces a half-power beamwidth equal to  $1.27 \frac{\lambda}{D}$  radians or  $72.8 \frac{\lambda}{D}$  degrees. The data show that the correlation between measured points and the theoretical curves is within less than 0.1°.

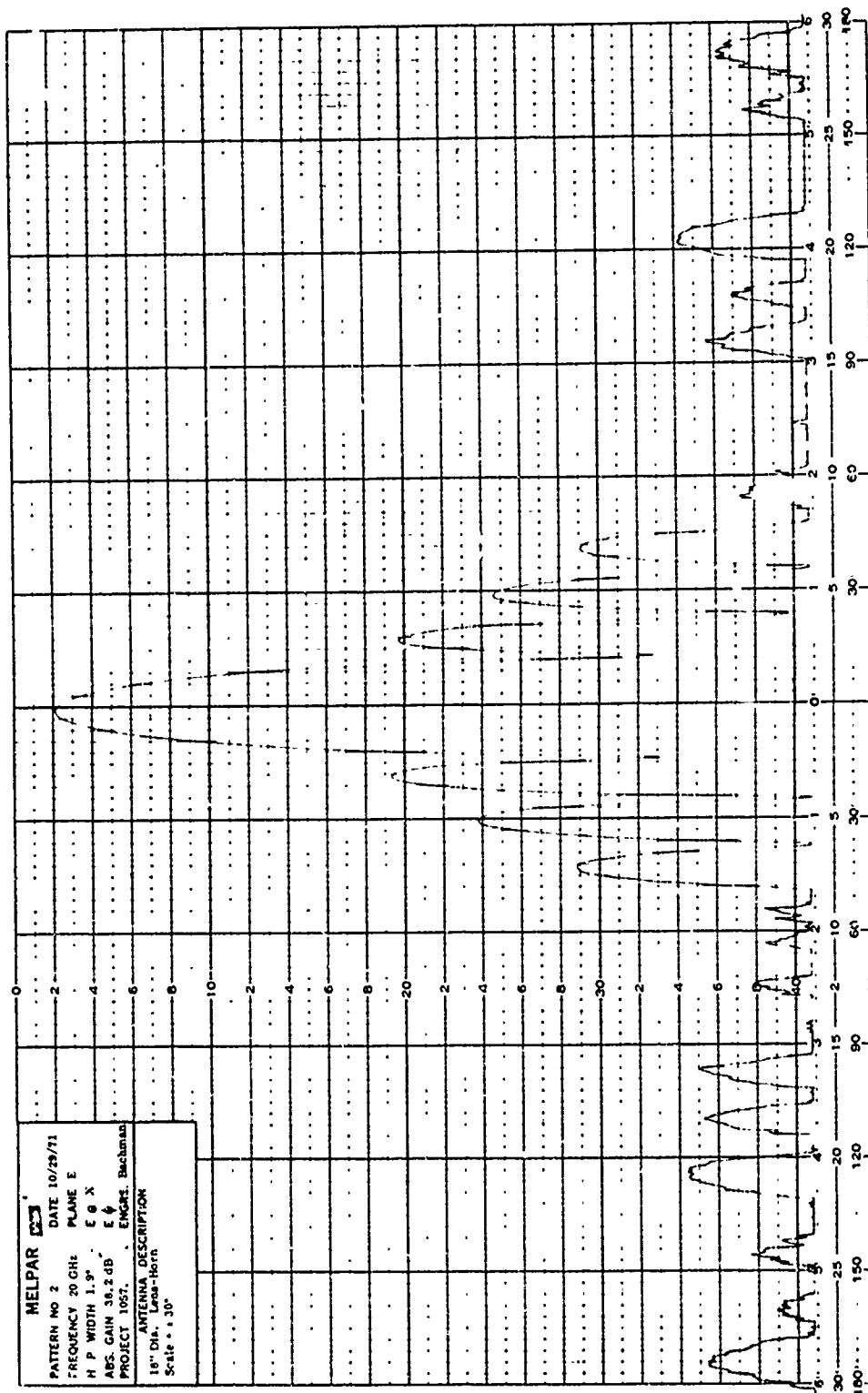


Figure 20. E-Plane Element Pattern, 20 GHz

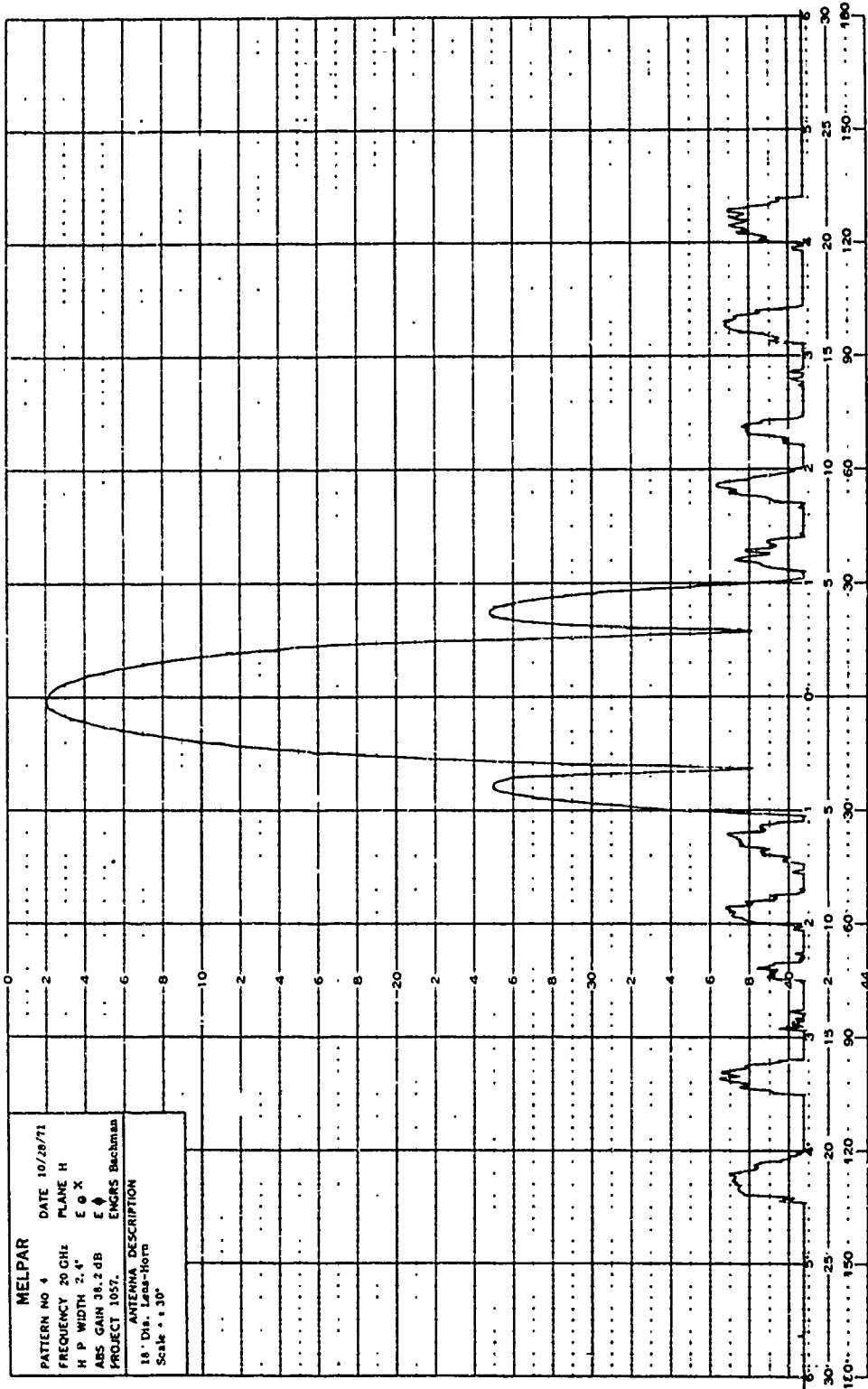


Figure 21. H-Plane Element Pattern, 20 GHz

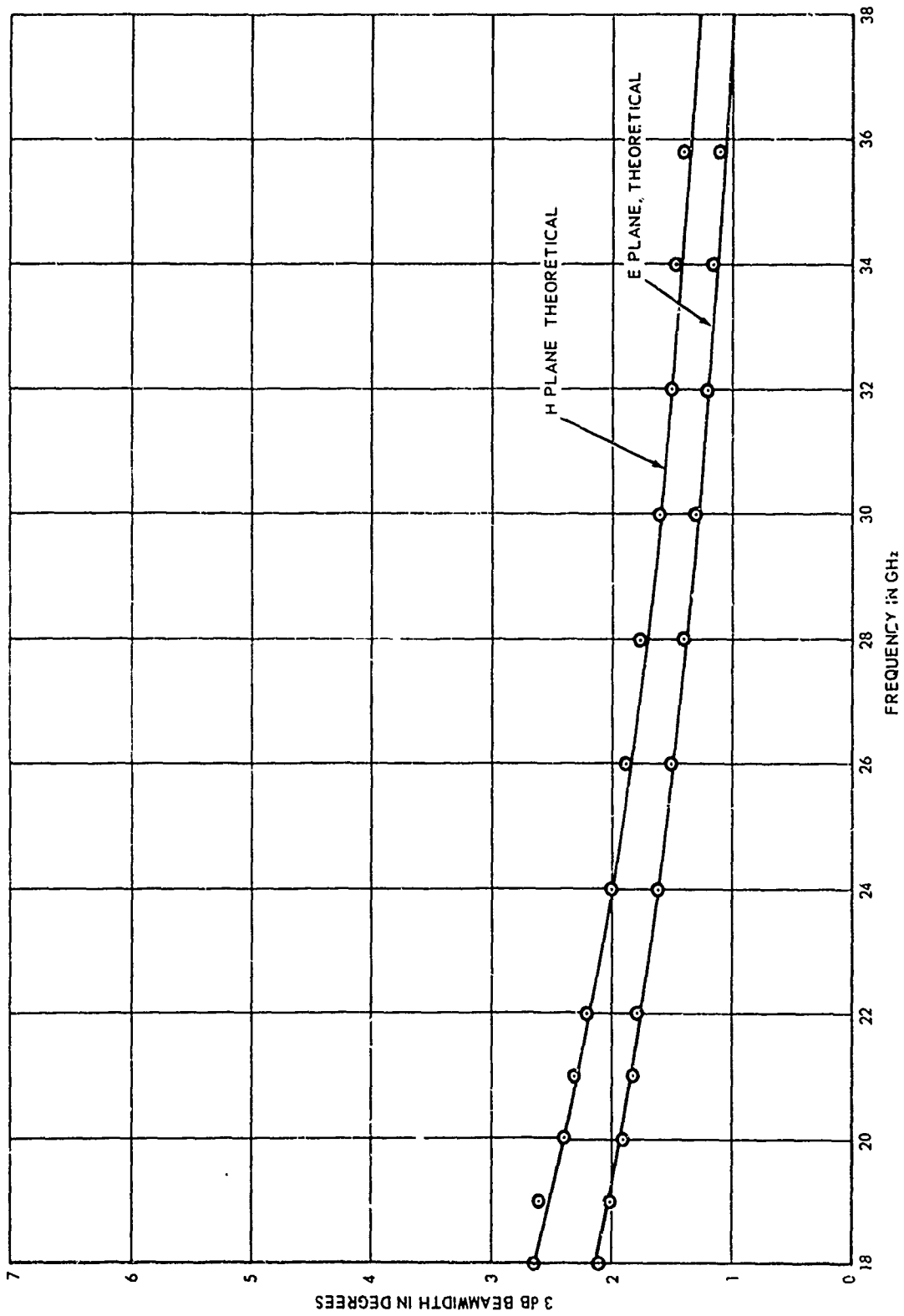


Figure 22. Measured Points and Theoretical Antenna Beamwidths

The first side-lobe levels in the E and H planes versus frequency are shown in figure 23. The theoretical values correspond to a uniformly illuminated aperture of the E plane and the tapered illumination for the H plane. The uniformity of performances across the frequency band is considered to be very good and the fluctuations in side-lobe levels are within reasonable tolerances. The average level in the E plane is approximately one dB higher than predicted and the reason for this difference is not apparent.

The fluctuations in side-lobe levels are attributed to low power reflections from the lens. These fluctuations are caused by constructive or destructive interference between direct and reflected waves and vary as a function of frequency. For example, a reflection level as low as -35 dB will cause up to 5-dB variations in the side lobes about the 24.6-dB level. No significant effect on peak gains was noted as a result of the varying H-plane side lobes.

The measured E-plane pattern corresponds to the case for uniform amplitude across the circular aperture. The comparison of theoretical and measured pattern features is given in figure 24. The correspondence is extremely close which proves that the desired lens design has been achieved.

The H-plane -3 dB beamwidth equals  $2.40^\circ$  and the first side-lobe level is at -23 dB from the peak. Other H-plane lobes are below -34 dB from the peak of the beam. Beyond  $\pm 30^\circ$  of the main beam for both the E and H planes there were no side lobes or back lobes above the limit of the recorder at -39 dB from the beam peak. The lens-horn antenna would be good for low noise applications where side or back radiated signals must be avoided.

The measured VSWR of a lens-corrected horn element showed no appreciable change with the lens in place or removed. The VSWR of the antennas was practically the same as that looking into the transistions and adapters and is plotted in figure 11. The energy that was reflected off the lens surfaces and back into the feed was of such a low value that it can be considered to be insignificant. The lens geometry is a factor in this low level of reflected energy as seen by the feed. The use of matching layers on the lens surfaces would ensure that the energy that is scattered and lost by reflections is conserved and directed into the main beam with a resultant increase in gain.

The effect of the environment on the lens and its performance was observed during testing. One lens was outdoors a high percentage of the time, for 6 months, from October through March. No noticeable change in performance characteristics occurred during this time. The only physical effect observable

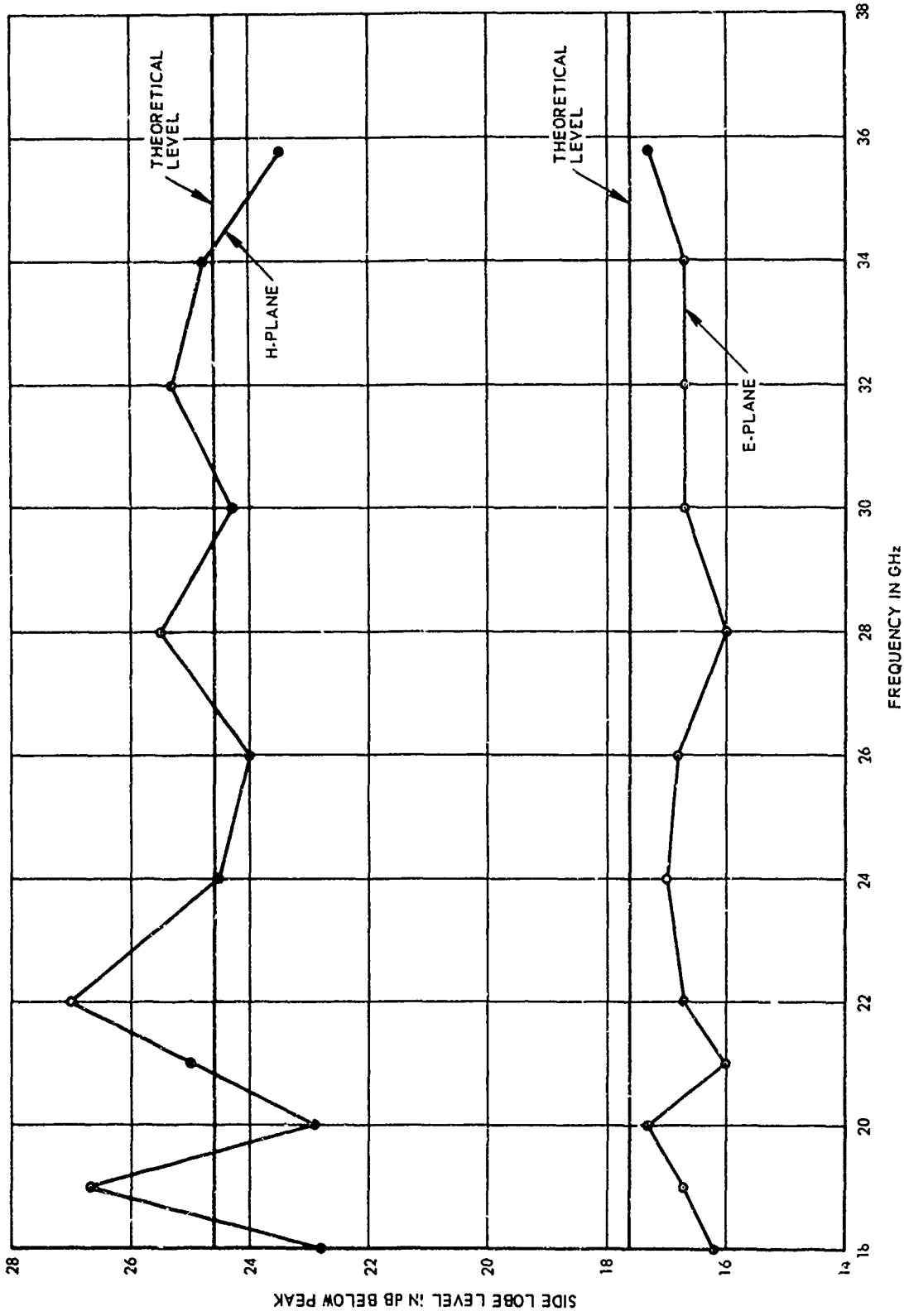


Figure 23. E- and H-Plane Element Side-Lobe Levels

PATTERN FEATURE	THEORETICAL	MEASURED
WIDTH, MAIN BEAM, -3 dB	1.84°	1.90°
WIDTH, MAIN BEAM, -10 dB	3.26°	3.22°
FIRST NULL POSITION	±2.30°	±2.25°
FIRST SIDE LOBE POSITION	±3.05°	±3.00°
FIRST SIDE LOBE LEVEL	-17.6 dB	-17.3 dB
SECOND NULL POSITION	±4.20°	±4.10°
SECOND SIDE LOBE POSITION	±5.05°	±5.00°
SECOND SIDE LOBE LEVEL	-23.8 dB	-22.2 dB
THIRD NULL POSITION	±6.10°	±6.10°
THIRD SIDE LOBE POSITION	±6.95	±7.00°
THIRD SIDE LOBE LEVEL	-28.0 dB	-27.0 dB

Figure 24. E-Plane Antenna Pattern Comparison for Uniform Amplitude, 20 GHz

was a slight yellowing of the plastic, but no crazing, cracking, or other defects occurred. It is believed that the change in appearance is primarily a surface effect because the surface finish was partially polished from exposure and handling, making it somewhat more transparent than its original frosty finish.

Temperature changes and light coatings of moisture in the form of condensation had no noticeable effects. Therefore, tests were made of gain and patterns at 20 GHz under different degrees of surface wetting. With a light wetting of the outer lens surface by wiping with wet towels, a reduction in gain of approximately 0.1 dB was observed. A heavy surface wetting, applying water by rubbing and dripping until no more would cling to the surface, caused a gain reduction of 0.8 dB. Antenna patterns measured under this heavy wetting showed no significant changes other than slight unevenness in lower side-lobe levels. Water was then dripped onto the lens to simulate a heavy rain. Under this test a maximum loss in gain of 2.3 dB occurred.

## 2. MATCHING LAYERS

Tests were performed to measure and evaluate the desirability of the one-quarter-wavelength-thick matching layers. Comparative gain and pattern measurements were taken using: (a) a lens without matching layers, (b) a lens with curved surface matching, (c) a lens with plane surface matching, and (d) a lens with both surfaces matched. Two lenses were used to perform the measurements; both lenses were checked for performance and found to be virtually identical. The curved (outer) surface on one lens was covered by cutting a flat layer into wedge-shaped pieces and gluing them to the lens. The adhesive was a thin sprayed-on coating of a rubber-based adhesive suitable for RF applications. A second flat layer was machined for use against the plane (inner) surface of the lenses. Using a minimal amount of adhesive, a lens was tested with and without the flat layer. The flat layer was then attached to the lens with the curved layer to get the data from both layers on the same lens.

The resulting data, showing the improvement in gain at different frequencies over an uncoated lens, are shown in the following tabulation:

<u>Frequency</u> <u>(GHz)</u>	<u>Inner and Outer Layers</u> <u>(dB)</u>	<u>Inner Layer</u> <u>(dB)</u>	<u>Outer Layer</u> <u>(dB)</u>
18	+0.4	+0.2	+0.2
20	+0.3	+0.2	+0.2

<u>Frequency (GHz)</u>	<u>Inner and Outer Layers (dB)</u>	<u>Inner Layer (dB)</u>	<u>Outer Layer (dB)</u>
22	+0.4	+0.2	+0.2
30	+0.15	+0.05	+0.05

The data points for total element gain with both layers added are shown in figure 19.

The measured results compare favorably with the predicted values. The improvement in gain due to cancellation of reflections occurs at dielectric thicknesses of  $\frac{\lambda}{4}$ ,  $\frac{3\lambda}{4}$ ,  $\frac{5\lambda}{4}$ , etc., but is approximately correct at bands of frequencies about these values. It is of interest to note that, although the layer was designed for 0.250 wavelengths at 20 GHz, there is still some reduction of reflection losses at 30 GHz, where the layers are 0.375 wavelengths thick. The layer should have no benefit at 40 GHz where its thickness is one-half wavelength. No explanation can be offered for the apparent reduction by 0.1 dB when both inner and outer layers are used at 20 GHz.

The improvement in element aperture efficiency with the matching layers is as follows:

<u>Frequency (GHz)</u>	<u>Efficiency without Matching Layers (%)</u>	<u>Efficiency with One Layer (%)</u>	<u>Efficiency with Two Layers (%)</u>
18	74.5	78.0	81.7
20	73.0	76.5	78.2
22	72.8	76.2	79.8
30	69.8	70.6	72.3

The matching layers were able to recover nearly all the losses attributed to reflections when layers were used on both lens surfaces. The maximum measured efficiency approaches very closely the efficiency of 83% that was predicted for the lens-corrected horn antenna.

The effect of the matching layers on the antenna patterns and side lobes was relatively small. This attests to the fact that measured element patterns were very nearly the same as the predicted performance. Variations of less than  $\pm 1$  dB in side-lobe levels were measured in most cases for both E and H planes. At the design frequency of 20 GHz, the effect on the antenna patterns was the most pronounced. The comparative results for 20 GHz are listed below:

<u>Pattern Plane</u>	<u>No Layers on Lens (dB)</u>	<u>Layer on Curved Side (dB)</u>	<u>Layer on Flat Side (dB)</u>	<u>Layers on Both Sides (dB)</u>
E plane:				
1st Side-lobe Level	-18	-18.3	-17.0	-16.8
2nd Side-lobe Level	-22	-23.5	-24.5	-24.0
3rd Side-lobe Level	-26	-28.7	-26.0	-27.5
H plane:				
1st Side-lobe Level	-23.5	-24.7	-25.5	-26.0

The matching layers on the lens-corrected horn antenna elements, as designed for use in this study, enhanced the gain and aperture efficiency by as much as 0.4 dB. This was an improvement in antenna gain for large-aperture antennas having gains on the order of 40 dB. In terms of physical size, the increase in equivalent aperture diameter is 5.5%. The layers made little improvement in the antenna element performance characteristics such as lower side lobes or lower VSWR. This is attributed to the fact that the basic antenna design, using a two-surface lens and horn feed, is a very efficient antenna and the effects of reflections are smaller than may be exhibited by other designs.

Fabrication of matching layers can take several forms such as homogeneous layers or artificial dielectric surface treatments. In either case, it is more difficult and costly to make matching layers for the curved, outer lens surfaces. The outer surface is also most subject to degradation due to environmental effects. The use of flat homogeneous matching layers on the inside surface of the lens is more readily accomplished and can be designed for the desired frequencies by changing the thickness of the layer. The relative value of the matching layers should be determined on the basis of the particular application involved.

### 3. ARRAY PERFORMANCE

The four lens-corrected horn antennas were assembled into three different configurations to obtain measured data on the performance characteristics of the array. The three array configurations are shown in figures 25, 26, and 27. Figure 25 is the 2 x 2 array. Figure 26 shows the 4 x 1 array, and the view showing the waveguide feed network was selected. Figure 27 shows the four-element diamond array, and the transmitting tower can be seen in the background. The method of mounting and aligning the array antenna elements can be seen in the photographs. Great care was taken to accurately align the elements because of the very narrow beamwidths involved.

The feed networks for the arrays are diagrammed in figure 28. The components are all purchased parts for the 18.0- to 26.5-GHz waveguide size. The flexible waveguide sections are each 12 inches long and attach directly to the feed on the lens-horn. The E- and H-plane bends are made with the flexible waveguide; then the guides are attached to the waveguide magic tees. The magic tees provide the desired power split with lower VSWR than waveguide tees and also give good isolation between the elements in the array. The difference ( $\Delta$ ) ports on the magic tees are used for the outputs rather than the sum ( $\Sigma$ ) ports because the relative phases are opposite. This can be seen by reference to the polarization and phase arrows in the figure. Little or no signal appears at the sum ports but a waveguide termination was used to absorb any reflected components.

The 90° waveguide twist sections were added between the flexible waveguide and the antenna feed in order to obtain both E- and H-plane data for a given orientation of the array. The twists are merely a convenience for test purposes and need not be used in an operational model. The flexible waveguide allows for minor adjustments in the pointing of the lens-horn elements. In an operational model the amount of physical adjustment will be small and the flexible sections can be shortened if desired. The flexible waveguides also allow the arrangements between elements to be varied as in the case of the diamond array.

The 2 x 2 array of four elements was assembled and tested for gain, patterns, VSWR, and efficiency. The feed network was assembled first, and checked for electrical length. Adjustments in phase were accomplished by the use of machined waveguide shims. The maximum phase difference between any of the four elements in the array was only 0.092 cm or 15.8 electrical degrees at 20 GHz. Insertion loss through the feed network was less than 0.5 dB. Elements were checked individually and in pairs to ensure that alignment and phasing were correct and the beams were properly boresighted.

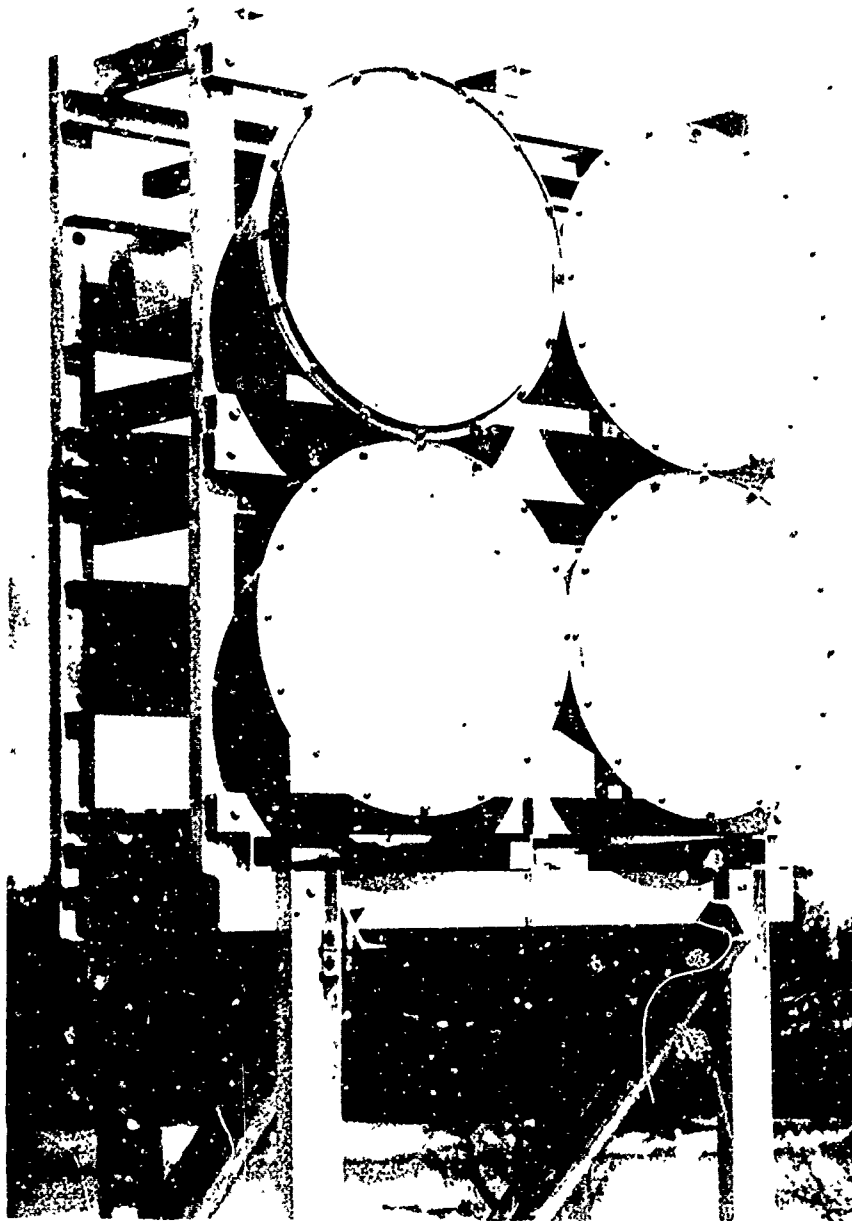


Figure 25. 2 x 2 Lens-Horn Array

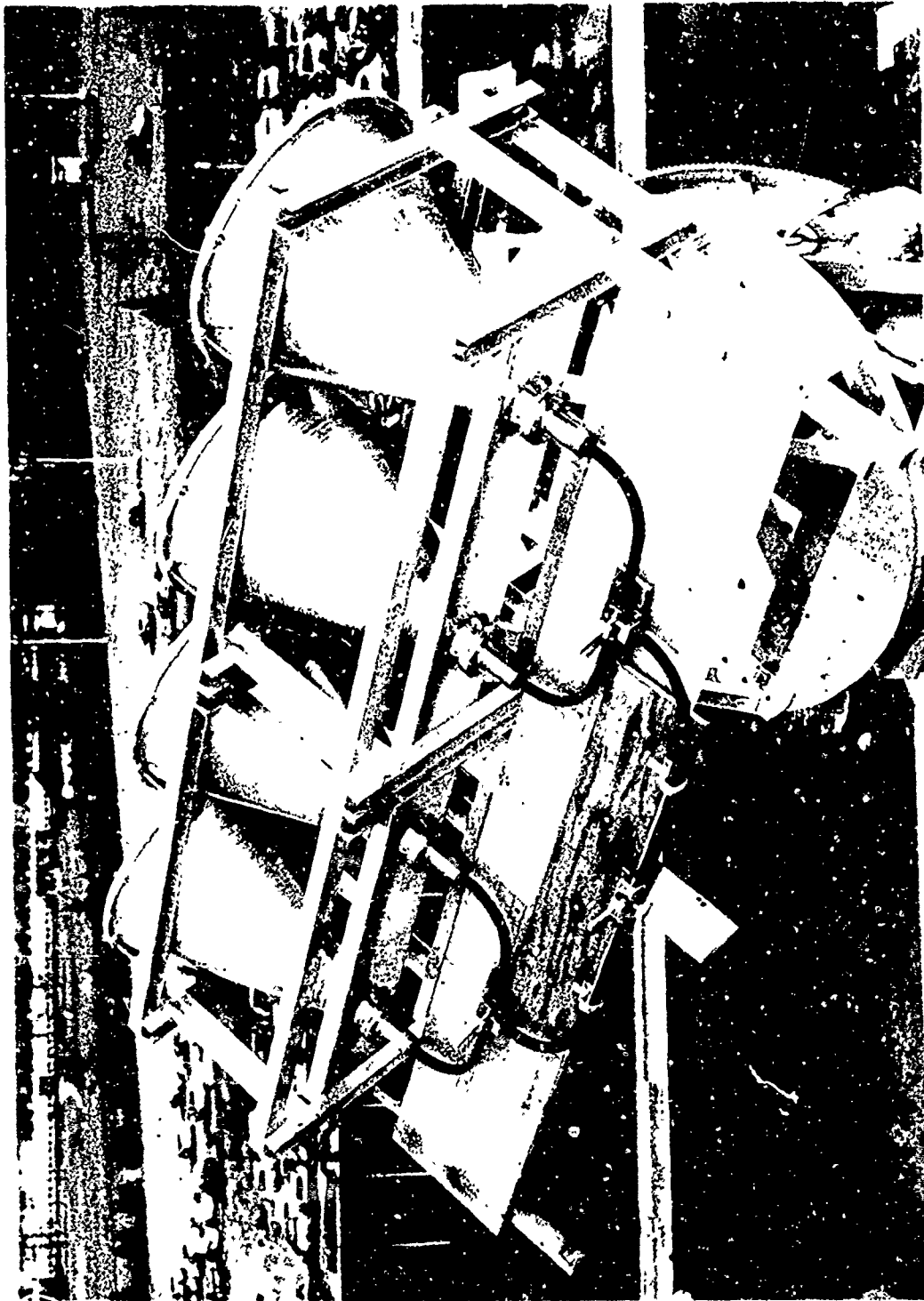


Figure 26. 4 x 1 Lens-Horn Array and Waveguide Feeds

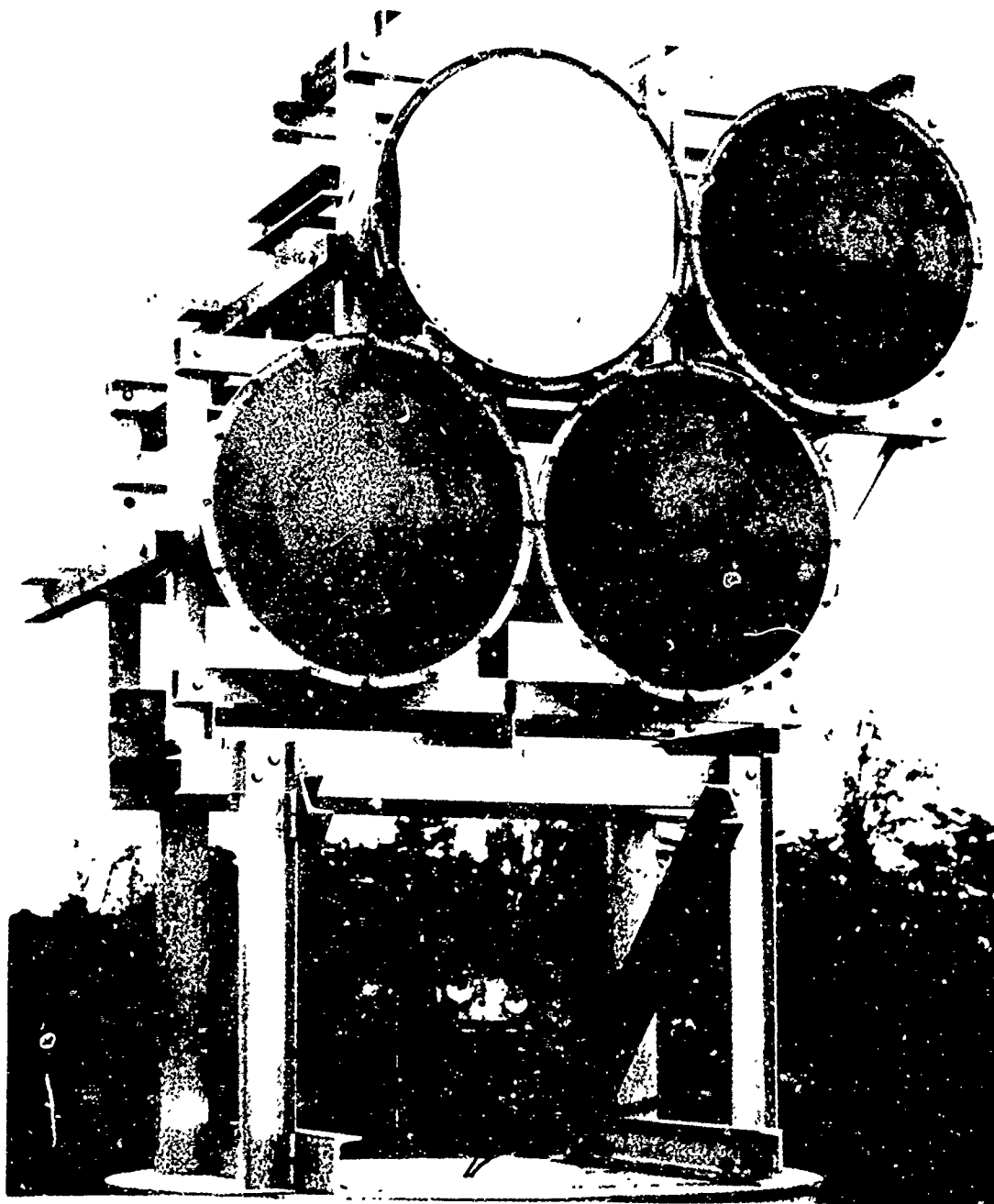


Figure 27. Diamond-Shaped Array of Lens-Corrected Horns

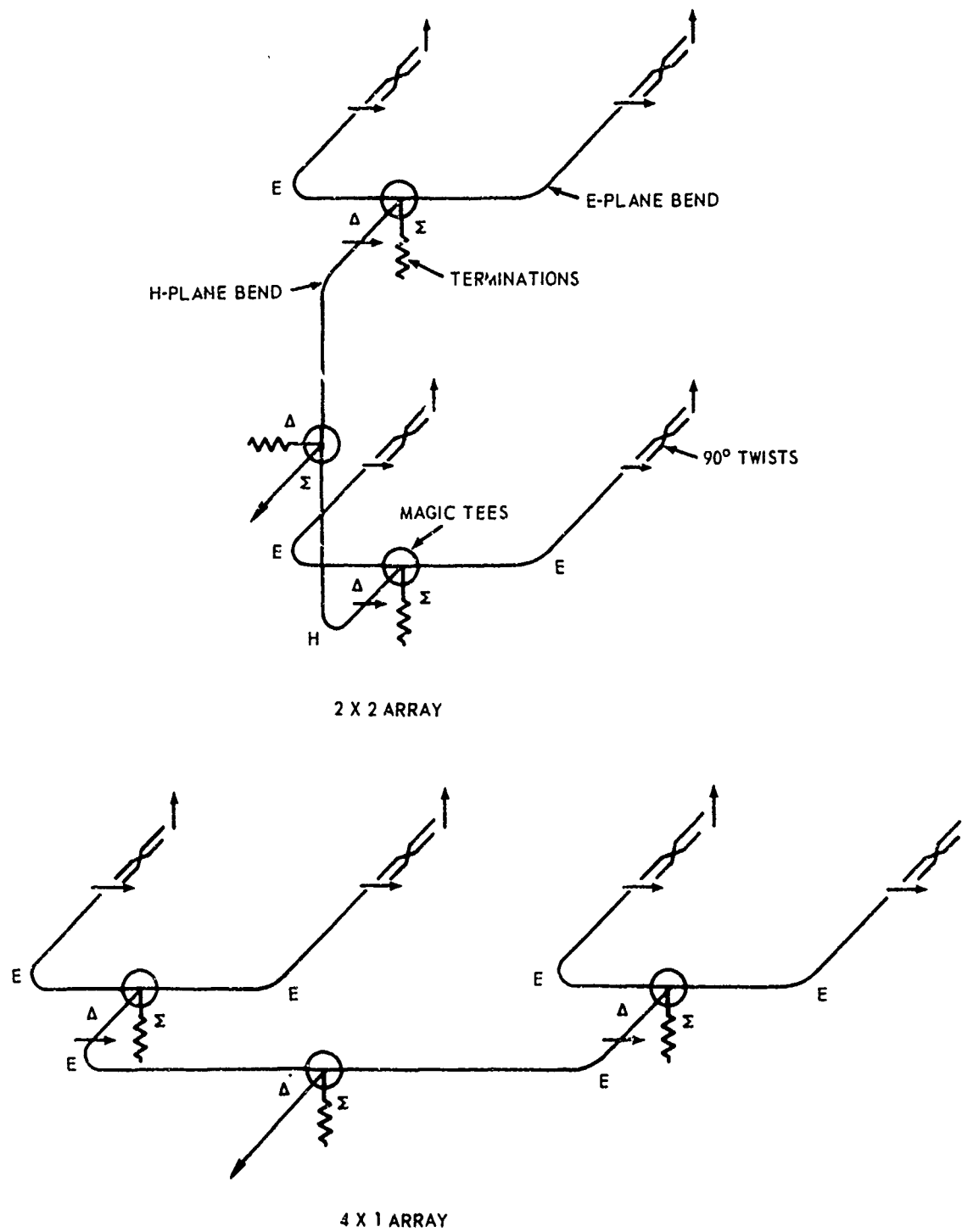


Figure 28. Feed Arrangements Showing Relative Polarizations, Planes of Bends, and Ports

The measured gain of the 2 x 2 array was 43.5 dB over an isotropic radiator at 20 GHz. This is 5.3 dB over the single element gain as compared to a theoretical 6.0 dB improvement. The measured feed network insertion losses account for 0.4 to 0.5 dB leaving only a loss of 0.2 to 0.3 dB that may be attributed to factors such as imperfect alignment or phase variations. The gain of a 4 x 4 array of 16 elements would be approximately 6 dB above 43.5 or equal to 49.5 dB. These figures are without the 0.4 dB potential improvement in gain due to the addition of surface matching layers.

For comparison purposes, a 3-foot diameter parabolic dish operating at a normal efficiency of 55% would correspond to the 2 x 2 array and the gain of a 6-foot diameter parabolic dish can be compared to the 4 x 4 array. The 3-foot dish has a gain of 43.0 dB and the 6-foot dish is 49.0 dB, neglecting any additional feed line losses.

The E- and H-plane patterns of the 2 x 2 array are shown in figures 29 and 30. The measured half-power beamwidths are  $0.80^\circ$  in the E plane and  $0.83^\circ$  in the H plane. Beamwidths for the 3-foot dish would be approximately equal to  $1.20^\circ$  with typical side-lobe levels of 20 dB below beam peak. The levels of the first side lobes for the 2 x 2 array are high, but they are consistent with the array theory for the actual element spacings of 19.5 inches and the element pattern levels at the displacement angles of these lobes. Only an effective tapering of the amplitude distribution across the two-element array can lower the first side-lobe levels. In the case of the 2 x 2 array, amplitude tapering cannot be done by altering the feed distribution, but it can be done by rearranging the elements into a diamond configuration to put greater concentration of signal in the center of the array and less on the edges.

The 4 x 1 array of elements was assembled and carefully aligned to put all the lenses in the same plane. The feed network was checked for equal electrical line lengths and adjusted by the use of machined waveguide shims. Maximum phase error between the four waveguide branches was only 0.070 cm or 12 electrical degrees. Insertion loss through the feed network was 0.4 to 0.5 dB. Measured gain of the array was 4.9 dB above a single array element or a total of 43.1 dB over an isotropic source. The E- and H-plane patterns across the four elements are shown in figures 31 and 32. The measured E- and H-plane beamwidths are both  $0.4^\circ$ .

The effect of tapering the amplitude of the 4 x 1 array was tested by inserting 3 dB of attenuation into the feedlines of the two outer elements. In this manner a 1, 2, 2, 1 distribution was obtained. The results showed a decrease in array gain of 0.45 dB after the attenuated power was accounted

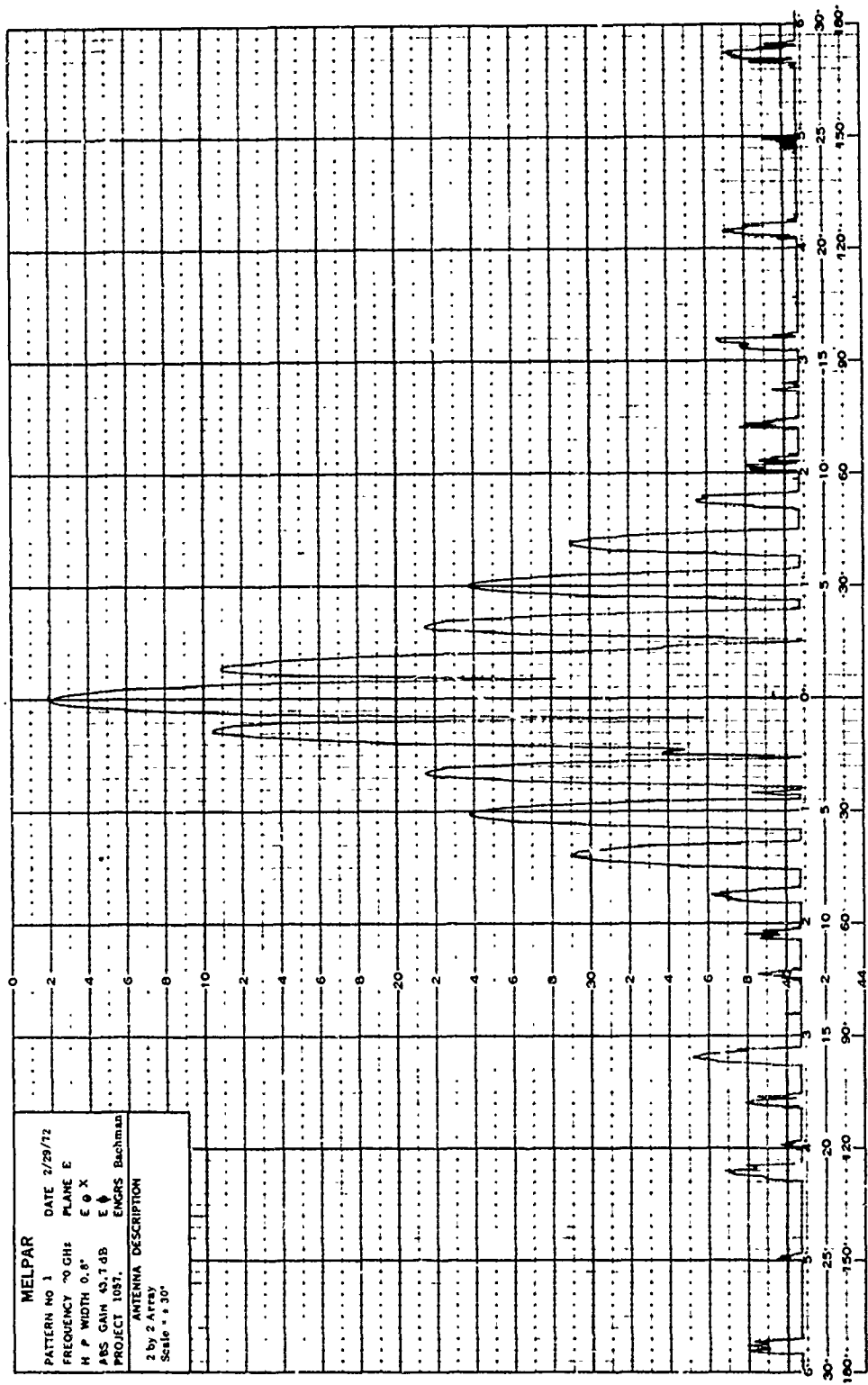


Figure 29. E-Plane Pattern of 2 x 2 Array

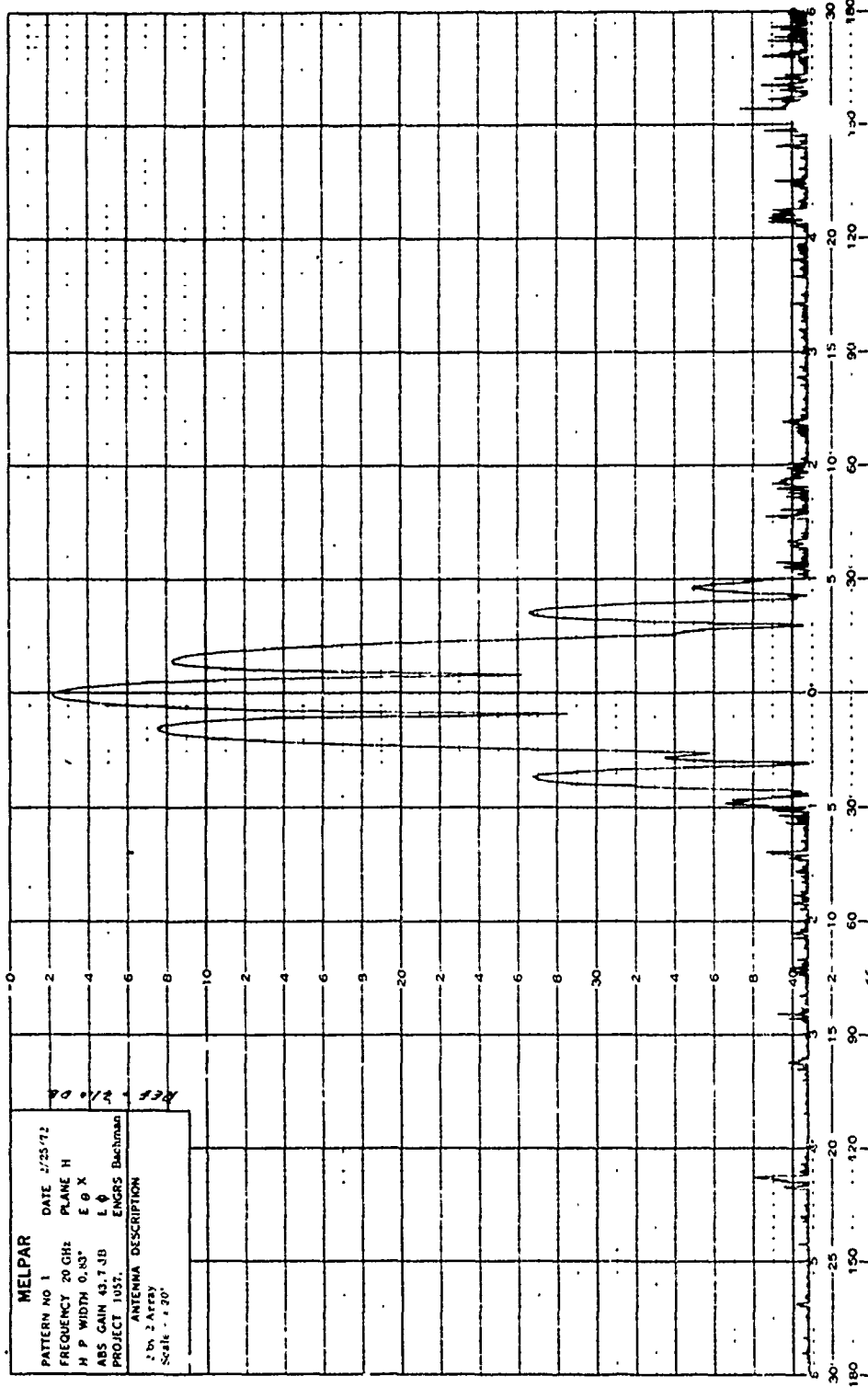


Figure 30. H-Plane Pattern of 2 x 2 Array



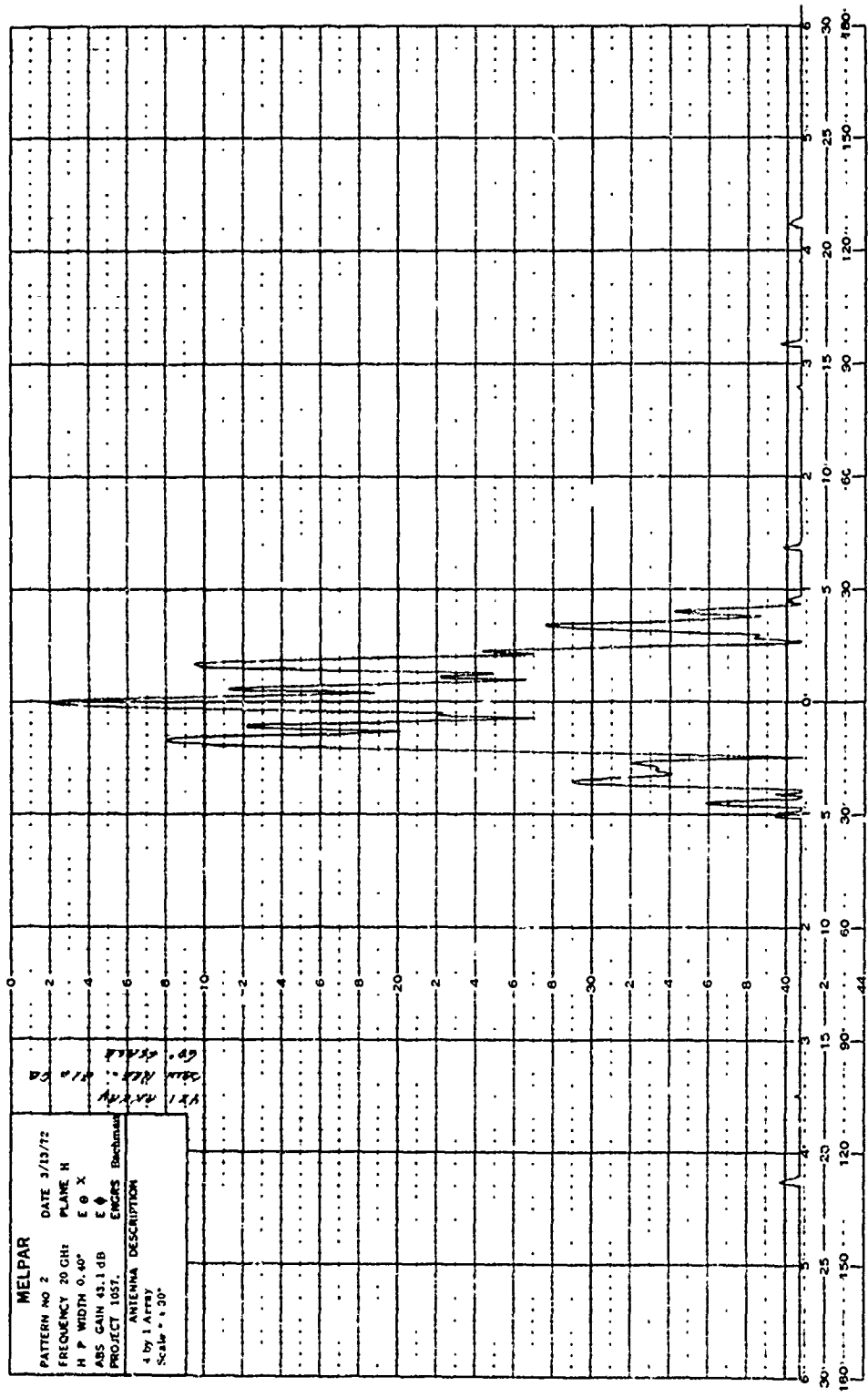


Figure 32. H-Plane Pattern of 4 x 1 Array

for in the calculation. The patterns and side-lobe levels were essentially unaffected. The only improvement occurred in the reduction of lesser internal lobes. In other words, the major grating lobes caused by the array spacing were not reduced significantly.

The diamond array of four elements was assembled in a similar manner to the 2 x 2 array and tested. The gain was measured as 43.1 dB over an isotropic source. E- and H-plane patterns are shown in figures 33 and 34. The cuts correspond to the "D" cut shown in the diagram in figure 17. The E-plane cut was with horizontal polarization and the H-plane cut was with vertical polarization. Other cuts were also taken by tilting the array in elevation and by taking azimuth cuts at different elevation tilt angles to obtain data on side lobes not seen in the principal E- and H-plane patterns. The E- and H-plane patterns corresponding to the "A" cut in figure 17 were taken by varying the elevation angle on the antenna rotator. These cuts represent the worst case for side-lobe levels and are shown in figures 35 and 36. The side lobes seen at 8° to the right of the main beam are caused by range reflections when tilting the array in elevation and can be ignored.

The data can be compared to the theoretical calculations tabulated in figure 18. The E-plane patterns (uniform amplitude distribution) compare very closely to the calculated values for the corresponding cuts. The actual antennas were spaced 19.5 inches between centers as opposed to 19.0 inches for the calculated values. It is concluded that the effective tapering of the aperture by the diamond element arrangement does offer the potential of lower side-lobe levels in arrays. This may be further enhanced by orienting the polarization to correspond to the principal axes of the diamond instead of the horizontal or vertical options used in the experiments.

A summary of the measured results of the different array configurations and that of a single element at 20 GHz is shown in figure 37. The summary eliminates the measured insertion losses of the array feed networks because this is an independent variable depending upon the design details and component selections.

The VSWR of the arrays is determined by the feed network components and the transition from rectangular waveguide to circular waveguide at the lens



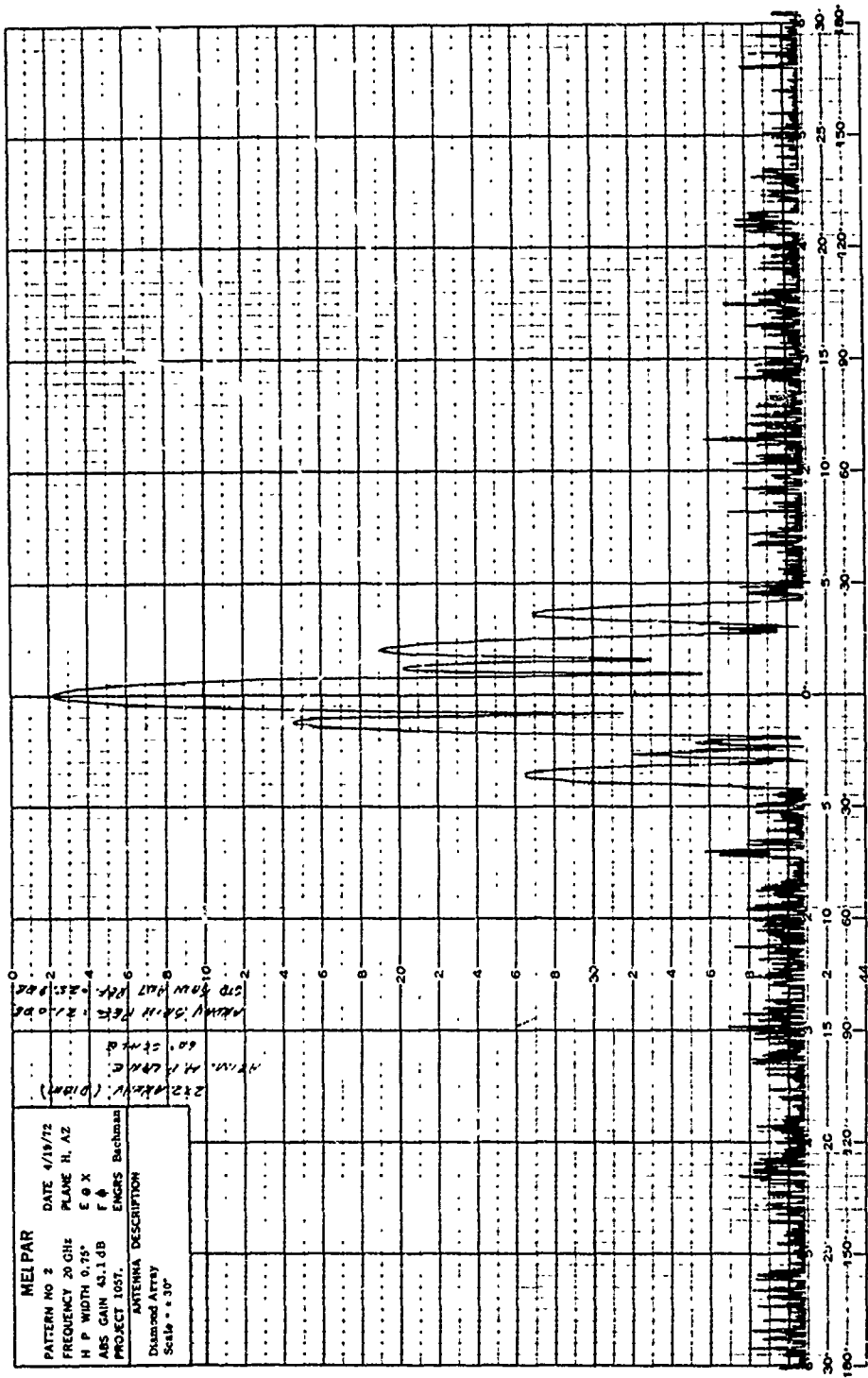


Figure 34. H-Plane of Diamond Array Azimuth Rotation

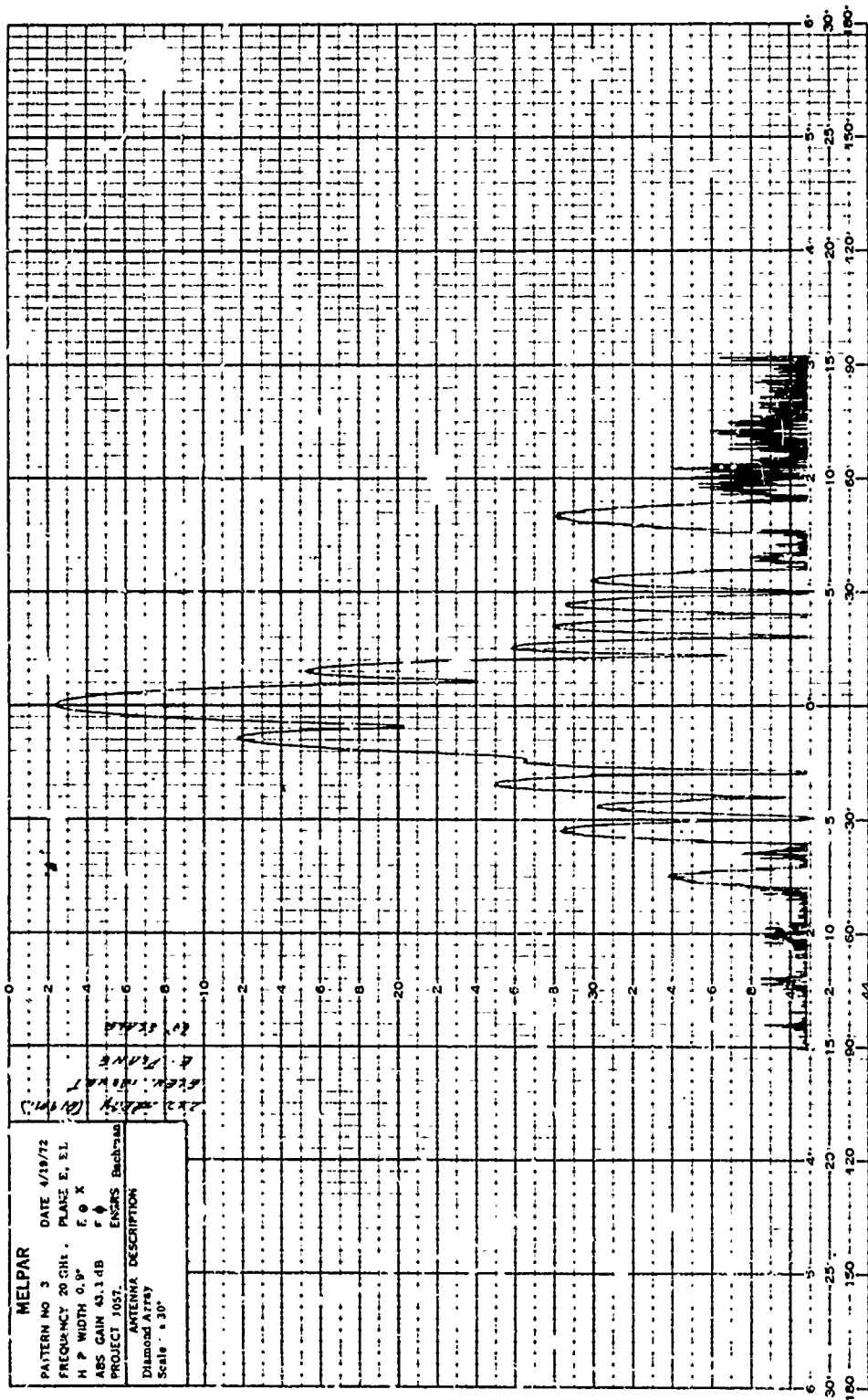


Figure 35. E-Plane Pattern of Diamond Array Elevation Rotation



Configuration	Measured Gain	Aperture Efficiency	3 dB Beamwidths		Highest Average Side Lobes	
			E	H	E	H
Single Element	38.2 dB	73.0%	1.90°	2.40°	-17.3 dB	-23.0 dB
2 by 2 Array	44.0	69.0%	0.80°	0.83°	- 8.5	- 6.0
4 x 1 Array	43.6	63.0%	0.42°*	0.40°*	- 9.5*	- 6.5*
Diamond Array	43.6	63.0%	0.77°	0.93°	-11.0	- 7.5

\* Measured across 4 elements.

Figure 37. Comparison of Performance of Element and Arrays

feed. The lenses and horns had little effect on VSWR. Typical measured values of VSWR for the arrays were as follows:

<u>Frequency</u> <u>in GHz</u>	<u>VSWR</u> <u>2 x 2 Array</u>	<u>VSWR</u> <u>4 x 1 Array</u>
18.0	1.50	1.60
19.0	1.95	1.43
20.0	1.24	1.36
21.0	1.23	1.23

The effects of weather on the arrays was the same as that for a single element with respect to gain. Using the 4 x 1 array as a worst case, no beam skewing was measured under heavy wetting, even when applied to only one-half of the array. Fluctuations of one dB or less were measured on the lower side lobes of the 4 x 1 array under heavy wetting but no main beam distortion occurred. The feed network behavior was stable; effects due to temperature should be self-compensating in a symmetrical feed arrangement; and excessive temperature gradients should not exist across the array.

#### 4. BEAM-STEERING CHARACTERISTICS

Measurements to determine beam-steering characteristics were made when using the 4 x 1 array configuration. Phase shifts were introduced into the waveguide feed network by inserting short sections of guide. Three lengths of waveguide are needed for a given beam tilt; the lengths have the phase relationship of  $\phi$ ,  $2\phi$ , and  $3\phi$  for the equally spaced array. The first element of the array remains at zero relative phase.

Calculated values for the relative element phases at 20 GHz, with a 19.5-inch element spacing, are as follows:

Beam Tilt	Element Number and Phase			
	1	2	3	4
0.5°	0°	104°	208°	312°
1.0°	0°	208°	415°	623°
1.5°	0°	312°	623°	934°

The lengths of the waveguide phasing sections were determined by converting from electrical degrees to distances at the waveguide wavelengths and were machined to accurate dimensions.

The 1.5° tilt was tried first and the results followed the theory described previously. The main beam was scanned by 1.5° but was at a level of approximately -7 dB from the peak gain value of the array while a second lobe appeared at -0.23° at a level of -0.2 dB from the peak value. In other words, the scan limit criteria discussed in section V, part 3, has been exceeded. Phasing sections for a 0.5° tilt were then fabricated and installed into the feed network. The resultant pattern in figure 38 also follows theoretical performance and shows the main beam scanned 0.5° to the left. The positions of the grating lobes, from left to right, occur at approximately +5.75°, +4.00°, +2.25°, +0.50° (main beam), -1.25°, -3.00°, -4.75°, etc. The levels of the main beam and the highest side lobe correspond very closely to the calculated values of -0.82 dB and -5.0 dB, respectively, from the peak gain. The peak gain level was set at the -2.0 dB line on the recorder paper shown in figure 38.

The availability of variable phase shifters, the amount of phase shift attainable, and insertion losses of typical devices were also investigated in evaluating beam-steering characteristics. Both mechanical- and ferrite-type phase shifters are available from manufacturers specializing in millimeter wave test equipment. The ferrite devices have the disadvantage of high insertion losses and smaller bandwidths. The typical insertion loss for a 180° ferrite phase shifter can be expected to be 1.5 dB. Mechanical phase shifters use dielectric vanes and can be made to provide 360° of phase shift but are generally available with up to 180°. The insertion loss of 180° units is typically not less than 0.3 dB, while the maximum losses for 360° units go up to 1.0 dB. It is felt that the typical insertion losses for the phase shifters in an array feed network are high and lessen the desirability of the beam-steering feature.

The alternative to beam-steering a stationary array is to mount the array on a dual axis antenna positioner with drives and controls for positioning the array. Positioners and control systems have been highly developed, are readily available, but are expensive. A significant cost savings may be realized if the beam-steering techniques are used for fine control in conjunction with a coarse positioner or other forms of mounting the array. Such a technique would be useful for fine beam alignment in setting up communications links. The limits in array beam steering and the insertion losses of the phase-shifting devices must be considered for the particular application involved.



## SECTION VII

### LASER OPTICAL SIMULATOR

#### 1. TECHNIQUE

Optical simulation of antenna arrays is possible with a laser light source which produces the coherent energy similar to a microwave source. Figure 39 is a diagram of the experimental apparatus used to obtain the image of the far field diffraction pattern of a two-dimensional antenna array. The complex pattern of the side-lobe structure that is obtained on film gives a useful visual presentation which shows the planes of symmetry and the relative intensity of the side lobes. Similar experiments have been reported in reference 12.

The far field pattern of a two-dimensional antenna array can be described by the two-dimensional Fourier transform of the field distribution at the antenna aperture. The coherent optical image processing apparatus shown in figure 39 employs the two-dimensional Fourier transform property of a lens to produce the far field pattern of a simulated antenna array. The pattern thus formed is identical to the intensity distribution as the film does not preserve phase information and records as a function of incident intensity.

The apparatus consists of a source of monochromatic light energy, a laser, which is spatially filtered to remove beam noise. The energy is collimated by lens  $L_1$  and provides a Gaussian intensity distribution over the simulated antenna array pattern,  $O$ . A small fraction of the collimated beam covers the array so that uniform illumination is well approximated. The Fourier transform lens images the far field pattern of the array from infinity to the focal length of the lens,  $L_2$ .

Small photographic transparencies of different apertures were made and placed at the object plane. Simple objects such as circles and slits produce the classic diffraction patterns of concentric rings and interference fringes usually found in optics text books. Different arrays of circles show matrices of dots or pencil beams with different patterns of symmetry for the various array configurations. Although the scale factor  $d/\lambda$  for the arrays are not identical to that of the arrays simulated, accurate patterns are obtained because the basic structure of the pattern is preserved.

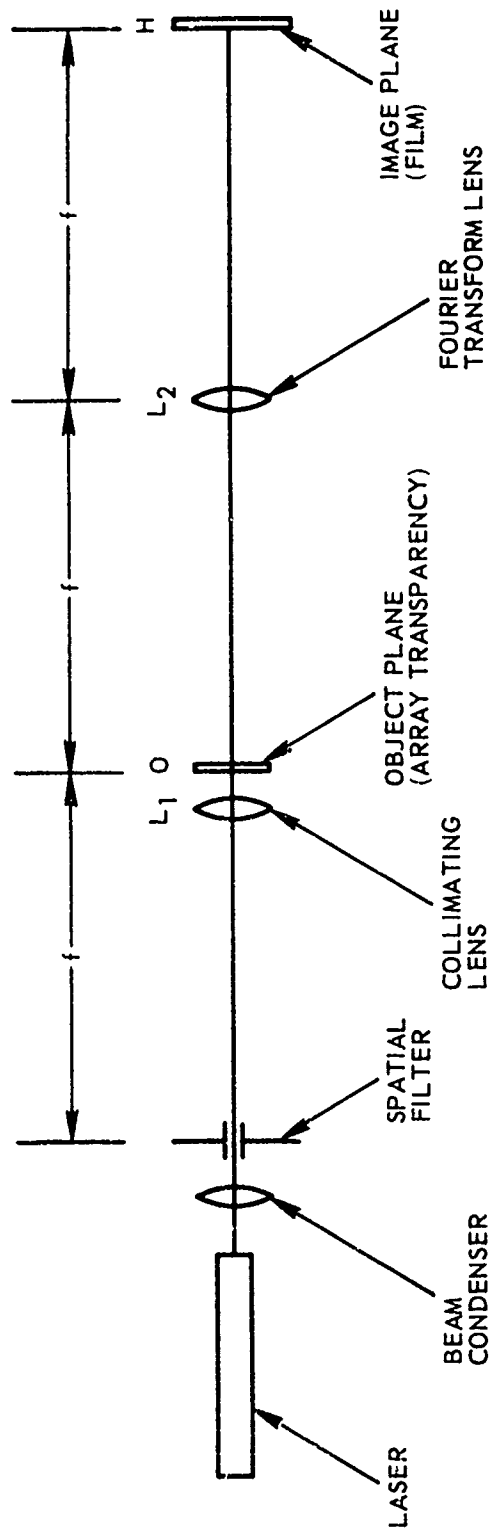


Figure 39. Coherent Optical Image-Processing Apparatus

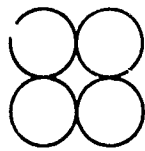
## 2. RESULTS

The different array configurations that were tested in the optical simulator are shown in figure 40. The four element configurations correspond to the array measurements performed at the microwave frequencies, and the larger arrays correspond to the system objectives. The significant differences are: The optical simulation has uniform amplitude in all planes while the microwave antennas are uniform in the E-planes but tapered in the H-planes. Also, the optical array elements are tangent circles while the microwave antennas have a 1-1/2 inch spacing between the 18-inch diameter apertures. Good correspondence is noted between the optical simulation and the microwave pattern measurements and calculations.

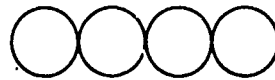
Variations in exposure times for the laser image on the film must be carefully controlled to obtain the significant main beam and first side-lobe structure. The tendency is to overexpose the central part of the pattern which shows the significant side-lobe levels down to approximately -25 dB. In general, a short exposure time shows the main beam and significant side lobes. Longer exposure times show the lesser side-lobe structure and are interesting because of their symmetry, but the levels are usually below the significant values for an antenna. Control of exposure time and measurement of relative intensity levels could be a subject for additional study. For example, color films tend to give better definition of wide variations in intensity because of the differences in sensitivity between the color layers on the film.

Two patterns taken of the 4 x 4 array are shown in figures 41 and 42 which demonstrate the effect of different exposure times. Figure 41 shows the main beam and the first three side lobes. Calculated results giving the relative side-lobe levels of this array are shown in the last line of figure 15. The fourth side lobe is calculated at -24.8 dB and did not appear on the exposure. Figure 42 shows a longer exposure which obscures the main beam but shows the symmetry of the lower level structure. Longer exposures continue to show the increasing matrix pattern.

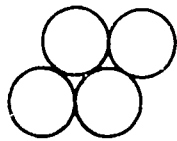
A promising array configuration that was not treated theoretically is the 12-element cross illustrated in figure 40. Its diffraction pattern appears in figure 43. The 14-element diamond pattern is shown in figure 44. The photograph obscures the main beam which has a circular cross section in the center. The calculated levels for different cuts through the diamond pattern are given in figure 15. The longer exposure shows a continuing six-sided arrangement of dots at the lower intensities.



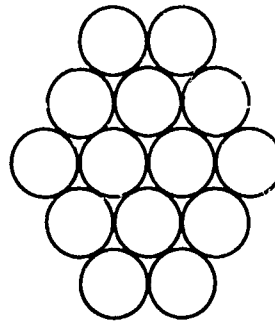
2 X 2



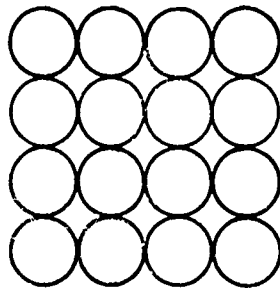
4 X 1



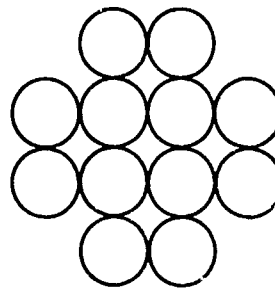
4 ELEMENT  
DIAMOND



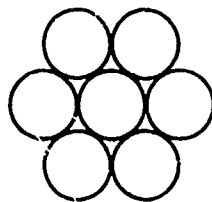
14 ELEMENT  
DIAMOND



4 X 4



12 ELEMENT  
CROSS



7 ELEMENT  
HEXAGON

Figure 40. Variations in Array Configurations

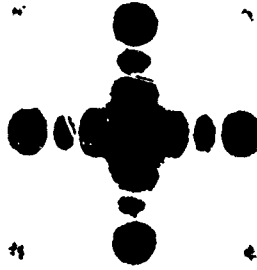


Figure 41. Diffraction Pattern of 4 x 4 Array, Short Exposure

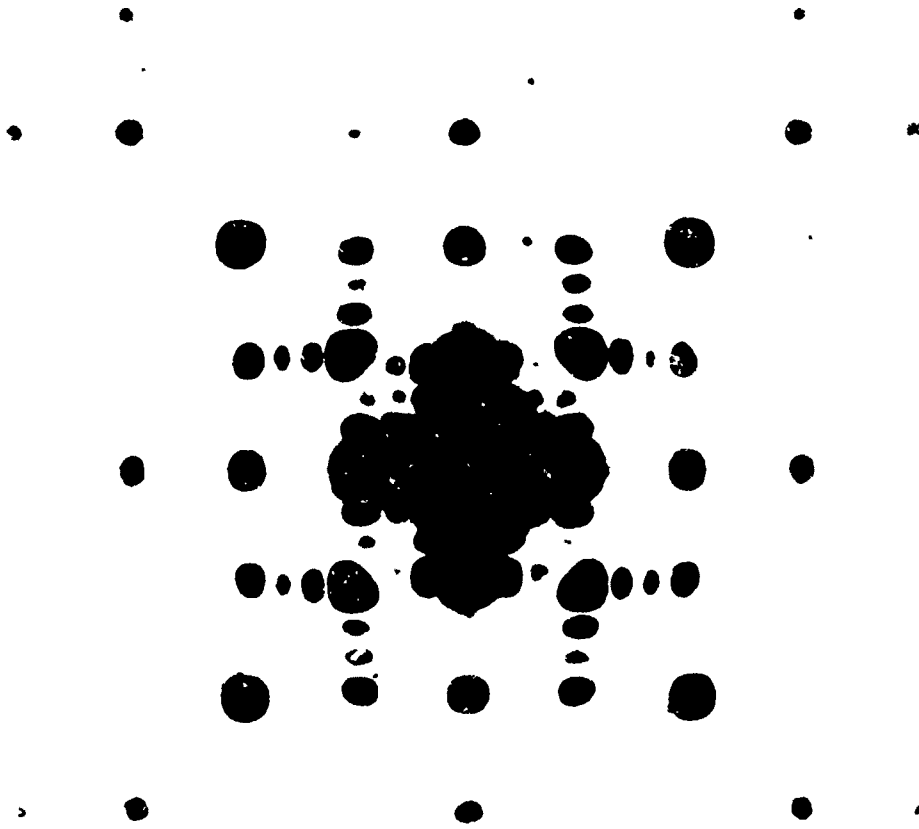


Figure 42. Diffraction Pattern of 4 x 4 Array, Long Exposure



Figure 43. Diffraction Pattern of 12-Element Cross

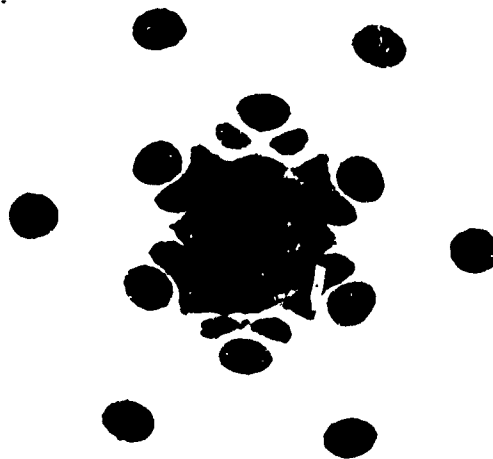


Figure 44. Diffraction Pattern of 14-Element Diamond

Patterns of the 2 x 2, 4 x 1, and 4-element diamond configurations that were also tested at microwave frequencies are shown in figures 45, 46, and 47, respectively. Figure 47 is a relatively long exposure which tends to blend the lobes together but the main features are discernible and can be compared to the theoretical results in figure 18. Experimental data at 20 GHz was obtained by taking principal plane cuts for the three arrays, and the results were substantially in agreement with the optically simulated patterns.

The 7-element hexagon is another configuration that was not treated theoretically during the study but showed promise as a useful antenna array by virtue of the optical simulation, figure 48. This type of array with closely spaced, overlapping apertures appears to be worthy of additional investigation to obtain high gain, low side-lobe performance.

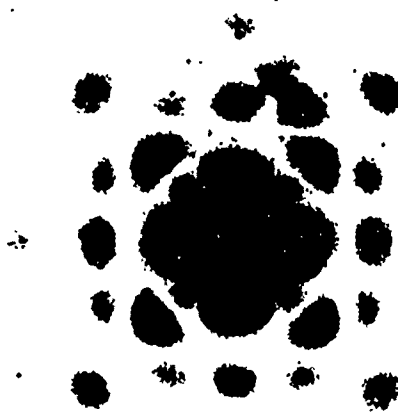


Figure 45. Diffraction Pattern of 2 x 2 Array



Reproduced from  
best available copy.

Figure 46. Diffraction Pattern of 4 x 1 Array

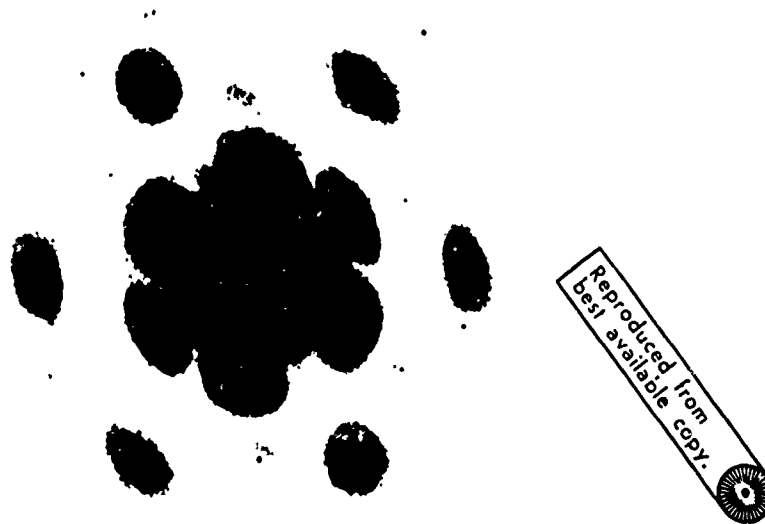


Figure 47. Diffraction Pattern of 4-Element Diamond

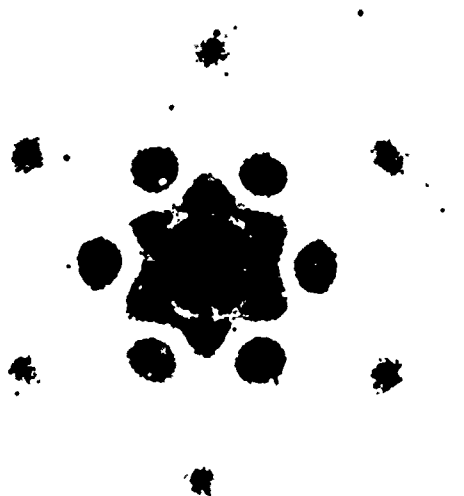


Figure 48. Diffraction Pattern of 7-Element Hexagon

## SECTION VIII

### CONCLUSIONS

1. The theory of design and design criteria for two-surface, dielectric lens-corrected horn elements and arrays of elements were applied to the practical development and accurate measurement of performance data under the study.
2. The dielectric lens with two refracting surfaces was designed and was fabricated of cross-linked styrene material. The computer design programs for the constant-amplitude aperture distribution and the conventional plano-convex design offered equivalent element performance. Aperture efficiency was 70% to 74.5% over an 18- to 36-GHz frequency bandwidth and approached maximum calculated values when used with surface-matching layers. Antenna pattern characteristics closely followed theoretical values.
3. The dielectric lens-corrected horn elements are excellent antennas for use in the 15- to 60-GHz frequency range and offer 3 to 1 advantages in fabrication tolerance that encourages operation at even higher frequencies. The lens is not frequency limited and bandwidth is determined by the feed design. The basic design is efficient, has no aperture blockage by the feed, has no spillover losses, and has very low wide angle side lobes.
4. Quarter-wave matching layers applied to both lens surfaces reduced reflections, increased efficiency to as high as 81.7% at design frequencies and did not degrade performance at other frequencies. This represents a 0.4 dB improvement which is nearly all the predicted loss. The reduction in side-lobe levels was as much as 2.5 dB at the design frequency but less than 1 dB at other frequencies. Any improvement in VSWR was obscured by the residual VSWR of the input feeds. The difficulty of fabricating matching layers for the outer, curved lens surface and the fragility of the layer must be weighed against the advantages. A flat layer on the inner side of the lens is easier to construct and is protected but has approximately one-half the advantages of layers on both surfaces.
5. Analytical methods of determining array performance were programmed and computations of array performance were run. Spacing between array elements must be minimized to keep side-lobe levels low and maintain high efficiency. Improved performance can be obtained from array configurations which have a more compact grouping of the element apertures and provide a tapered amplitude distribution while still feeding all array elements equally. A 14-element, diamond-shaped array offers the type of improved array performance desired for the system objective.

6. Experimentation with other array configurations was performed with a laser optical simulator, and a continuation of the theoretical array design analysis is suggested. The optical simulator produces a record on film of the two-dimensional array diffraction pattern as viewed in the plane of the array. This is a useful analytical tool that could be developed further.

7. Consideration was given to electronic beam steering with the arrays. The lens-corrected horns are electrically large apertures; this means that the array factor has narrow, closely spaced, grating lobes and severe limitations in the beam-steering capabilities. Beam steering was limited to one-half the grating lobe spacing or  $0.85^\circ$  at 20 GHz for the four-element array. Low-loss phase shifting devices and low-loss feed networks are needed to steer the array beam and maintain the high element efficiency. Beam steering appears to be most useful for making fine alignment adjustments coupled with a coarse mount.

## SECTION IX

### RECOMMENDATIONS

1. The dielectric lens-corrected horn antenna is a high-gain, broad-band, low-loss, antenna having nearly optimum aperture efficiency and is recommended for use in the upper microwave frequencies, approximately 15 GHz and above.
2. The antenna has many desirable features to recommend its use such as: no aperture blockage by the feed; low back- and side-lobe levels beyond the narrow main pattern; and built-in weather protection; and it can be fabricated to close tolerances needed for millimeter wave applications.
3. The use of quarter-wave surface matching layers on the lens offers a 5% to 7% improvement in efficiency and some improvements in side-lobe levels at the design frequency.
4. Arrays of these elements offer high gain capability where relatively high side-lobe levels do not affect system capability as in the case of satellite links. High efficiency and gain can be maintained for arrays if lens surface-matching layers are used and the insertion losses of the feed network are minimized.
5. Further study, using the analytical methods and data obtained during this program, is recommended to determine optimum array configurations having low side-lobe structures and high array efficiencies.
6. The laser optical simulator for array pattern analysis is recommended as a useful analytical technique which should be developed further.
7. Electronic beam steering of arrays of these electrically large aperture-sized elements is limited to very small angles, and low-loss phase shifting devices are needed for high efficiency. The beam-steering techniques can be used for making fine alignments to more coarse settings.
8. Applications which utilize single elements or several elements independently will make optimum use of the desirable features of the high-gain, lens-corrected horns. Such applications might involve tracking systems that use amplitude comparison or lobe switching techniques.

## APPENDIX I

### COMPUTER PROGRAM FOR CONSTANT-AMPLITUDE LENS DESIGN

This program was originally developed by J. F. Kauffman and described in technical report No. RADC-TR-70-109 dated July 1970. The program was modified by W. V. Goodell and J. Kuhns of the Melpar Division of LTV Electrosystems, Inc., in June 1971. The program is written in FORTRAN II for use in Melpar's terminal for the IBM-360/25 computer. It calculates the nonspherical X and Y coordinates of the two surfaces of a dielectric microwave lens. The lens is designed to have uniform amplitude and phase distribution across its aperture. The computations are based upon a point source radiator at the lens focus which provides spherical waves of constant intensity over the angle subtended by the lens. The geometry of the problem is depicted in figure 2.

Input data consists of indices of refraction (ADEX) and the included half angles of the lens subtended at the feed (DEG). The program performs the following operations, with referenced equation numbers referring to the original report, reference 1: A trial value of  $\theta_0$  is entered (TH) and an initial value generated by a Newton-Raphson method (equation 58). The differential equation (equation 48) of the first surface is integrated by a fourth order Runge-Kutta integration within which the repeated value of  $\theta$  is computed by a Newton-Raphson subroutine called NEWT. The second surface is computed by equations 51 and 52 using values of C1 through C4.

The data output tables of X and Y coordinates for each of the two surfaces start at the maximum value of the included half angle and end on the axis of the lens. Values of Y for each surface are referred to zero at the intersection of the second surface at the lens axis. The first surface is that surface nearest the focal point of the lens. A copy of the program and a typical data printout are given in the following pages of this appendix.

C THIS DECK MUST BE USED WITH THE IBM-360/25  
 C  
 C PROGRAM TITLED DIELECTRIC LENS DESIGN  
 C PROGRAM AUTHOR DR. J. F. KAUFMAN, UNC, RALEIGH, N.C., MODIFIED BY  
 C W.V. GOODELL AND J. KUNNS OF HELPAR/LTV ELECTROSYSTEMS, INC.  
 C THE PROGRAM WAS ORIGINALLY DEVELOPED AND DESCRIBED IN RADG-TR-70-100  
 C OF JULY 1970.

C HOW TO USE THE PROGRAM  
 C THE PROGRAM IS WRITTEN IN FORTRAN 2 FOR USE IN HELPARS 503-910. IT COMPUTES  
 C THE NON-SPHERICAL CONTOURS OF A DIELECTRIC LENS. INPUT DATA CONSIST OF  
 C FIVE (5) INDICES OF REFRACTION (ADEN) AND ELEVEN (11) INCLUDED HALF-  
 C ANGLES OF THE LENS SUBTENDED AT THE FEED (DEG).  
 C WHAT THE PROGRAM DOES  
 C A TRIAL VALUE OF THETA ZERO IS ENTERED (TH) AND AN INITIAL VALUE GEN-  
 C ERATED BY A MENTON - RAPHSON METHOD (EQ 5B). THE DIFFERENTIAL EQUATION  
 C (EQ 4B) OF THE FIRST SURFACE IS INTEGRATED BY A FOURTH ORDER RUNGE-KUTTA  
 C INTEGRATION WITHIN WHICH THE REPEATED VALUE OF THETA IS COMPUTED BY A  
 C MENTON-RAPHSON SUB-ROUTINE CALLED ABNT. THE SECOND SURFACE IS COMPUTED  
 C BY EQUATIONS 5I AND 5J USING VALUES OF CI THROUGH C4. THE PROGRAM  
 C COMPUTES A FAMILY OF 11 LENS CONTOURS PER INDEX FOR 5 INDICES FOR A  
 C GRAND TOTAL OF 55 LENS COMBINATIONS.  
 C LIST OF VARIABLES  
 C DEL - MAXIMUM APERTURE ANGLE  
 C TH - INDEPENDENT VARIABLE OF THETA ZERO  
 C H - INCREMENT OF INDEPENDENT VARIABLE ALPHA  
 C Y - DEPENDENT VARIABLE R  
 C RC - RADIAL COORDINATE AT ALPHA ZERO  
 C DIMENSION X(100),Y(100),Z(100),XP(200),YP(200),LINE(100),DEG(11),  
 C IADEN(5)

C0001 PRINT 153  
 C0002 FORMAT (1M1)  
 C0003 114X, INDEX OF REFRACTION N=,F5.3/  
 C0004 2) ELECTRO-OPTICS LABORATORY, 23X, PACC/GAFB, 27X, DIAMETER OF LENS  
 C 3 (INCHES) D=,F5.1/5X, APRIL-MAY 1971, 22X, TOTAL SUBTENDED ANGLE  
 C 4 (DEGREES) 2 =,F5.1/5X, THICKNESS OF LENS AT VERTEX (INCHES) T=  
 C 5,F6.2)

C0005 FCMPAT(1M0), THIS DIELECTRIC LENS IS DESIGNED TO GIVE A UNIFORM AMP  
 C 1LITUDE AND PHASE DISTRIBUTION ACROSS THE APERTURE. THE LENS WATER  
 C 2IAL IS, ° RECNLITE 1422 WITH INDEX OF REFRACTION, N=1.59 FROM 3-2  
 C 3000 GHz. VALUES OF X,Y FOR EACH SURFACE ARE REFERRED TO THE SECOND  
 C 477° SURFACE WHICH IS ZERO TO THE FIRST SURFACE WHICH IS A POSITIVE  
 C 5 NUMBER. TABLES OF X,Y FOR EACH SURFACE START AT THE MAXIMUM VALUE  
 C 67% OF THE INCLUDED HALF-ANGLE, ° AND END ON THE AXIS AT =0.777)

C0006 159  
 C0007 FCMPAT(1M0)  
 C0008 01A=20.0  
 C0009 READ 165,ADEN  
 C0010 169 FORMAT(5F10.3)  
 C0011 READ 170,DEG  
 C0012 170 FORMAT (11F7.1)  
 C0013 00, 201, 6-155  
 C A=ADEN(1)

```

0014      DD_200 N=1,11
C
C      INITIAL VALUE OF THETA IS COMPUTED USING TRIAL VALUE (TH) WITH NEWTON-
C      RAPHSON ROUTINE (NEWTON THETA)
C
C      CONVERT DEGREES TO RADIANS
0015      DEL=DEG(1)/57.2957795
C
0016      IF(DEL) 5,200,9
C      MAXIMUM VALUE OF RADIUS OF LENS
0017      E=SI(DEL)
C
C      TOTAL INCLUDED ANGLE DEL
0018      ANGLE=2*DEL
C
C      VERTEX THICKNESS
0019      T=(1-COS(DEL))/(A-1)
C
C      SCALE LENS TO .10 INCH RADIUS
0020      THICK=TOIG/E
0021      PRINT 156,A,CIA,ANGLE,THICK
0022      PRINT 155
0023      PRINT 156
0024      FORMAT (15X,'THETA 0')
0025      CO=1-(A-1)*E
0026      SI=SQRT(1-CO*CO)
C
C      COMPUTATION OF THETA ZERO
C
C      TRIAL INITIAL VALUE OF THETA ZERO
0027      TH=3
0028      B=1-CO
0029      DO 10 J=1,7
0030      CA=COS(TH)-1/A
0031      ARG=DEL-J*PI
0032      TOP1=B*CA/2-SI*SI(TH)
0033      BOT1=-SI(TH)*B-SI*CA
0034      TOP2=SI(ARC)
0035      BOT2=A-COS(ARC)
0036      FU=TOP1/BCT1-TOP2/BOT2
0037      TOP3=-B*SI(TH)/2-SI*CO(TH)
0038      TCP4=-B*CO(TH)+SI*SI(TH)
0039      FUP=TOP3/BOT1-TCP4/BOT2+(3*BOT1*BOT2)/(SI*CO(TH)+SI*SI(TH))
1002
0040      TO=TH-FU/FUP
0041      PRINT 105,TC
0042      FORMAT(10X,F12.9)
0043      TH=TO
C
C      FIRST SURFACE COMPUTATION
0044      M=(DEL+CO*CO)/100
0045      XI=DEL
C
C      NORMALIZED VALUE OF REAR

```

```

003  PORTMAN IV 340N-PC-473 3-4      MAINPCH      DATE 09/09/71      TIME          PAGE 0003

0044      Y1=1.0
0047      Z1=51N170)
0048      SQ=SQRT(1-2J*Z1)
0049      B=10*(A-1)
0050      M2=M/2
0051      C=SIN(X1)/SQRT(1-COS(X1))
0052      DD 75  J=1,100

C
C  START OF RUNGE-KUTTA INTEGRATION. SEE SCARBOROUGH, P. 299
0053      FUN=V1*AOZ1/(AO50-1)

C
C  COMPUTE R0
0054      Y1=HOFUM1
0055      X1=X10H2
0056      Y1=V1*Y1/2

C
C  CALL NENTCH-RAPSCN FOR COMPUTING THETA. SEE SCARBOROUGH, P. 192
0057      CALL NENT(X1,Y1,Z1,A,B,C,SQ)
0058      FUN2=Y1*AOZ1/(AO50-1)

C
C  COMPUTE M1
0059      T2=HOFUM2
0060      Y1=V1-T1/2+T2/2
0061      CALL NENT(X1,Y1,Z1,A,B,C,SQ)
0062      FUN3=Y1*AOZ1/(AO50-1)

C
C  COMPUTE M2
0063      T3=HOFUM3
0064      X1=X10H2
0065      Y1=V1-T2/2+T3
0066      CALL NENT(X1,Y1,Z1,A,B,C,SQ)
0067      FUN4=Y1*AOZ1/(AO50-1)

C
C  COMPUTE M3
0068      T4=HOFUM4

C
C  COMPUTE EQ. 68 FOR R'(H0)
0069      Y1=V1-T3+T1+2*T2+T3+T4)/4
0070      CALL NENT(X1,Y1,Z1,A,B,C,SQ)

C
C  LOAD AN ARRAY FOR PLOTTING ROUTINE
0071      X(J)=X1
0072      Y(J)=Y1
0073      Z(J)=Z1
0074      CONTINUE
0075      PRINT 107,Y(100)
0076      FORMAT (1H0,5X,'R0 =',F8.5,' MMAR')

C
C  SECOND SURFACE CONTOUR COMPUTATION
0077      DD=V1/100)
0078      PRINT 153
0079      PRINT 154,A,DI,ANGLE,THICK
0080      PRINT 157
0081      PRINT 160
0082      FORMAT(22X,'X SURF. 1',13X,'Y SURF. 1',12X,' X SURF. 2',13X,'Y SUR

```



```

0001      SUBROUTINE NENT(X,Y,Z,A,B,C,IQ)
0002      C SUBROUTINE NENT
0003      SQ=SQRT(1-Z**2)
0004      BOT1=A-SQ*CCS(X)-Z*SIN(X)
0005      TOP2=C*SQRT(1-COS(X))-YOS(RTX)
0006      BOT2=B-Y*(1-COS(X))
0007      F=TOP1/BOT1-TOP2/BOT2
0008      TOP3=-(Z*SIN(X)+SQ*CCS(X))
0009      TOP4=Z*CCS(X)-SQ*SIN(X)
0010      FP=TOP3/(SQ*BOT1)-TOP2*TOP4/(SQ*BOT1*BOT1)
0011      W=Z-F/FP
0012      V=ABS(Z-W)
0013      IF(V-.000001)10,10,11
0014      Z=W
0015      GO TO 15
0016      SQ=SQRT(1-M**2)
0017      Z=W
0018      RETURN
0019      END

```

HELPAR/LIVELECTROSYSTEMS  
ELECTRO-OPTICS LABORATORY

DIELECTRIC LENS DESIGN  
RADC/GAFB  
APRIL-MAY 1971

INDEX OF REFRACTION N=1.590  
DIAMETER OF LENS (INCHES) D= 20.0  
TOTAL SUBTENDED ANGLE (DEGREES) 2 $\theta$ = 45.0  
THICKNESS OF LENS AT VERTEX (INCHES) T= 3.37

	X SURF. 1	Y SURF. 1	X SURF. 2	Y SURF. 2
1	9.88632	3.01931	9.90127	2.94216
2	9.77304	3.01716	9.80250	2.88160
3	9.66920	3.03333	9.70685	2.82104
4	9.56581	3.03732	9.60597	2.76048
5	9.46242	3.04393	9.50705	2.70387
6	9.35903	3.05049	9.40803	2.64597
7	9.25564	3.05200	9.30910	2.58874
8	9.15225	3.06345	9.21008	2.53217
9	9.04886	3.06985	9.11102	2.47627
10	8.94547	3.07620	9.01192	2.42103
11	8.84208	3.08249	8.91275	2.36646
12	8.73869	3.08872	8.81363	2.31256
13	8.63530	3.09490	8.71443	2.25928
14	8.53191	3.10102	8.61520	2.20668
15	8.42852	3.10708	8.51594	2.15473
16	8.32513	3.11308	8.41664	2.10343
17	8.22174	3.11902	8.31731	2.05279
18	8.11835	3.12491	8.21795	2.00279
19	8.01496	3.13073	8.11856	1.95344
20	7.91157	3.13650	8.01914	1.90474
21	7.80818	3.14220	7.91969	1.85668
22	7.70479	3.14784	7.82020	1.80924
23	7.60140	3.15342	7.72069	1.76249
24	7.49801	3.15894	7.62115	1.71635
25	7.39462	3.16439	7.52158	1.67085
26	7.29123	3.16978	7.42198	1.62599
27	7.18784	3.17511	7.32235	1.58177
28	7.08445	3.18037	7.22270	1.53817
29	6.98106	3.18557	7.12301	1.49521
30	6.87767	3.19070	7.02330	1.45288
31	6.77428	3.19577	6.92357	1.41119
32	6.67089	3.20077	6.82380	1.37012
33	6.56750	3.20571	6.72401	1.32967
34	6.46411	3.21057	6.62420	1.28985
35	6.36072	3.21537	6.52436	1.25066
36	6.25733	3.22011	6.42450	1.21209
37	6.15394	3.22477	6.32461	1.17414
38	6.05055	3.22937	6.22469	1.13682
39	5.94716	3.23390	6.12474	1.10011
40	5.84377	3.23836	6.02476	1.06402
41	5.74038	3.24275	5.92478	1.02855
42	5.63699	3.24708	5.82478	99.265
43	5.53360	3.25133	5.72474	95.946
44	5.43021	3.25551	5.62472	92.532
45	5.32682	3.25962	5.52467	89.122
46	5.22343	3.26366	5.42457	85.714
47	5.12004	3.26761	5.32443	82.308

48	4.94488	3.25161	5.12244	.79746
49	4.84638	3.27153	5.12633	.76689
50	4.74808	3.29141	5.02514	.73632
51	4.64998	3.27912	4.92401	.70758
52	4.55207	3.28280	4.82292	.67883
53	4.45434	3.28661	4.72281	.65069
54	4.35681	3.28995	4.62338	.62316
55	4.25956	3.29342	4.52414	.59623
56	4.16257	3.29681	4.42258	.56990
57	4.06586	3.30013	4.32260	.54417
58	3.96843	3.30338	4.22240	.51905
59	3.87125	3.30655	4.12199	.49453
60	3.77523	3.30965	4.02167	.47061
61	3.67887	3.31268	3.92132	.44729
62	3.58267	3.31563	3.82096	.42457
63	3.48661	3.31850	3.72059	.40244
64	3.39069	3.32131	3.62020	.38092
65	3.29491	3.32403	3.51980	.35999
66	3.19927	3.32669	3.41939	.33966
67	3.10376	3.32926	3.31896	.31992
68	3.00837	3.33177	3.21852	.30077
69	2.91312	3.33419	3.11807	.28223
70	2.81797	3.33654	3.01760	.26427
71	2.72295	3.33882	2.91712	.24691
72	2.62804	3.34102	2.81663	.23015
73	2.53323	3.34314	2.71614	.21397
74	2.43853	3.34519	2.61563	.19839
75	2.34393	3.34716	2.51511	.18340
76	2.24942	3.34906	2.41458	.16900
77	2.15501	3.35087	2.31404	.15520
78	2.06068	3.35262	2.21349	.14198
79	1.96644	3.35428	2.11294	.12935
80	1.87228	3.35587	2.01237	.11731
81	1.77819	3.35738	1.91180	.10587
82	1.68418	3.35881	1.81122	.09501
83	1.59023	3.36017	1.71063	.08474
84	1.49635	3.36145	1.61004	.07506
85	1.40254	3.36265	1.50944	.06596
86	1.30877	3.36378	1.40884	.05746
87	1.21507	3.36483	1.30823	.04954
88	1.12144	3.36580	1.20761	.04221
89	1.02779	3.36669	1.10699	.03546
90	.93422	3.36751	1.00637	.02931
91	.84065	3.36825	.90574	.02374
92	.74719	3.36891	.80511	.01874
93	.65372	3.36949	.70447	.01436
94	.56028	3.37000	.60383	.01055
95	.46686	3.37043	.50319	.00733
96	.37346	3.37077	.40255	.00462
97	.28008	3.37105	.30191	.00264
98	.18670	3.37124	.20127	.00117
99	.09334	3.37136	.10062	.00029
100	.00002	3.37140	.00007	.00000

## APPENDIX II

### COMPUTATION OF APERTURE AMPLITUDE DISTRIBUTION FOR A PLANO-CONVEX LENS

This computer program was written to determine the X and Y coordinates and to calculate the amplitude distribution across the aperture of a two-surface, plano-convex lens. The geometry of the problem is presented in figure 2. References 3 and 4 were used to set up the basic equations. Constant increments of  $\theta$  were chosen for the incident ray and the (X, Y) coordinates were then calculated for the "entrance ray," at  $(X_{1k}, 0)$ , and the "exit ray," at  $(X_{2k}, Y_{2k})$ , where k ranged from 0 to 45 for a range of  $\theta$  from 0 to 22.5° and the  $\Delta\theta$  was chosen as 0.5°. Therefore, for equal angle spacing of entrance rays, we calculate the distance between two adjacent exit rays and compare their separation to the separation of two exit rays adjacent to the Y axis. If this ratio has the value of one throughout the range of  $\theta$ , then the lens has a uniform or constant amplitude distribution across its aperture.

The equations used are stated below. The focal length f is determined by:

$$f = \frac{X_1 \text{ max}}{\tan \theta_0}$$

where  $X_1 \text{ max}$  is the maximum radius of the lens and  $\theta_0$  is one-half the total subtended angle. The X coordinate of the entrance ray is determined by:

$$X_{1k} = f \tan \theta_k$$

where  $\theta_k$  is the particular angle the entrance ray makes with the axis of the lens, leaving the focal point.

The maximum thickness of the lens is then found by:

$$t = \frac{(f^2 + X_{1 \text{ max}}^2)^{1/2}}{n - 1}$$

where n is the index of refraction of the lens material, and the other factors have already been determined.

The X and Y coordinates of the exit ray can now be determined. For the Y coordinate,

$$Y_{2k} = \left[ \frac{(n-1) t + f - (f^2 + X_{1k}^2)^{1/2}}{n - \left(1 - \frac{X_{1k}^2}{n^2 (f^2 + X_{1k}^2)}\right)^{1/2}} \right] \left[ 1 - \frac{X_{1k}^2}{n^2 (f^2 + X_{1k}^2)} \right]^{1/2}$$

This equation is the same as the one illustrated in figure 14.2 (e) in reference 4 except for the transposing of the X and Y coordinates. This was done to be consistent with the previous work in reference 1.

The X coordinate is then obtained by using the following expression:

$$X_{2k} = X_{1k} \left\{ 1 + \frac{Y_{2k}}{\left[ n^2 (f^2 + X_{1k}^2) - X_{1k}^2 \right]^{1/2}} \right\}$$

These equations are true for the case where the index of refraction is greater than 1.

To determine the amplitude distribution from the above data, we calculate a new term called W.

$$W = \frac{X_{2k} - X_{2(k-1)}}{X_{2_1}}, \text{ for } k = 0, 1, 2, \dots 45.$$

To convert this to dB, we use,

$$W \text{ (dB)} = 20 \log (W).$$

**This program was run using the following input data:**

$$X_1 \text{ max} = 10 \text{ inches}$$

$$\theta = 0.5^\circ$$

$$\theta_0 = 0^\circ$$

$$\theta \text{ max} = 22.5^\circ$$

$$n = 1.590$$

**The program is presented on the following pages.**

JUN 30 1971

....

```

▲JOB
▲REWIND MT1,
▲ASSIGN S=MT0,S1=CR,L0=LP,B0=MT1,
▲FORTRAN SI,L0,B0,
. 1 C PLAN0-CONVEX DIELECTRIC LENS
. 2 C THIS PROGRAM CALCULATES THE ERROR INTRODUCED IN THE APERTURE
. 3 C DISTRIBUTION WHEN USING A PLANO-CONVEX INSTEAD OF A LENS
. 4 C CALCULATED FOR UNIFORM APERTURE DISTRIBUTION
. 5 C ETA=INDEX OF REFRACTION 1.590
. 6 C D= DIAMETER OF LENSE [INCHES] = 2*XMAX
. 7 C T= THICKNESS OF LENS AT THE AXIS [INCHES]
. 8 C TH1= LOWER LIMIT ON ANGLE [DEGREES] 0
. 9 C TH2= UPPER LIMIT ON ANGLE [DEGREES] 22.5
. 10 C DELTA= INCREMENT OF THETA [DEGREES] 0.5
. 11 C XMAX= RADIUS OF LENSE [INCHES] 10
. 12 C DIMENSION X2[0/100]
. 13 C PI=3.141593
. 14 C READ INPUT DATA
. 15 C READ 10, XMAX, TH1, TH2, DELTA, ETA
. 16 10 FORNAT [5F12.6]
. 17 C RTH1=PI*TH1/180
. 18 C RTH2=PI*TH2/180
. 19 C RDELTA=PI*DELTA/180
. 20 C CALCULATE F
. 21 C F=XMAX/[SIN[RTH2]/COS[RTH2]]
. 22 C CALCULATE T
. 23 C T= [SORT[F**2*XMAX**2].F]/[ETA-1.]
. 24 C ANG=2.*TH2
. 25 C PRINT HEADING
. 26 C PRINT 20, ETA, T, ANG
. 27 20 FORMAT [1H1, INDEX OF REFRACTION >, F6.3/1X, $THICKNESS OF
. 28 1LENS>, F5.1, $INCHES$/1X, $TOTAL SUBTENDED ANGLE>,
. 29 2F5.1, $DEGREES$//)
. 30 C PRINT 21
. 31 21 FORMAT [1H0, $THETA$, 4X, $X1 [INCHES]$, 2X, $X2 [INCHES]$, 2X,
. 32 1 $Y2 [INCHES]$, 2X, $W [RATIO]$, 2X, $W [DB]$///)
. 33 C COMPUTE NUMBER OF ITERATIONS
. 34 C NT=(RTH2-RTH1)/RDELTA
. 35 C THETA=RTH1
. 36 C THETR=RTH1
. 37 C DO 30 K=0,NT
. 38 C X1=F*SIN[THETR]/COS[THETR]
. 39 C P=ETA**2*[F**2+X1**2]
. 40 C A=[ETA-1.]*T+F-SQRT[F**2+X1**2]
. 41 C B=ETA-SQRT[1.-X1**2/P]
. 42 C C=SQRT[1.-X1**2/P]
. 43 C Y2=A*C/B
. 44 C X2[K]=X1+[1.+Y2/SQRT[P.X1**2]]
. 45 C CALCULATE W
. 46 C [F[K] 31,31,35
. 47 35 W=[X2[K]-X2[K-1]]/[X2[1]-X2[0]]
. 48 C W=ABS[W]
. 49 C WDB=20.*ALOG[W]*[0.43429 ]

```

```

• 50 31 PRINT 40,THETA,X1,X2(K),Y2,W,WDB
• 51 40 FORMAT(1X,F4.1,4X,F7.4,5X,F7.4,5X,F7.4,5X,F7.4)
• 52 1 2X,F7.4)
• 53 THETA=THETA+DELTA
• 54 THETR=THETR+RDELTA
• 55 30 CONTINUE
• 56 END

```

PROGRAM ALLOCATION

00013 X2	00325 NT	00326 K	00327 PI
00331 XMAX	00333 TH1	00335 TH2	00337 DELTA
00341 ETA	00343 RTH1	00345 RTH2	00347 RDELTA
00351 F	00353 T	00355 ANG	00357 THETA
00361 THETR	00363 X1	00365 P	00367 A
00371 B	00373 C	00375 Y2	00377 W
00401 WDB			

SUBPROGRAMS REQUIRED

SIN	COS	SQRT	ABS	ALOG
THE END				

INDEX OF REFRACTION > 1.590  
 THICKNESS OF LENS > 3.4 INCHES  
 TOTAL SUBTENDED ANGLE > 45.0 DEGREES

THETA	X1(INCHES)	X2(INCHES)	Y2(INCHES)	W(RATIO)	W(DB)
.0	.0000	.0000	3.3714	.0000	.0000
.5	.2107	.2292	3.3697	1.0000	.0000
1.0	.4214	.4583	3.3646	.9999	-.0009
1.5	.6322	.6874	3.3561	.9997	-.0027
2.0	.8431	.9165	3.3443	.9994	-.0053
2.5	1.0541	1.1454	3.3290	.9990	-.0089
3.0	1.2652	1.3743	3.3104	.9985	-.0133
3.5	1.4766	1.6029	3.2884	.9979	-.0186
4.0	1.6882	1.8315	3.2630	.9972	-.0248
4.5	1.9000	2.0598	3.2342	.9963	-.0318
5.0	2.1122	2.2880	3.2021	.9954	-.0397
5.5	2.3246	2.5159	3.1666	.9944	-.0485
6.0	2.5374	2.7435	3.1277	.9933	-.0581
6.5	2.7506	2.9709	3.0855	.9921	-.0685
7.0	2.9643	3.1980	3.0399	.9909	-.0797
7.5	3.1784	3.4247	2.9910	.9895	-.0918
8.0	3.3930	3.6512	2.9387	.9880	-.1047
8.5	3.6081	3.8773	2.8832	.9865	-.1183
9.0	3.8237	4.1030	2.8242	.9848	-.1327
9.5	4.0400	4.3283	2.7620	.9831	-.1479
10.0	4.2569	4.5532	2.6964	.9813	-.1638
10.5	4.4745	4.7776	2.6276	.9794	-.1805
11.0	4.6928	5.0017	2.5554	.9775	-.1979
11.5	4.9118	5.2252	2.4799	.9754	-.2159
12.0	5.1316	5.4483	2.4012	.9733	-.2346
12.5	5.3522	5.6708	2.3192	.9712	-.2540
13.0	5.5737	5.8929	2.2339	.9689	-.2740
13.5	5.7960	6.1144	2.1453	.9666	-.2947
14.0	6.0193	6.3354	2.0535	.9643	-.3159
14.5	6.2436	6.5559	1.9585	.9619	-.3377
15.0	6.4689	6.7758	1.8602	.9594	-.3600
15.5	6.6952	6.9951	1.7586	.9569	-.3828
16.0	6.9226	7.2138	1.6539	.9543	-.4062
16.5	7.1512	7.4319	1.5459	.9517	-.4300
17.0	7.3810	7.6494	1.4347	.9491	-.4542
17.5	7.6120	7.8663	1.3202	.9464	-.4788
18.0	7.8443	8.0825	1.2026	.9436	-.5038
18.5	8.0778	8.2982	1.0818	.9409	-.5292
19.0	8.3128	8.5132	.9578	.9381	-.5549
19.5	8.5492	8.7275	.8305	.9353	-.5808
20.0	8.7870	8.9412	.7001	.9325	-.6070
20.5	9.0264	9.1543	.5665	.9297	-.6335
21.0	9.2673	9.3667	.4296	.9268	-.6601
21.5	9.5098	9.5784	.2896	.9240	-.6868
22.0	9.7541	9.7896	.1464	.9211	-.7136
22.5	10.0000	10.0000	.0000	.9183	-.7406

## APPENDIX III

### APERTURE EFFICIENCY VERSUS AMPLITUDE DISTRIBUTIONS

#### 1. THEORETICAL INVESTIGATION

Antenna patterns and gain have been calculated for rectangular and circular apertures having various amplitude illuminations. The standard reference on this subject is reference 3, chapter 6, and several examples have been worked out. These examples are not sufficient to analyze the expected results for the present lens-corrected horn application. A more detailed treatment of the subject is reference 10 in which families of aperture distributions have been studied and the integrations carried out to provide the theoretical efficiencies of circular apertures. The theory utilized here makes the basic assumptions that phase errors are negligible, aperture blocking is not a factor, and spillover losses are not present. These assumptions are considered valid for the case of lens-horn antennas but could not be assumed for conventional parabolic dish antennas.

Typical aperture distributions are shown in figure 49. It will be seen that the functions  $e^{-pr^2}$  apply most nearly to typical E-plane illuminations while the functions  $(1-r^2)^p$ , in which the edge illumination drops essentially to zero, are typical of H-plane illuminations. The aperture efficiency for varying values of  $p$  for these functions has been calculated and is given in reference 10. Figure 50 is a plot of the efficiency curves, with a dB scale for corresponding percentages.

#### 2. MEASURED DATA

Measurements were made of the amplitude distributions across the front of the lens-horn antennas. These measurements were accomplished by traversing a small pickup horn across the E and H planes (vertical and horizontal) and measuring the relative received power levels. The plane of measurement was taken at 4 inches from the center of the lens which is considered as being in the near-zone region with characteristics, as described by Silver in reference 3, pages 170 and 171. The measurement data are given in figures 51 through 54. The shape of the plotted amplitudes corresponds to the characteristic features shown in reference 11, page 173, figure 6.2(a).

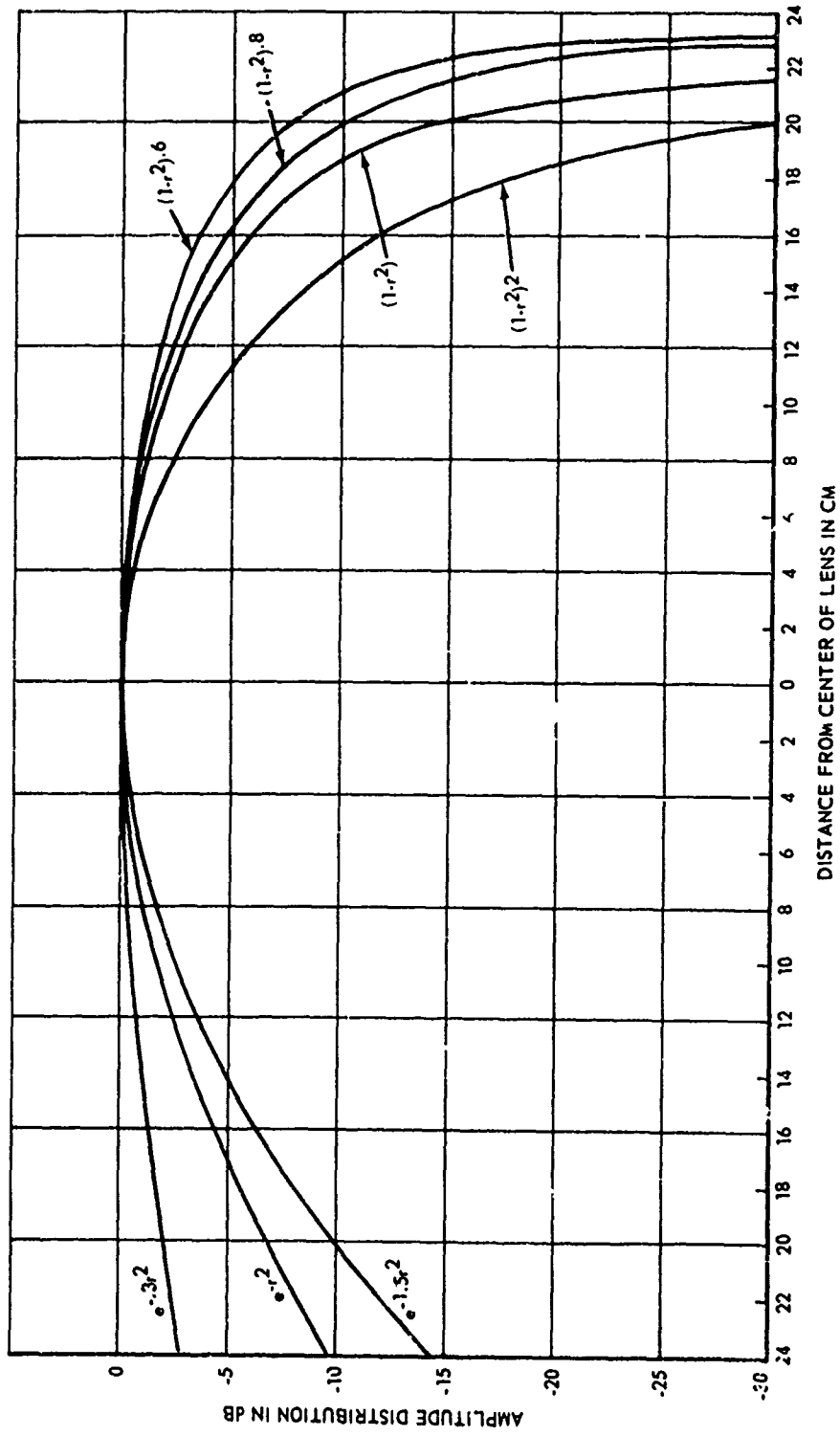


Figure 49. Typical Aperture Distribution Functions

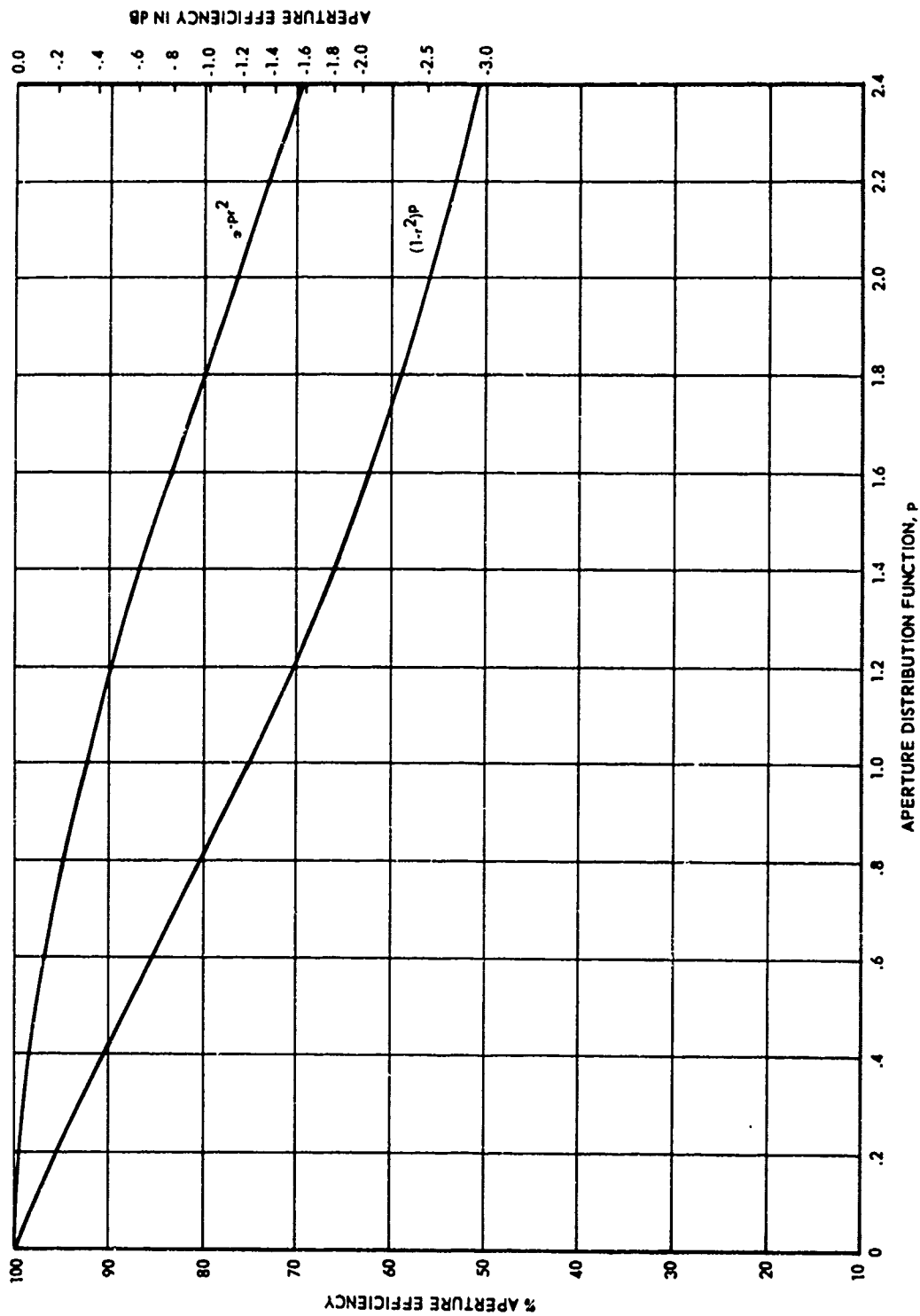


Figure 50. Aperture Efficiency Relative to Uniform Illumination

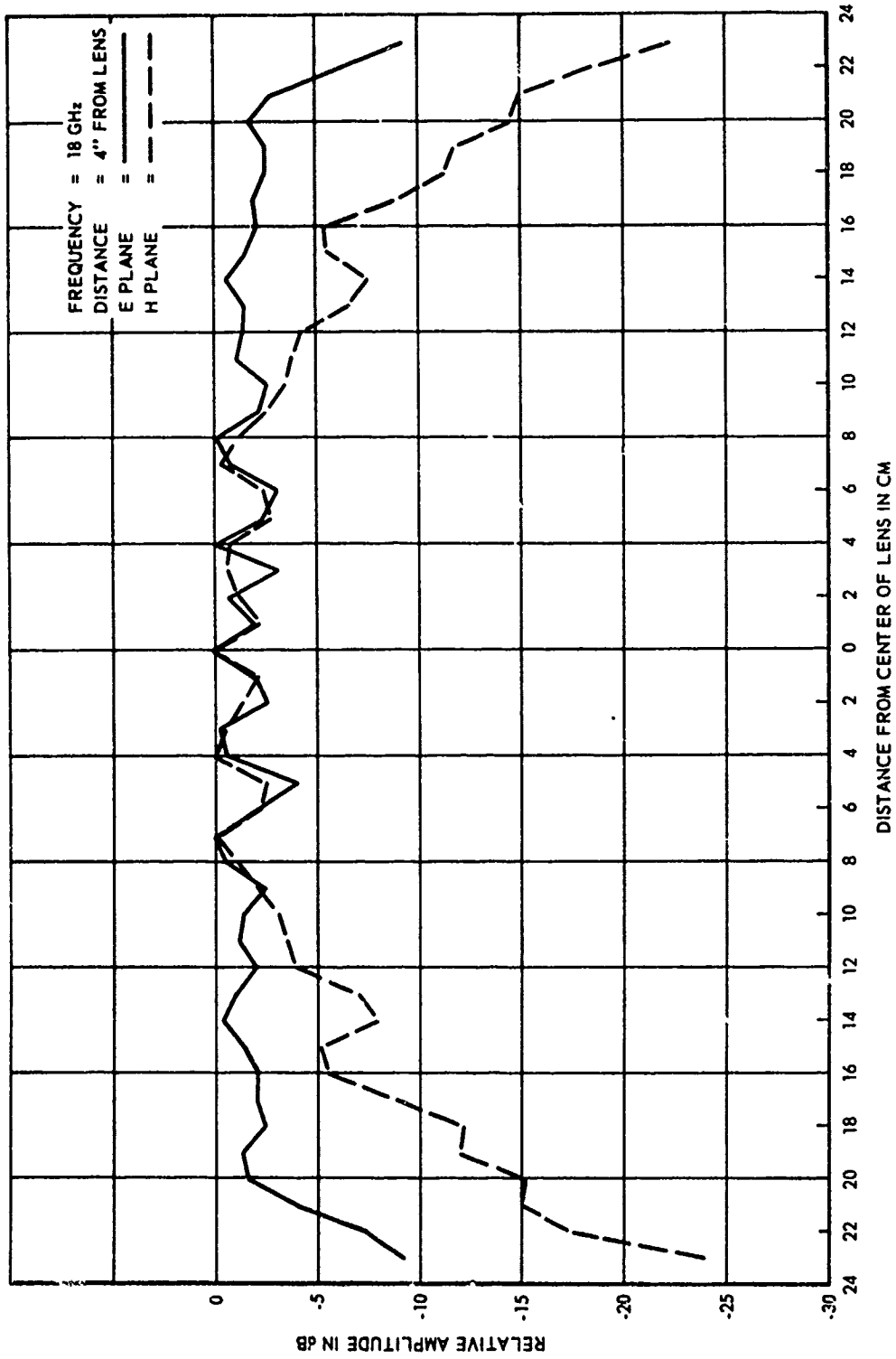


Figure 51. Measured Aperture Distributions of Lens-Horn, 18 GHz

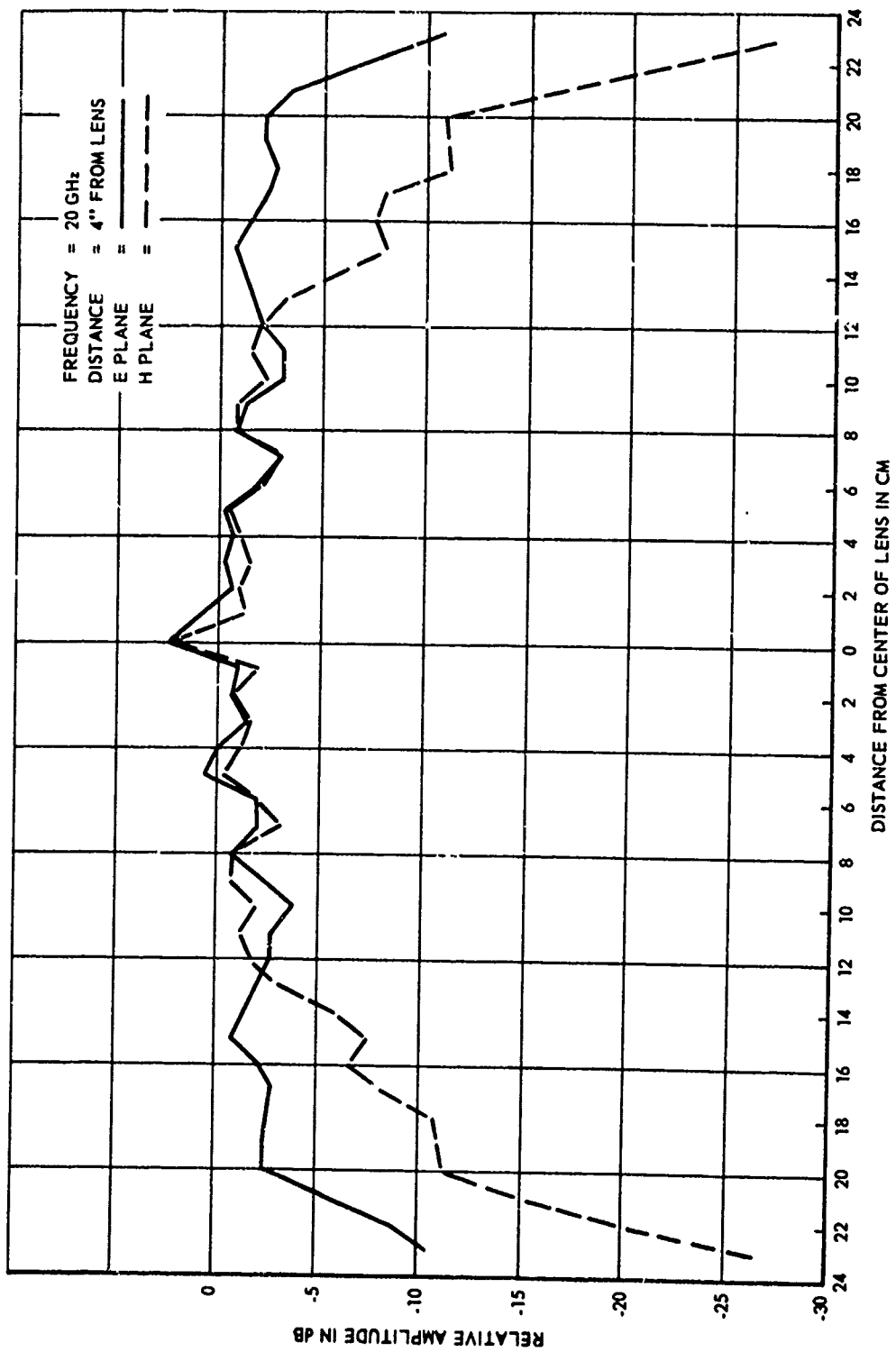


Figure 52. Measured Aperture Distributions of Lens-Horn, 20 GHz

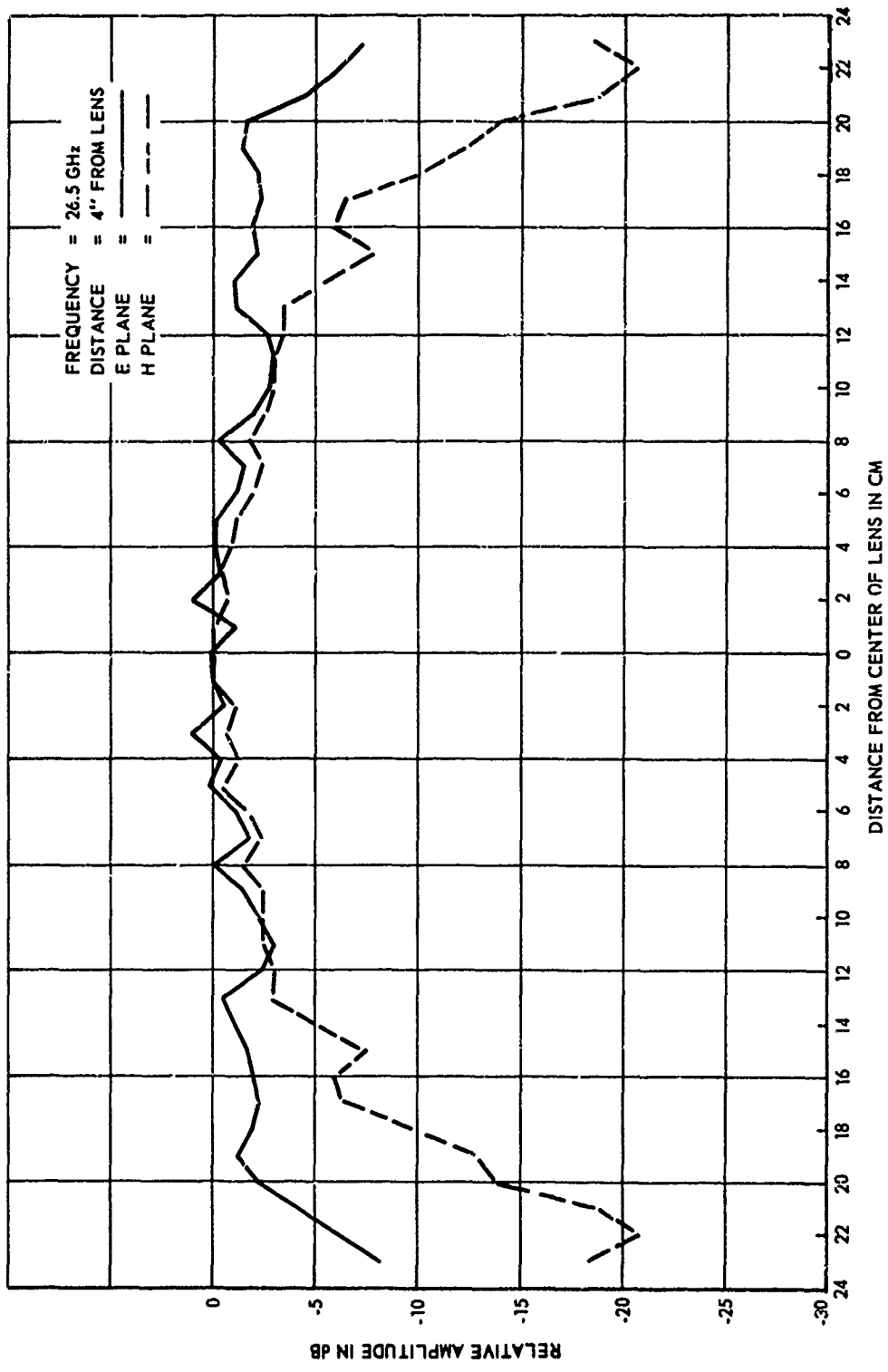


Figure 53. Measured Aperture Distributions of Lens-Horn, 26.5 GHz

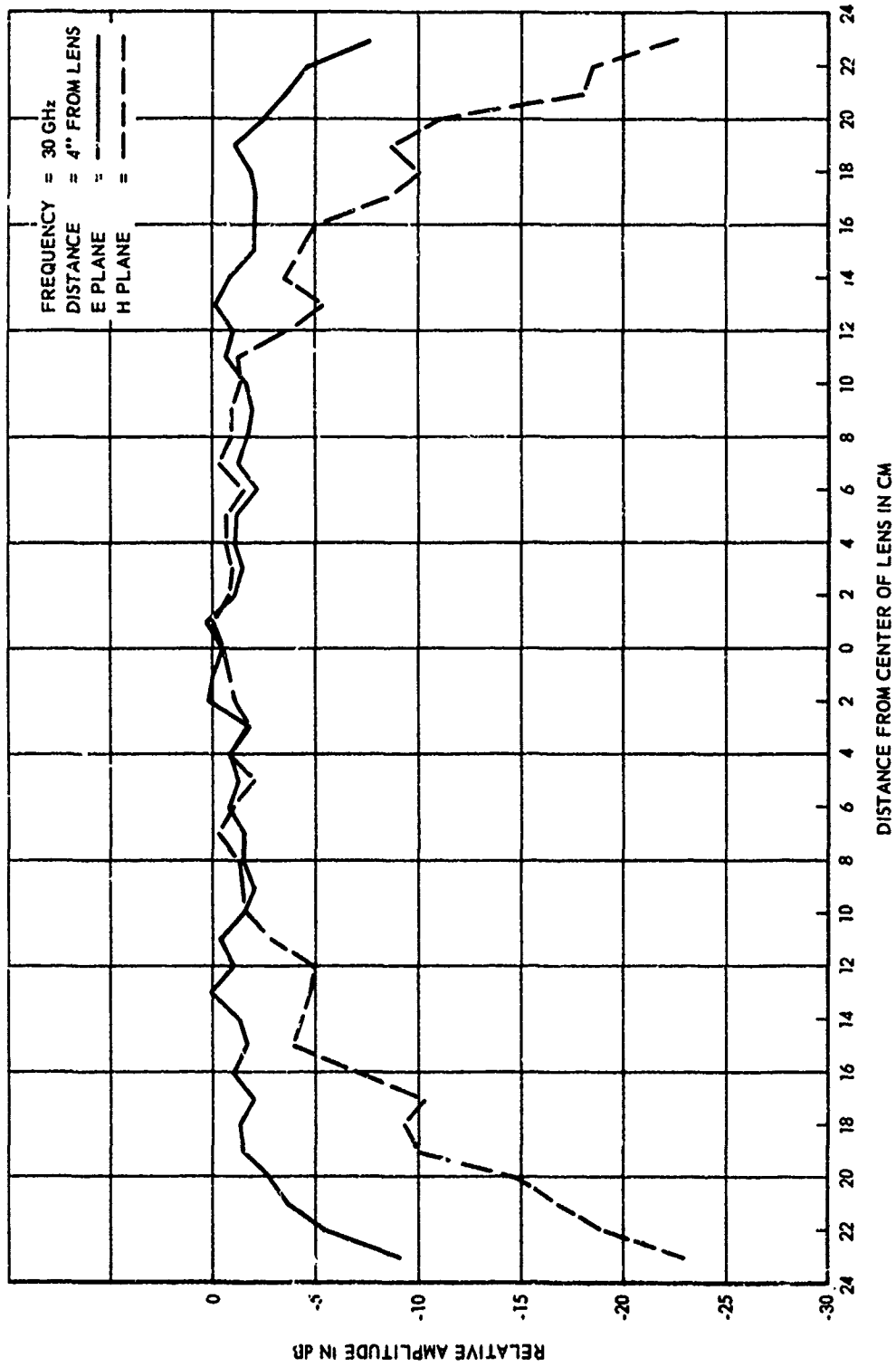


Figure 54. Measured Aperture Distributions of Lens-Horn, 30 GHz

There are several significant features which can be observed from the amplitude plots:

- a. The average E-plane amplitudes are nearly uniform over approximately 85% of the lens diameter of 18 inches (46 centimeters).
- b. The H-plane amplitude approaches zero at the edges of the conical horn due to the same boundary conditions that are characteristic of waveguide or of conventional pyramidal horns.
- c. The fluctuations in amplitude are due to interference effects determined by the geometrical propagation from equivalent point sources (Huygens sources) across the aperture (see reference 3, pages 170 and 171). These fluctuations become smaller as the wavelength decreases and the aperture becomes greater in terms of wavelengths.
- d. The fluctuations described above will alternately reinforce and interfere along the axis of the lens as the distance from the field probe to the lens varies in wavelengths.
- e. The average amplitude characteristics are essentially invariant with frequency.

### 3. COMPUTATION OF EFFICIENCY

The efficiency of the radiating aperture, relative to that of a uniformly illuminated aperture, can be determined on the basis of the amplitude distribution across the lens-horn aperture. All available references make the basic assumption that the amplitude across a circular aperture is circularly symmetric. This assumption is made because of the difficulty in integrating the gain function. Unfortunately, most practical applications exhibited different amplitude distributions in the E and H planes, as evidenced by the measured amplitude plots and the actual antenna patterns. Thus, an average distribution must be assumed in arriving at a figure for aperture efficiency.

The distribution across the aperture in the E plane is considered to be uniform on the basis of the close correspondence between theoretical and measured pattern data and on the basis of the measured amplitude plots. The distribution across the aperture in the H plane most nearly corresponds to the function  $(1-r^2)^p$ , where  $p = 1.0$  and  $r$  is the normalized radius on the basis of the measured amplitude plots and the antenna pattern side-lobe level and beamwidth.

The aperture efficiency for the uniform E-plane distribution is 100%. The efficiency for the  $(1-r^2)$  distribution in the H plane is 75% which represents a maximum loss in gain of 1.25 dB. The effective aperture efficiency lies between these limits.

To determine more closely the aperture efficiency, a look at the efficiency of rectangular horn apertures such as gain-standard horns can be taken as an approximate example. Basic work by Schelkunoff, Braun, and others is summarized in reference 4, chapter 10. For the case of pyramidal horns the gain can be computed from:

$$\text{Gain in dB} = 10(1.008 + \log \frac{\text{area}}{\lambda^2}) - (L_e + L_h)$$

where  $L_e$  and  $L_h$  are decibel loss figures as a function of aperture phase deviation. For the present case it is assumed that both  $L_e$  and  $L_h$  are 0 dB because no phase errors are present under conditions of maximum efficiency. Using as an example the case of an 18-inch-square aperture at 20 GHz, the maximum theoretical gain works out to be 39.77 dB.

Compare this value to the gain of a uniformly illuminated aperture of the same size:

$$\text{Gain in dB} = 10 \log \frac{4\pi (\text{area})}{\lambda^2}$$

which equals 40.68 dB. The efficiency is the difference of -0.91 dB, or, expressed as a percentage, 81%.

It can be expected that the efficiency of a circular aperture would be slightly greater than that of a square aperture. Reference 4 indicates that the gain of a comparable conical horn should be:

$$\text{Gain} = 20 \log \frac{C}{\lambda} - L$$

where:  $C$  is the aperture circumference,  $\lambda$  is the wavelength, and  $L$  is a decibel loss figure which is equal to 0.8 dB if no phase errors are present. This value for gain is 38.8 dB if we use the 18-inch diameter at 20 GHz as an example.

The maximum theoretical gain for a uniformly illuminated aperture with a plane phase front is determined from:

$$\text{Gain in dB} = 10 \log 4\pi \left( \frac{\text{area}}{\lambda^2} \right)$$

or for a circular aperture this is equal to:

$$\text{Gain} = 10 \log 9.87 \left( \frac{D}{\lambda} \right)^2$$

This works out to be 39.6 dB gain over an isotropic source.

The difference between the maximum theoretical gain of 39.6 dB (100% efficiency) and the figure of 38.8 dB is -0.8 dB or an efficiency of 83%. The difference is attributed to nonuniform distribution in the circular aperture and is the maximum efficiency that can be expected.

## APPENDIX IV

### COMPUTER PROGRAM FOR LINEAR ANTENNA

The computer program was written in a general form to enable one to perform a detailed study of arrays of elements. The capability of nonuniform amplitudes for the elements has been added. This was done to investigate the effect on radiation patterns and the effect on beamwidths and side-lobe levels for variations in the design of the array.

The array pattern  $F(\theta) = g(\theta) f(\theta)$

where

$g(\theta)$  = the element pattern factor

$f(\theta)$  = the array pattern factor

The element pattern factor for a uniformly illuminated circular aperture is:

$$g(\theta) = 2\pi a^2 \frac{J_1(\mu)}{\mu}$$

where

$a$  = element aperture radius

$$\mu = \frac{2\pi a}{\lambda} \sin \theta$$

$\lambda$  = wavelength at test frequency

$J_1$  = Bessel function of order one

The array pattern factor for even and odd numbers of elements ( $m$ ) is as follows; the parameters are identified in figure 55.

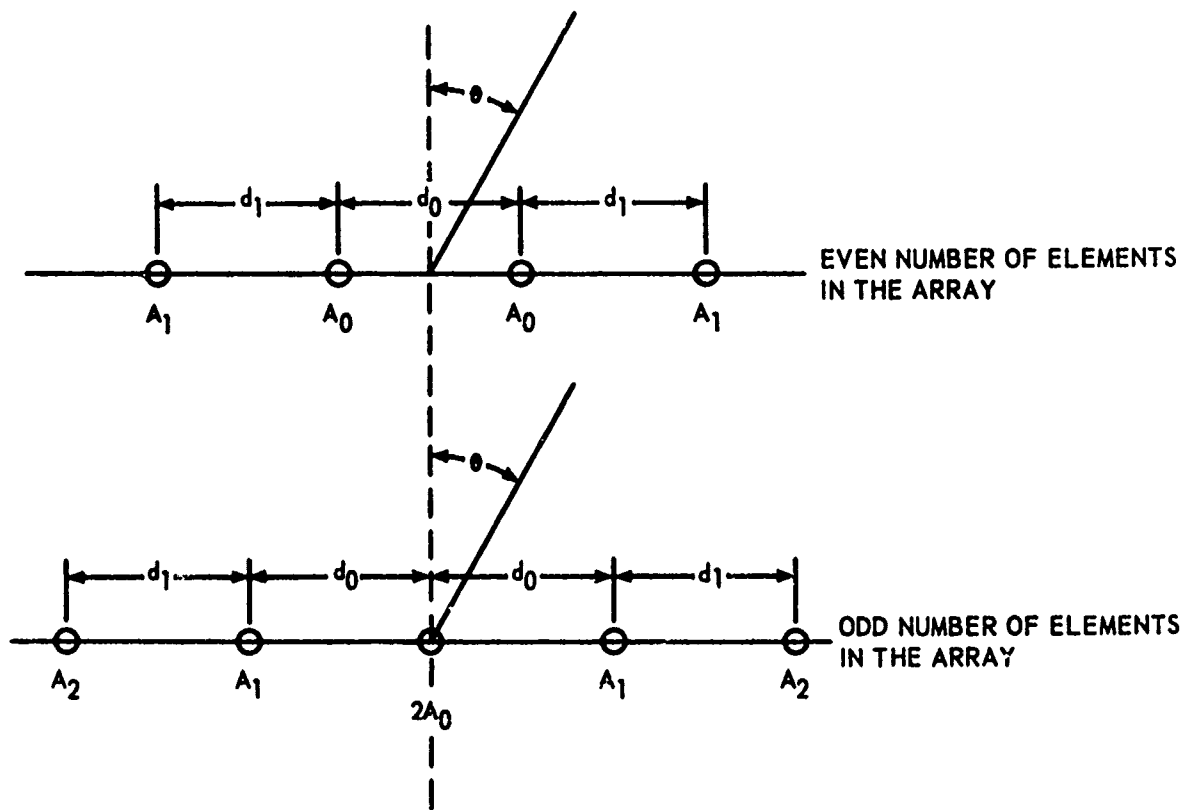


Figure 55. Array Parameters Used in Computer Program

For the case  $m =$  an even number:

$$f(\theta) = 2 \sum_{K=0}^{N-1} A_K \cos \left( \frac{2k+1}{2} \psi \right)$$

where

$$N = \frac{m}{2}, \quad \psi = \frac{2\pi l}{\lambda} \sin \theta$$

$l =$  distance between isotropic sources

For the case  $m =$  an odd number:

$$f(\theta) = 2 \sum_{K=0}^{N-1} A_K \cos \left( 2k \frac{\psi}{2} \right)$$

where

$$N = \frac{m-1}{2}, \quad K = 0, 1, 2, 3 \dots$$

The computer program takes three data input cards which contain the following information:

Card 1:

$$a, \lambda, m, \theta_1, \theta_n, \Delta\theta$$

Card 2:

$$d_0, d_1$$

Card 3:

$$A_0, A_1$$

Where  $a$  is the radius of circular horn aperture, in inches

$\lambda$  is the wavelength of the frequency of interest, in inches

$m$  is the number of antennas in the array

$\theta_1$  is the lowest angle from boresight in which the patterns are to be calculated, in degrees

$\theta_n$  is the largest angle from boresight of interest, in degrees

$\Delta\theta$  is the increment, or step size, between  $\theta_1$  and  $\theta_n$ , in degrees

$d_0$  is the distance between the innermost antennas, in inches

$d_1$  is the distance between the antennas next to the innermost ones, in inches

$A_0$  is the voltage excitation coefficient of the innermost element

$A_1$  is the voltage excitation coefficient of the next to the innermost element.

A subroutine has been used in the computer to produce a rough plot of the antenna pattern. The patterns are plotted as a function of theta and dB from 0 to 10 degrees and 0 to 50 dB. The program is given on the following pages.

```

▲JOB
▲REWIND MT1.
▲ASSIGN S=MT0,S1=CR,L0=LP,B0=MT1.
▲FORTRAN S1,L0,B0.
  1 C LINEAR MULTI-ELEMENT ANTENNA ARRAY
  2 C
  3 C A=RADIUS OF SINGLE APERTURE (INCHES)
  4 C M=NUMBER OF HORNS IN ARRAY
  5 C XLAM=WAVELENGTH (INCHES)
  6 C DIAM(I)=DISTANCE BETWEEN SOURCES
  7 C CNST(I)=ELEMENT FACTOR CONSTANTS
  8 C RTHETA=ANGLE THETA IN RADIANS
  9 C TH=LOWER LIMIT OF THETA (DEGREES)
 10 C TH2=UPPER LIMIT OF THETA (DEGREES)
 11 C TH3=STEP SIZE OF THETA (DEGREES)
 12 C ELEM=A*(THETA)*ELEMENT FACTOR
 13 C ARRAY=ARRAY FACTOR
 14 C ANSWER=F(THETA) BEFORE NORMALIZING
 15 C FTH=F(THETA) AFTER NORMALIZING
 16 C FDB=F(THETA) IN DB
 17 C
 18 C DIMENSION ANSWER(501),CNST(0/8),DIAM(0/8),ANS(501)
 19 C READ INPUT VARIABLES
 20 300 READ 1,A,XLAM,M, TH,TH2,TH3
 21 READ 3,(DIAM(I),I=0,8)
 22 READ 3,(CNST(I),I=0,8)
 23 PI=3.14159
 24 S=360.*L/XLAM
 25 C CONVERT S TO RADIANS
 26 S=S*PI/180.
 27 PRINT S
 28 C COMPUTE NUMBER OF THETA VALUES
 29 N=(TH2-TH)/TH3 +1
 30 DO 10 I=1,N
 31 THETA=TH+(I-1)*TH3
 32 RTHETA=THETA*PI/180.
 33 U=2.*PI*A/XLAM*SIN(RTHETA)
 34 IF(U<3.) 20,20,25
 35 20 X=U/3.
 36 X2=X*X
 37 X4=X2*X2
 38 X6=X4*X2
 39 X8=X6*X2
 40 X10=X8*X2
 41 X12=X10*X2
 42 APPROX=0.5 + .56249985*X2 + .21093573*X4 + .03954289*X6 +.0044331*
 43 X8 + .00031761*X10 + .00001109*X12
 44 BESSEL=APPROX*U
 45 GO TO 11
 46 25 X=3./U
 47 X2=X*X
 48 X3=X2*X
 49 X4=X3*X
 50 X5=X4*X

```

```

• 51 X6=X5*X
• 52 F1=.79788456 + .00000156*X + .01659667*X2 + .00017105*X3 +
• 53 1 .00249511*X4 + .00113653*X5 + .00020033*X6
• 54 TH1=U = 2.35619449 + .12499612*X + .00005650*X2 + .00637879*X3
• 55 1 + .00074348*X4 + .00079824*X5 + .00029166*X6
• 56 APPROX=F1*COS(TH1)
• 57 BESSEL=APPROX/SQRT(U)
• 58 11 IF(RTHETA) 12,12,13
• 59 12 ELEM=2.*PI*A**2*APPROX
• 60 GO TO 17
• 61 13 ELEM=2.*PI*A**2*BESSEL/U
• 62 C COMPUTE ARRAY FACTOR
• 63 17 IF(MOD(M,2)) 60,60,70
• 64 C M EVEN
• 65 60 LIMIT=M/2-1
• 66 SUM=0.
• 67 SUMD=DIAM(0)/2.
• 68 DO 61 K=0,LIMIT
• 69 SUM=SUM+CNST(K)*COS(2.*PI/XLAM*SUMD*SIN(RTHETA))
• 70 61 SUMD=SUMD+DIAM(K+1)
• 71 ARRAY=SUM*2.
• 72 GO TO 14
• 73 C M ODD
• 74 70 LIMIT=(M+1)/2
• 75 SUM=0.
• 76 SUMD=0.
• 77 DO 71 K=0,LIMIT
• 78 SUM=SUM+CNST(K)*COS(2.*PI/XLAM*SUMD*SIN(RTHETA))
• 79 71 SUMD=SUMD+DIAM(K)
• 80 ARRAY=SUM*2.
• 81 14 ANSWER(I)=ELEM*ARRAY
• 82 10 CONTINUE
• 83 C
• 84 C PRINT INPUT VARIABLES
• 85 PRINT 2,A,XLAM,M, TH ,TH2,TH3
• 86 PRINT 100, (I,DIAM(I),I,CNST(I),I=0,LIMIT)
• 87 PRINT 49
• 88 DO 50 I=1,N
• 89 THETA=TH*(I-1)*TH3
• 90 FTH=ANSWER(I)/ANSWER(1)
• 91 FDB=20.*.43429*ALOG(ABS(1./FTH))
• 92 IF(FDB=50.) 90,90,91
• 93 91 FDB=50.
• 94 90 ANS(I)=FDB
• 95 50 PRINT 51,THETA,ANSWER(I),FTH,FDB
• 96 1 FORMAT(2F10.5, 14,3F10.3)
• 97 5 FORMAT(1H1,3X,THETAs,7X,ANSWERS,8X,US,9X,BESSELs,7X,ELEMs,7X,
• 98 1*ARRAY//)
• 99 23 FORMAT(6F12.4)
• 100 2 FORMAT(1H1,*INPUT VARIABLES--LINEAR MULTI-ELEMENT ANTENNA ARRAY*
• 101 1 //1X,*A*s,F8.4/1X,*LAMBDA *s,F8.4/1X,*M *s,I4/1X,
• 102 2 *THETA RANGES FROM*s,F5.1,* DEGREES TO*s,F5.1,* DEGREES IN*s,F5.2,
• 103 3 * DEGREE STEPS*)
• 104 100 FORMAT(1X,*D*,I1,* *s,F7.3,5X,*A*,I1,* *s,F7.3)

```

```

• 105 49 FORMAT(1H1,5THETA(DEG)8,3X,5F(THETA)8,6X,5NORMALIZED8,7X,8F IN DB8
• 106 1 //)
• 107 51 FORMAT(1X,F6.2,3F15.3)
• 108 3 FORMAT(9F8.4)
• 109 CALL PLY(ANS,N,1,1)
• 110 GO TO 300
• 111 END

```

PROGRAM ALLOCATION

00021 ANSWER	01773 CNST	02015 DIAM	02037 ANS
04011 M	04012 I	04013 L	04014 N
04015 LIMIT	04016 K	04017 A	04021 XLAM
04023 TH	04025 TH2	04027 TH3	04031 PI
04033 S	04035 THETA	04037 RTHETA	04041 U
04043 X	04045 X2	04047 X4	04051 X6
04053 X8	04055 X10	04057 X12	04061 APPROX
04063 BESSFL	04065 X3	04067 X5	04071 F1
04073 TH1	04075 ELEM	04077 SUM	04101 SUMD
04103 ARRAY	04105 FTH	04107 FDB	

SUBPROGRAMS REQUIRED

SIN	COS	SQRT	MOD	ALOG	ABS
PLY					
THE END					

## REFERENCES

1. J. F. Kauffman, "Dielectric Antenna Study," RADC-TR-70-109, Rome Air Development Center, Air Force Systems Command, Griffiss Air Force Base, New York, July 1970.
2. J. F. Kauffman, "Lens Antennas that Provide Both Amplitude and Phase Transformation," Applied Optics, Vol. II, No. 2, page 435, February 1972.
3. Samuel Silver, Microwave Antenna Theory and Design, Radiation-Laboratory Series, No. 12, McGraw-Hill, New York, 1949.
4. Henry Jasik, Antenna Engineering Handbook, McGraw-Hill, New York, 1961.
5. E. M. T. Jones and S. B. Cohn, "Surface Matching of Dielectric Lenses," IRE Convention Record, Part I, pages 46-53, March 1954.
6. E. M. T. Jones and S. B. Cohn, "Surface Matching of Dielectric Lenses," Journal of Applied Physics, pages 452-457, April 1955.
7. T. Morita and S. B. Cohn, "Microwave Lens Matching by Simulated Quarter-Wave Transformers," IRE Transactions, Vol. AP-4, pages 33-37, January 1956.
8. T. Morita and S. B. Cohn, "Measured Performance of Matched Dielectric Lenses," IRE Transactions, Vol AP-4, pages 31-33, January 1956.
9. R. E. Collin and F. J. Zucker, Antenna Theory, Part I, McGraw-Hill Book Co., New York, pages 650-653, 1969.
10. G. Doundoulakis and S. Gethin, "Far Field Patterns of Circular Paraboloidal Reflectors," IRE National Convention Record, Part I, March 1959.
11. J. D. Kraus, Antennas, McGraw-Hill Book Co., New York, 1950.
12. A. L. Ingalls, "Optical Simulation of Microwave Antennas," IEEE Trans on Antennas and Propagation, Vol. AP-14, No. 1, Jan. 1966.